ELECTROSPUN NANOFIBER ELECTRODES FOR HYDROGEN/AIR PROTON EXCHANGE MEMBRANE FUEL CELLS

By

Matthew Ward Brodt

Dissertation

Submitted to the Faculty of the

Graduate School of Vanderbilt University

in partial fulfillment of the requirements

for the degree of

DOCTOR OF PHILOSOPHY

in

Chemical Engineering

December, 2015

Nashville, Tennessee

Approved:

Professor Peter N. Pintauro

Professor G. Kane Jennings

Professor M. Douglas LeVan

Professor David E. Cliffel

To my family.

ACKNOWLEDGEMENTS

I am enormously grateful for all the people that contributed to this dissertation. First, I would like to thank my thesis advisor, Professor Peter Pintauro, for welcoming me into his lab and supporting my project. His excitement for research and incredible vision were instrumental to the success of this work. I am also very thankful for my committee members Professors Kane Jennings, Douglas LeVan, Janet Macdonald, and David Cliffel for their helpful guidance and encouragement.

Many external collaborators made important contributions to this project. Researchers at Nissan Technical Center North America shared their facilities and conducted extensive laboratory testing. A special thank you goes to Dr. Taehee Han, Dr. Nilesh Dale, and Dr. Ely Niangar for sharing their valuable knowledge and insight through numerous conversations. Discussions and laboratory collaborations with researchers at EMD Millipore/Merck KGaA were also a great asset to this dissertation. In this regard, Dr. Onur Kas and Dr. Ashley Moore were particularly helpful. I would also like to thank Dr. Karren More from Oak Ridge National Laboratory for collecting high magnification SEM images of the electrode nanofibers.

I would like to thank my research colleagues and the Vanderbilt community as a whole for their assistance and making the lab a fun place to work. Dr. Angela Zhang started this project on electrospun fuel cell electrodes and taught me everything she had learned. Dr. Jason Ballengee and Dr. Andrew Park were very helpful in sharing their expertise and answering all my questions when I joined the lab. Tori Trout was an undergraduate researcher who proved to be a great asset in the lab. Dr. Ryszard Wycisk was invaluable for his advice, troubleshooting assistance, paper critiques, and overall for just being the go-to guy whenever I needed anything.

Most importantly, I want to thank my family, who have always been there to support me.

This dissertation research was funded by the U.S. Department of Energy's Hydrogen Program (DE-FG36-06GO16030), and by the NSF-funded TN-SCORE program, NSF EPS-1004083, under Thrust 2. This research was also funded by Nissan Technical Center North America, and Merck KGaA, Darmstadt.

TABLE OF CONTENTS

LIST OF TABLES

Table Page

LIST OF FIGURES

Figure Page

CHAPTER I

INTRODUCTION AND BACKGROUND

The creation of a sustainable energy solution to fulfill the requirements of a rapidly growing global energy demand is one of the most important challenges of the 21st century. We use energy to produce and transport our food and water, to heat and light our buildings, to power industry, to communicate and travel long distances; energy is vital for our welfare, security, and prosperity. As the global energy demand skyrockets from 500 quadrillion Btu in 2010, of which 85% was produced with fossil fuels, to a projected 700 quadrillion Btu by 2030[1], our ability to harvest, transmit, and store energy must expand and scale accordingly. The Earth's supply of fossil fuels will not run out in the near future, yet coal, oil, and natural gas remain non-renewable resources with finite supply. The burning of fossil fuels also pollutes our atmosphere and continued large-scale use may have severe environmental ramifications. Alternate energy sources and conversion devices are necessary to transition out of our dependence on fossil fuels and make strides towards a cleaner, sustainable strategy.[2, 3]

One promising energy conversion device that could replace the internal combustion engine, a leading contributor of fossil fuel consumption and localized air pollution, is the proton-exchange membrane fuel cell (PEMFC). The hydrogen/air fuel cell, which electrochemically converts energy from hydrogen gas into electrical power with water as a byproduct, is particularly suited to generate electricity for automotive power plants due to its high power output, high energy conversion efficiencies, moderate

operating temperature, and quick start-up. Integration of a hydrogen-fueled fleet of fuel cell vehicles into the transportation sector would mitigate our reliance on foreign oil and reduce emissions of localized environmental pollutants.[3-5] While there have been many fuel cell vehicle prototypes released by car manufactures including General Motors, Chrysler, Ford, Nissan, Honda, Toyota, Mitsubishi, Kia, Hyundai, BMW, Mercedes Benz, Mazda, Fiat, Audi, and Volkswagen, several obstacles are making mass commercialization of fuel cell vehicles challenging.

1.1 Principles of Hydrogen/Air Fuel Cells

A proton exchange membrane fuel cell (PEMFC) is an electrochemical device that directly converts chemical energy into electricity, as opposed to a spark ignition internal combustion engine, which burns a fuel to create heat that is converted into mechanical energy. With hydrogen as the energy carrier, a PEMFC can operate at thermodynamic efficiencies over 55%, compared to internal combustion engines that have efficiencies around 20%.[6] This is one of the primary advantages of fuel cells.

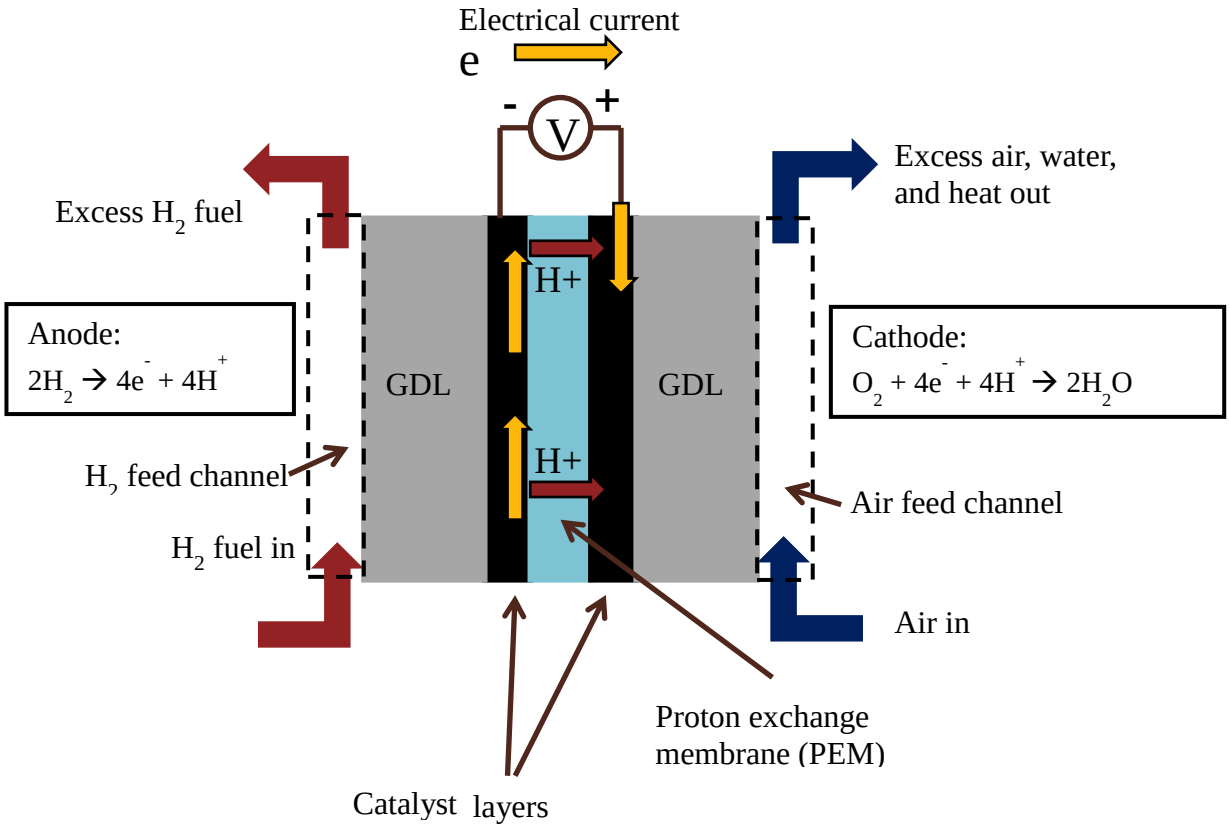

Figure 1.1. Schematic of a typical PEMFC

A hydrogen/air PEMFC cell schematic is shown in Figure 1.1. At the anode, hydrogen gas is electrochemically oxidized to protons and electrons. The protons travel through the proton exchange membrane (PEM), while electrons travel through an external circuit where a portion of their energy is extracted to generate power. At the cathode, oxygen reacts with electrons and protons from the anode in a reduction reaction to form water. Porous carbon, electrically conductive layers with specific/controlled hydrophobic/hydrophilic properties, known as the gas diffusion layers (GDLs) are attached to the electrodes. The structure consisting of the membrane, electrodes, and GDLs is known as a membrane-electrode-assembly (MEA). The GDLs allow passage of

gases, aid in water management at the electrode surface, and electrically connect the electrodes to the bipolar plates (graphitic or metallic plates that separate but electronically connect cells) in a fuel cell stack (an assembly of cells that produce a higher voltage and power than a single cell). The standard material for the PEM is Nafion, a perfluorosulfonic acid ion exchange polymer with excellent thermal and chemical stability that was developed by DuPont in the 1960's.[7] In a hydrogen/air PEMFC, the kinetics of the oxygen reduction reaction (ORR) are much slower than hydrogen oxidation, thus the cathode is the problematic electrode and is the focus of most research studies.

Presently, the most common catalyst for the anode and cathode of a hydrogen/air PEMFC is platinum supported on carbon powder. A proton-conductive ionomer is dispersed with the Pt/C powder to bind the particles to one another and to the membrane. A schematic picture of a catalyst layer, located between the membrane and GDL (the GDL is shown as electronically conductive fibers) in an MEA is shown in Figure 1.2. To efficiently utilize Pt during fuel cell operation, the "triple phase" contact area must be maximized, where catalyst (for reaction sites), ionomer (for delivery of protons) and void space (for gas delivery and removal of product water) meet.[8]

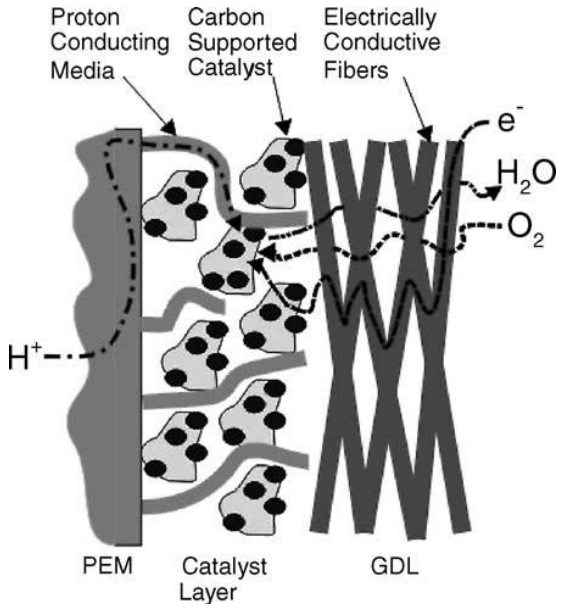

Figure 1.2. Schematic half of an MEA, depicting membrane, electrode as well as gas diffusion layer. Adapted from Reference 9.

1.1.1 Cathode Characterization

The most common method to assess the performance of the cathode in an MEA is to collect current-voltage polarization data, where the results are plotted as cell potential verse current density. These are steady-state measurements under constant load, where either a voltage is recorded at a set current (galvanostatic operation) or a current is recorded at a set voltage (potentiostatic operation) for each data point. The voltage is the potential difference between the two half cells (hydrogen oxidation at the anode and oxygen reduction at the cathode). As hydrogen is oxidized and oxygen is reduced, electrons travel from the anode to the cathode, producing current. In pure oxygen, the theoretical (thermodynamic) voltage of the four-electron oxygen reduction reaction is 1.23 V vs. a standard hydrogen reference electrode (SHE) when operating at 25°C and 1

atm oxygen. In a hydrogen/air fuel cell, this potential cannot be achieved at open circuit (zero current) because of finite feed gas crossover through the electrolyte membrane (most notably, H_2 from the anode to the cathode) and because the reversible open circuit voltage is a function of oxygen partial pressure and air is only 21% oxygen. The crossover of hydrogen fuel causes a mixed reaction at the cathode (hydrogen oxidation and oxygen reduction) that reduces the voltage from the thermodynamic ideal value. During steady-state current flow (i.e., during power generation) the voltage decreases further due to various overpotentials, which are explained below.

A fuel cell steady-state polarization curve generally has three distinct regions which are characterized by the primary source of voltage loss (due to overpotentials). A typical curve is depicted in Figure 2.3. At high potentials (and low current densities) activation (kinetic) losses of the ORR dominate. This region follows a non-linear Tafel behavior (an exponential drop in voltage with current density). The kinetics of the hydrogen oxidation reaction at the anode are much faster than the ORR, so the polarization curve kinetic voltage losses originate solely from the cathode reaction.[10] The second region of a fuel cell polarization curve at higher current densities (and lower voltages) is dominated by ohmic losses (resistances) in the membrane and electrode, i.e., losses are associated with finite transport rates for protons from the catalyst sites in the anode to sites within the cathode, through the membrane and electrode layer. Voltage losses associated with finite conductivity follow Ohm's law, thus they scale linearly with current density, as can be seen from the straight line region in the V-i polarization plot in the ohmic region. In the third region of the polarization curve (at very high current densities), mass transfer effects dominate. Here, the cathode reaction is oxygen

diffusion-limited as the reactant (O_2) concentration at the electrode surface becomes significantly lower than that of bulk air. Oxygen mass transfer limitations can be caused by any one of a number of effects, such as insufficient air flow rates, low catalyst layer porosity, and water accumulation in the cathode.[11] In order to minimize oxygen diffusion limitations, high stoichiometric air flow rates are often used, in which much more oxygen is fed to the cathode than is consumed in the ORR. High air flow rates maintain higher concentrations of oxygen near the Pt surface and also help to remove water generated in the cathode. There are no mass transfer limitations at the anode in a PEMFC because the feed is pure hydrogen gas.

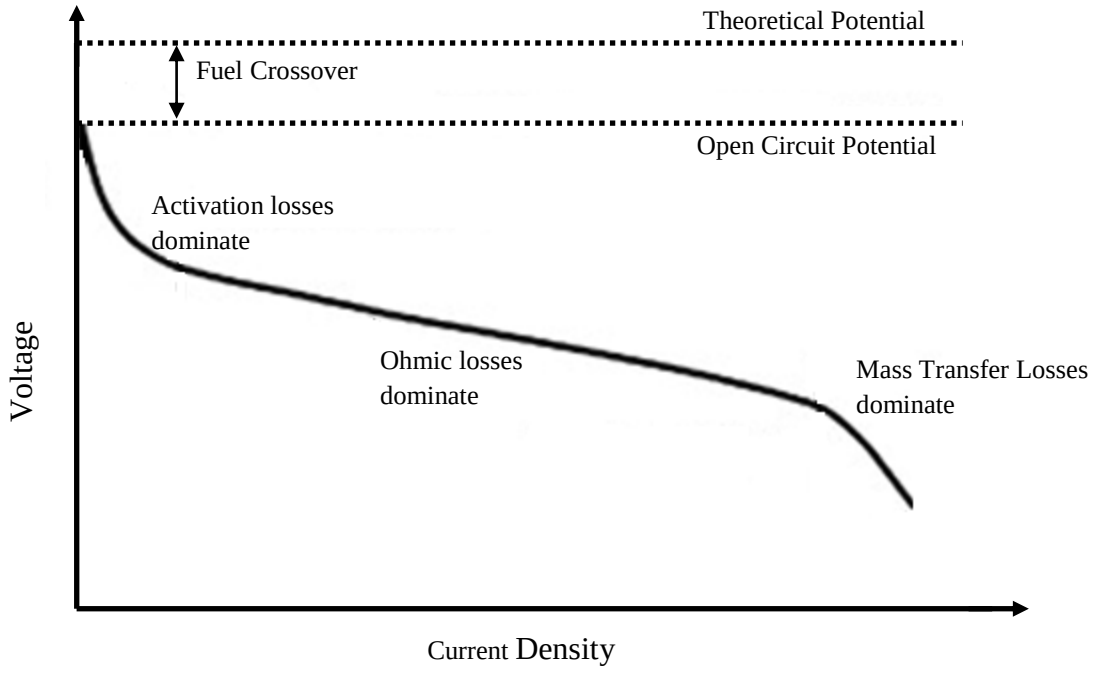

Figure 1.3. Typical polarization curve of a PEMFC with a hydrogen/air feed.

The accessible Pt surface area of an MEA cathode is often less than the actual surface area of the Pt on Pt/C powder due to imperfect triple-phase boundaries. Only metal surfaces in close contact with oxygen, electrons and protons contribute to catalysis and power generation.[12] The electrochemical surface area (ECA) of the Pt in a PEMFC cathode can be measured by *in-situ* cyclic voltammetry (CV), where the charge (integrated current) associated with hydrogen gas oxidation and reduction on catalyst sites is measured. The Pt surface area is calculated by assuming the charge required to reduce one monolayer of hydrogen atoms on Pt is 210 $\mu C/cm^2$. It is always assumed that the ECA measured via Eqn 1.1 is the same area available for oxygen reduction (i.e., $O_2 + 4H^+ + 4e^- \rightarrow 2H_2O$).

$$Pt\text{-}H_{ads} \rightarrow Pt + H^+ + e^- \qquad (1.1)$$

In a traditional/conventional Pt/C fuel cell cathode (made by painting a catalyst/binder/solvent ink on a GDL), the Pt ECA varies between 13 and 72 m^2/g, depending on the type/source of Pt/C catalyst powder as well as the binder loading and type of binder.[13-15]

Even though the high potential region in a polarization curve is dominated by activation (kinetic) losses at the cathode, mass transfer losses can effect power output for cell voltages as high 0.8 V when the cathode feed gas is air.[14] Thus, the kinetics of the oxygen reduction reaction in a fuel cell MEA are studied/measured using pure oxygen as the cathode feed and at a low current densities to minimize oxygen mass transfer effects.[14] Normally, the oxygen reduction reaction rate is quantified in terms of a mass activity which is reported as current per mass of Pt at a given fuel cell potential,

temperature, and oxygen partial pressure. The Tafel slope for the oxygen reduction reaction at an MEA cathode is obtained from the slope of a voltage vs. log(current) curve after the measured voltage is corrected for membrane ohmic resistance and the measured current is corrected from the current loss associated with hydrogen gas crossover from the anode to the cathode.[14] A typical Tafel slope for the four-electron oxygen reduction reaction in PEMFC at 80°C is 70 mV/decade. This value can increase if there is a significant contribution of the undesired two-electron transfer pathway in which oxygen is reduced to hydrogen peroxide, or if the Pt surface has oxide layers.[16] The Tafel slope can also be used to calculate the exchange current density, which is the current density at zero overpotential and a quantification of catalyst activity.

1.2 Objective and Rationale of Dissertation Research

The successful commercialization of fuel cell vehicles requires inexpensive and durable MEAs that produce high power at practical operating conditions. In order to meet these qualifications, fuel cell electrodes must have low materials and production costs, high electrochemical activity, and stability in a harsh automotive environment. In 2011, Zhang and Pintauro[17] published promising results on new electrospun nanofiber mat electrodes for fuel cells. The objective of this dissertation research, which is an extension of Zhang's preliminary work, is to fabricate and characterize MEAs with electrospun nanofiber particle/polymer electrodes for hydrogen/air fuel cells with an emphasis on (i) producing high power densities with low Pt loadings and (ii) demonstrating excellent durability. These new fuel cell electrodes made by electrospinning have the following advantages: a robust, high surface area nanofiber

structure with inter-fiber and intra-fiber porosity for efficient oxygen access to reaction sites and removal of product water, low production costs, and the ability to accommodate new catalyst powders and new ionomer or uncharged electrode polymer binders.

The remaining sections of this chapter are devoted to a literature search on the following topics that are directly related to this research topic: a history of PEMFC electrode development, durability issues of fuel cell electrodes in an automotive environment, alternative catalyst powders to Pt/C, alternative electrode binders to Nafion, alternative cathode morphologies, background information on electrospinning, and Zhang and Pintauro's[17] previous nanofiber electrode work.

1.3 PEMFC Electrode Development

1.3.1 PTFE-bound Catalyst Layers

In the 1960's, first-generation catalyst layers for PEMFC MEAs used Pt black (unsupported Pt) bound with polytetrafluoroethylene (PTFE, e.g., DuPont's Teflon®).[18, 19] These were designed for H_2/O_2 fuel cells and used as auxiliary power on space missions. Pt black was mixed with a PTFE emulsion and spread on a carbon paper GDL, which was subsequently hot-pressed to either a sulfonated polystyrene membrane or, later in the mid 1960's, a more stable Nafion membrane. The PTFE fixed the Pt to the GDL and its hydrophobicity aided in water management at the cathode by preventing excess water accumulation (flooding).[9] During the Gemini space flights in the 1960's, 3 stacks of 32 MEAs produced 620 W. The platinum loading was 28 mg/cm^2.[20] Thus, these early electrodes produced high power, but with very high amounts of Pt catalyst. MEAs

showed good durability over a timeframe of days, and only minimal power losses were reported.[21] However, these electrodes were not subjected to the harsh voltage cycling durability testing methods that are performed today.

1.3.2 Catalyst Layers with Nafion

The performance of PTFE-bound electrodes was improved when they were brushed with a Nafion dispersion, which dripped into and partially filled the porous catalyst layer (such a step is referred to as "impregnation"). The Nafion added hydrophilicity and proton conduction to the electrodes. An MEA with a Nafion-impregnated cathode and anode (5 mg_{Pt}/cm^2) and a Nafion membrane produced 900 mW/cm^2 at 0.6 V with humidified H_2/O_2 at 30 psi_g and 95 °C.[22] The Pt loading was reduced much further when the unsupported Pt was replaced with a Pt/C catalyst, which increased Pt utilization.[23] With a much lower Pt loading of 0.35 mg/cm^2, 180 mW/cm^2 at 0.6 V was produced in an H_2/O_2 fuel cell operating at 50°C and 1 atm_g, and 110 mW/cm^2 were produced at 0.6 V with H_2/air gas feeds at the same pressure and temperature.

The most common method of fabricating electrodes today for PEMFC is the thin film method, in which a carbon-supported Pt catalyst powder is dispersed with ionomer in an electrode ink (as opposed to only impregnation or the coating of an already dried catalyst layer with ionomer) in an alcohol/water solvent, and then applied directly to either the membrane (to create what is referred to as a catalyst coated membrane or CCM) or to the carbon paper gas diffusion layer (to transform the GDL into a so-called gas diffusion electrode or GDE).[24] For the CCM method, the ink may be painted or sprayed directly onto the proton conducting membrane that separates the two electrodes

in a MEA or it can first be coated on an inert polymer film such as Kapton and then transferred (during a hot-pressing step) onto the membrane using the so-called "decal method".[25] These thin film layers, which have typical Pt loadings between 0.10 and 0.5 mg/cm^2, have been shown to produce much higher power than the Nafion-impregnated layers, and have become the present day convention.[26-28] For example, a conventional thin film electrode MEA with 0.50 mg_{Pt}/cm^2 at the cathode and anode produced 360 mW/cm^2 at 0.6 V at 70°C with H_2/air feed gases at ambient pressure.[29] However, these thin film catalyst layers have durability issues in an automotive environment, as will be described in the next section.

1.4 Durability Issues of Pt/C Catalyst in an Automotive Environment

Carbon has many properties than make it an excellent support for Pt-based catalysts. Carbon blacks have a high electronic conductivity and high surface area, and they are also relatively inexpensive. Small platinum particles (~3 nm) can be grown on carbon with a much higher active surface area than Pt black powder.[30] However, the oxidation of carbon to gaseous carbon dioxide at a potential of 0.207 V vs. SHE makes carbon thermodynamically susceptible to corrosion (oxidation) reactions throughout most of the operational voltage range of a hydrogen/air fuel cell.[31]

$$C + H_2O \rightarrow C\text{-}O_{ad} + 2H^+ + 2e^-,\ E_0 = 0.207\ V \qquad \text{(Eq. 1.2)}$$

$$C\text{-}O_{ad} + H_2O \rightarrow CO_2 + 2H^+ + 2e^- \qquad \text{(Eq. 1.3)}$$

The presence of platinum also increases the rate of carbon corrosion because platinum catalyzes the carbon oxidation reaction and significantly reduces the overvoltage for the reaction shown in Eq. 1.3 .[32, 33] Fortunately, carbon oxidation kinetics are only fast above ~1.0 V vs SHE.[11] While hydrogen/air fuel cells typically do not experience such high voltages under normal operating conditions (the open circuit voltage in a hydrogen/air fuel cell, which represents the maximum potential of the system before current flow is typically ~0.95 V), the cathode potential can spike as high as 1.5 V during the start-up of a fuel cell stack. This spike in cathode voltage is explained next.

Air is typically present on both fuel cell electrodes after a long shutdown, because air enters the anode compartment by permeating across the membrane from the cathode and the remaining hydrogen in the anode is consumed by hydrogen oxidation. During start-up, when hydrogen fuel is fed to the anode, a hydrogen-air front passes through the anode. Due to this maldistribution of hydrogen, fuel-rich regions drive a "reverse current" in the fuel-starved regions.[34] During normal operation, hydrogen is consumed at the negative electrode (anode) via hydrogen oxidation and air is reduced at the positive electrode (cathode). These spontaneous reactions establish a potential difference across the cell (~0.95 V at open circuit) which is normally harnessed to drive an external load. This potential difference, however, can also drive reactions that would not otherwise occur spontaneously. During start-up with an external load, localized regions of the fuel cell where the anode does not have hydrogen, but are in parallel with regions where the anode does have hydrogen, have a potential of ~1.5 V vs. SHE. In the fuel-starved regions, in order to simultaneously maintain current and potential difference, the respective domains reverse, and the cathode catalyst layer is utilized as fuel while oxygen

on the anode side is reduced.[35] A schematic of this reverse current process is depicted in Figure 1.4a, which shows a H_2/air front moving through the anode on start-up (from left to right). Hydrogen is introduced in region A, which is in parallel to region B with air at the anode. Normal fuel cell operating conditions (Figure 1.4b) are restored shortly after start-up when normal H_2 distribution is restored.[32]

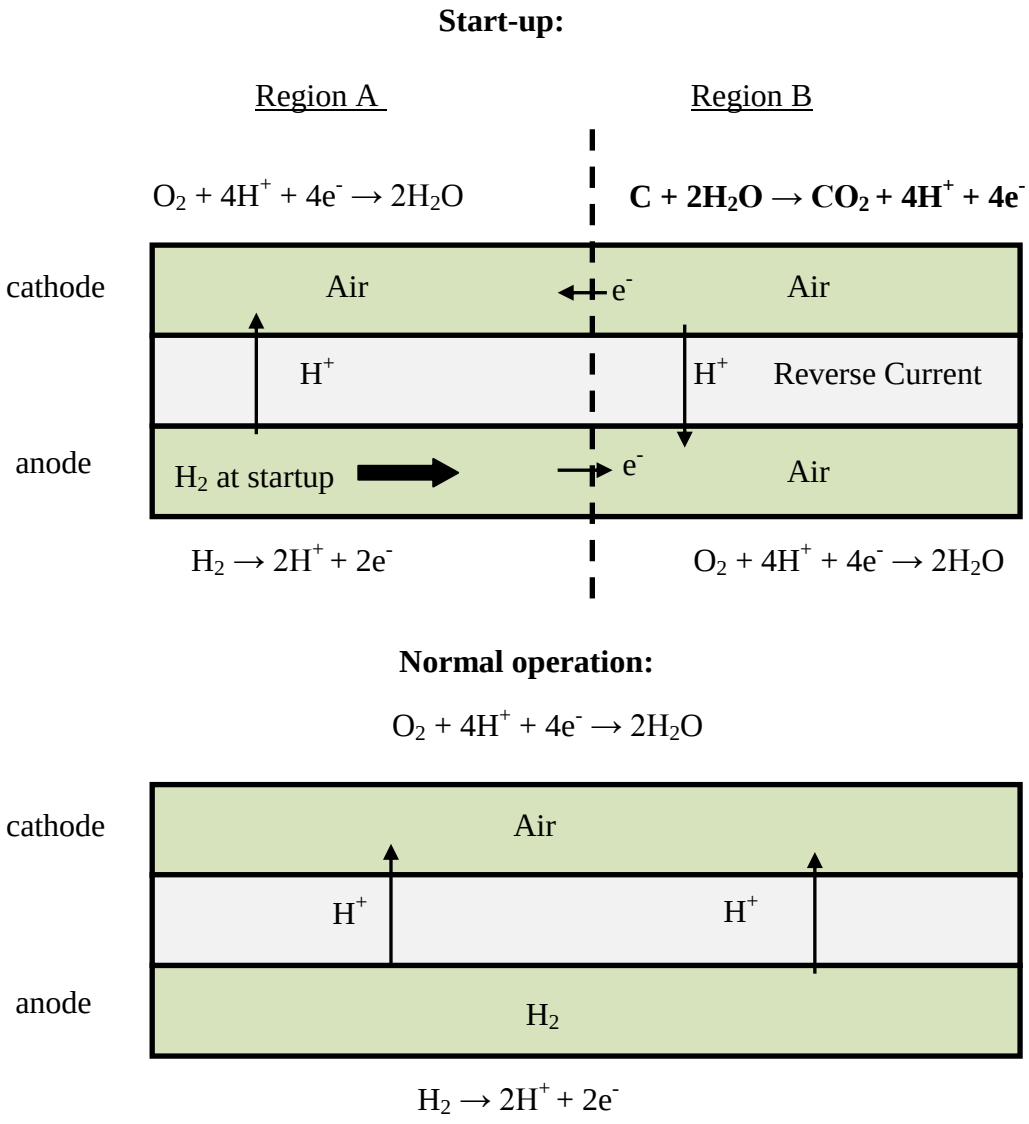

Figure 1.4. **(a)** Schematic of reverse current mechanism that causes cathode carbon corrosion during fuel cell stack start-up. Localized regions with hydrogen (Region A) polarize localize regions without hydrogen (Region B); **(b)** Normal fuel cell operation.

After many shut-down/start-ups cycles, there will be severe degradation of the cathode catalyst layer, including loss of carbon, electrode layer thinning and disintegration, and platinum nanoparticles agglomeration into larger particle sizes. These phenomena decrease the electrochemically active platinum surface area and lower the fuel cell power output. For example, a conventional thin film electrode MEA with a cathode loading of 0.50 mg_{Pt}/cm^2 and an initial power density of 360 mW/cm^2 at 0.6 V only produced 120 mW/cm^2 at 0.6 V after 750 stop-start cycles.[29] The formation of surface oxide species on the carbon support (e.g., C=O and C-OH), as intermediate/precursor species during CO_2 production, is also an issue. Such species make the cathode layer more hydrophilic and more prone to water flooding (excessive water build up in the cathode layer), which reduces oxygen access to active catalytic sites.[36] Engineering strategies have been sought to minimize these voltage spikes, such as using high velocity hydrogen at start-up, drying out the MEA at shut-down (carbon corrodes slower at low humidity), or using a shorting resistor to limit the cathode voltage spike, but no practical/simple solutions have emerged to eliminate the problem of carbon corrosion.[11]

Platinum nanoparticles are also subject to electrochemical degradation during typical automotive acceleration/deceleration events. An example of the platinum particle size distribution for fresh catalyst powder and for powder that has undergone potential cycling (10,000 cycles between 0.6 and 1.0 V vs. SHE) is shown in Figure 1.5.[37] As can be seen, the Pt islands on the carbon support material of a fuel cell Pt/C catalyst powder are very small (initially, the average Pt size is about 3 nm). After Pt degradation in a fuel cell, the average Pt particle size increases to 6 nm. During these voltage cycling tests, it

has been reported that platinum particle growth occurs predominantly via Ostwald ripening, in which smaller platinum particles dissolve at high potentials and diffuse nanometer length scales on the carbon support surface to redeposit as larger particles. Larger Pt particles have less electrochemically active surface area than the same mass of smaller particles. In addition to Pt particle growth, the total electrochemically active Pt surface area is also reduced during voltage cycling events due to the relocation of Pt into the membrane. Near the cathode/membrane interface, there is dissolution of Pt and migration of platinum ions over micrometer length scales with the subsequent precipitation of Pt particles in the membrane (due to the reduction of Pt ion species by H_2 gas that is crossing over the membrane from the anode side of the MEA).[11, 37] Pt particles that precipitate in the membrane have no electrical contact with the cathode, and therefore, are no longer electrochemically active.[23] After a durability test in which an MEA was cycled 24,000 times between 0.6 and 0.95 V, it was found that 16% of the initial cathode Pt had migrated into the membrane.[38] X-ray photoelectron spectroscopy showed that while there can be significant accumulation of platinum in the membrane, the total amount of Pt in an MEA does not change.[11] Thus, the total electrochemically active Pt surface area that can participate in the oxygen reduction reaction is reduced due to a combination of (i) an increase in the average Pt particle size and (ii) dissolution of Pt from the cathode and precipitation of Pt in the membrane. This loss in active Pt surface area decreases the power output of an MEA. For example, a 0.40 mg_{Pt}/cm^2 Pt/C conventional MEA lost 30% of its power output after it was cycled 21,600 times between 0.65 and 1.05 V vs. SHE.[39]

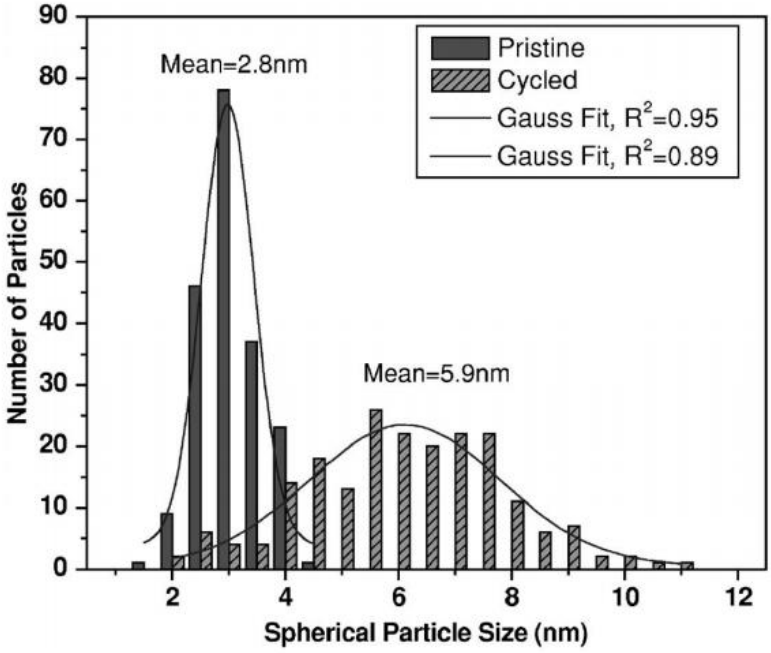

Figure 1.5. Size distributions of platinum nanoparticles in the pristine Pt/Vulcan sample and powders scraped from the MEA cathode surface after the voltage cycling (the Pt durability test). Figure adapted from Ferreira, P. J., G. J. la O, Y. Shao-Horn, D. Morgan, R. Makharia, S. Kocha, and H. A. Gasteiger (2005) Journal of the Electrochemical Society, 152, A2256-A2271.

1.5 Alternate Approaches for PEMFC Electrodes

Presently, the commercialization of fuel cell devices, especially for automotive applications, is challenging due to the high price and inadequate durability of the platinum catalyst electrodes.[9] Alternate approaches to the standard Pt/C/ionomer thin film methods of MEA preparation with commercial catalysts have shown some promise, and some limitations.[18, 40] The purpose of these studies was two-fold: (a) to decrease the cost of MEAs by minimizing or eliminating Pt and (b) to increase the lifetime of the cathode by stopping carbon corrosion and Pt particle growth and migration. These

alternate approaches can be broken down into two general strategies: (1) using new cathode catalyst powders or new catalyst binders, and (2) altering the morphology of the cathode catalyst layers.

1.5.1 Alternate Catalyst Powders to Replace Pt/C

A principal strategy to reduce the cost of MEAs is to minimize the amount of the costly platinum catalyst in the electrodes without sacrificing the power generated in a given fuel cell stack. One approach is the use of platinum metal alloys.[41, 42] Rotating disk electrode (RDE) tests are often used to screen the performance and durability of new catalysts. RDE testing is an ex-situ approach that uses a half-cell setup and is the quickest and most cost-effective method of characterizing new catalysts in terms of reaction rates and reaction mechanisms. Additionally, a smaller amount of catalyst is required for these experiments than is needed to prepare an MEA. In an RDE experiment, a thin mixture of catalyst and ionomer is deposited on a glassy carbon substrate and its ORR activity is measured in an acidic electrolyte, often 0.5 M H_2SO_4.[43] In such tests, the concentration of oxygen at the surface of the electrode can be controlled by varying rotation speed. Reports have shown that the catalytic activity of bimetallic platinum alloys can be 2-4 times higher than that of platinum.[14] Higher ORR catalyst activity with Pt-alloy catalysts has been attributed to shortening of the Pt-Pt interatomic distance after alloying[44] and an improved d-electron vacancy of the alloyed Pt.[45] Notable work in this area includes the preparation and evaluation of PtCr, PtMn, PtFe, PtCo, and PtNi with 75 Pt:M by Mukerjee *et al.*[46] Of these alloys, PtCr showed the best activity for ORR in RDE studies, with an exchange current density of 7.15 $x10^{-4}$ mA/cm^2, as compared to 3.46 x 10^{-4} mA/cm^2 for Pt/C. The exchange current density is found by

extrapolating kinetically-controlled current density/voltage polarization data via a Tafel slope to zero overpotential, and it is one method to quantify catalyst activity. One limitation of Pt alloy catalysts, as reported by some groups,[45, 47, 48] is the dissolution of the non-noble metal from the carbon support into the electrolyte during a RDE polarization experiment or into the membrane during an MEA experiment, resulting in a loss of catalyst activity. For example, Colon-Mercado *et al*.[49] reported a 60% loss in catalytic activity for a Pt_3Ni/C catalyst after a 20 hour hold at 0.9 V, due to leeching of the non-noble metal from the catalyst layer into the sulfuric acid solution. The leeching of the non-noble metal can be mitigated with a "pre-leech" procedure in which the catalyst is heated in oxygen to form surface oxides and then washed with phosphorous acid. This procedure has been shown to remove a portion of the non-noble metal from the catalyst surface and create a more stable Pt-alloy catalyst.[50] In fact, the non-noble metal has been shown to increase the durability of the Pt nanoparticles; the presence of the non-noble metal decreases the mobility of Pt on carbon, thus reducing Pt agglomeration and an increase in particle size.[51] Protsailo and Haug[50] reported good Pt-alloy catalyst durability, where the Pt surface area loss of PtCo/C following 1800 voltage cycles at 120°C were only 18% as compared to 45% for Pt/C at the same conditions. Similarly, Hasche *et al*,[52] reported excellent activity and durability for a $PtNi_3$ catalyst, where some Ni was pre-leeched ("de-alloyed") prior to incorporation into an MEA. After an accelerated durability test of 10,000 voltage cycles between 0.5 and 1.0 V vs. SHE, the dealloyed $PtNi_3$ catalyst showed four-times the catalyst activity of a Pt catalyst. Thus Pt-alloy catalysts have shown superior activity and durability to Pt/C powder.

Besides alloying Pt with another metal to reduce cathode Pt loading without sacrificing power, researchers are also developing oxygen reduction reaction fuel cell catalysts that are platinum-free. Such catalysts are based on metal-nitrogen-carbon materials.[53-55] For example, Oleson, Chapman, and Atanassov[56] fabricated a 5, 10, 15, 20-tetrakis(4-methoxy-phenyl)-porphine cobalt(II) (CoTMPP) catalyst with a pyrolysis process. This catalyst powder was mixed with Nafion and Vulcan carbon and used as the cathode in an MEA. With an oxygen feed, the MEA produced 100 mW/cm^2 at 0.6 V, compared to 900 mW/cm^2 at 0.6 V that were produced with a 0.40 mg_{Pt}/cm^2 Pt/C cathode MEA. Similarly, in 2012 Zhao *et al.*,[57] fabricated an iron imidazolate framework non-platinum group metal (non-PGM) catalyst that achieved 200 mW/cm^2 at 0.6 V in an MEA with an oxygen feed. Zhao reported a 70% loss in power output after 100 hours of steady-state operation, conditions that have negligible impact on Pt/C based cathode MEAs. Bashyam and Zelany[58] fabricated a catalyst with slightly less power output as Zhao *et al*.[57], but with better durability. They prepared a cobalt-polypyrrole-carbon catalyst that produced a maximum power of 130 mW/cm^2 (75 mW/cm^2 at 0.6 V) in an MEA with an oxygen feed that maintained constant power over 100 hours of steady-state operation. While these novel catalysts have the potential to be much less expensive than Pt/C powder, the performance and durability of non-PGM catalysts is presently much lower than Pt-based catalysts powders.[59] It is also noted many groups that have used the same basic catalyst, e.g, M-N_4C,[60-63] have proposed different catalytically active reaction sites. These conflicting reports are most likely attributed to differences in synthesis procedures, such as choice of macrocycle precursor, pyrolysis temperature and duration.[64] Much more research is needed to understand the nature of the active catalyst

sites in metal-nitrogen-carbon materials, and to improve their activity and durability before they can compete with Pt-based catalysts for fuel cell applications.[57]

1.5.2. Alternative Catalyst Binders

In addition to studying novel catalyst powders, researches have investigated alternative binders to Nafion®, which has limitations when used in a fuel cell electrode. As with various catalyst powders, new binders can be incorporated into electrospun nanofiber electrode mats, the focus of this dissertation.

Nafion, a long side chain perfluorosulfonated acid (PFSA) developed by DuPont, is the standard catalyst binder in PEMFC electrodes due to its high electrochemical, thermal, and mechanical stability. One limitation of Nafion is it loses water with a subsequent drop in proton conductivity at temperatures above 90°C and at low humidity.[65] One strategy to overcome the limitations of Nafion is to use ion-exchange polymers with a higher concentration of charged groups. Aquivion® is a short side chain PFSA with a lower equivalent weight than Nafion, (e.g., 790 g/eq for Aquivion vs. 1100 g/eq for Nafion). It has been reported that while Aquivion has a higher concentration of sulfonic acid charge groups than Nafion, it still produces poor power in dry, hot environments. For example, when Aquivion was used as the membrane and catalyst binder in an MEA operated at 110°C and 33% relative humidity, 330 mW/cm^2 was produced at 0.6 V vs. SHE, which has only modestly higher than the 270 mW/cm^2 for a Nafion-based MEA at the same conditions, and much lower than when operated at fully humidified conditions.[66]

Charged hydrocarbon polymers have also been investigated as potential candidates for electrode binders, but none have demonstrated better performance than PFSAs in terms of fuel cell performance. Several groups have tested sulphonated polyarylene ethers as the electrode binder in PEM fuel cells.[67-69] In general, the fuel cell performance of this class of ionomers was found to be inferior to Nafion when used as an electrode binder. For example, Eastan *et al.*[69] reported that an MEA with sulfonated poly(ether ether ketone) (SPEEK) as the cathode binder and membrane only produced about 30% of the power of a Nafion MEA (Nafion membrane and binder). The authors wrote that that fuel cell performance of SPEEK was quite poor because it has lower oxygen permeability (~7 mol-cm^{-2}s^{-1} for SPEEK compared to ~53 mol-cm^{-2}s^{-1} for Nafion), lower proton conductivity (~0.04 S/cm for SPEEK and ~0.09 S/cm for Nafion), and lacks the hydrophobic PTFE backbone of PFSAs that aid in pore formation and water management in the cathode layer. A non-fluorinated polymer that has shown better performance than SPEEK as an electrode binder is sulphonated polyphosphazene (SPOP). Muldoon *et al.*[70] reported that SPOP has comparable proton conductivity and higher oxygen permeability than Nafion. At 0.65 V, an MEA with a SPOP cathode binder produced about 80% of the performance of a conventional Nafion cathode binder MEA. The authors associated the low power to poisoning of the Pt catalyst by the dimethylacetamide (DMAc) solvent that was used in the SPOP-based electrode ink (Nafion is typically dispersed in alcohol/water) and a non-optimized MEA fabrication procedure (i.e., hot pressing electrodes onto a Nafion membrane).

Polyvinylidene fluoride (PVDF) has been used as the electrode binder for high temperature (160^{o}C) hydrogen/air PEM fuel cells which employ a phosphorous acid

soaked polybenzimidazole (PBI) membrane. The electrodes for these high temperature fuel cells are a fundamentally different system as phosphorous acid is used for proton conduction so the binder does not require any ionic conductivity. PVDF has not been tested as the binder in low temperature hydrogen/air fuel cells with a Nafion membrane. Su *et al.*[71] reported that PVDF worked better than Nafion, PBI, and PBI/PVDF blends as an electrode catalyst binder. For example, a PVDF electrode binder MEA produced 230 mW/cm^2 at 0.65 V and 600 mW/cm^2 at maximum power, as compared to 100 mW/cm^2 at 0.65 V and 210 mW/cm^2 at maximum power for a Nafion cathode binder MEA. The authors claimed that catalyst layers prepared with PVDF had larger pores than with Nafion or PBI, and thus PVDF catalyst layers had less catalyst encapsulated with polymer (better catalyst activity) and less mass transfer limitations to phosphoric acid due to higher hydrophobicity of PVDF. All cathode layers were impregnated with phosphorous acid, which provided proton conduction. The PVDF electrode MEA showed stable current densities when operated at 0.6 V for 125 hours. Another group did not test neat PVDF as the electrode binder, but showed that increasing the PVDF binder content in PVDF/PBI blends increased fuel cell performance. Ergun *et al.*[72] reported a 26% increase in maximum power by increasing the PVDF:PBI ratio from 1:3 to 3:1 in the PBI/PVDF electrode binder of a PBI membrane MEA when operated at 150°C. The authors did not provide an explanation for this increase in power with higher PVDF content.

1.5.3. Alternative Cathode Morphologies

In addition to using better electrode materials (the catalyst power and/or the electrode binder), another strategy is to improve the power densities and durability of fuel cell electrodes at very low Pt loadings is to alter the electrode morphology itself (i.e., alternative structures to the standard thin film CCM and GDE electrodes described in Section 1.2.2).

Many groups have fabricated Pt catalyst structures for fuel cell cathodes that have no binder. Such layers must be very thin and situated near the proton conducting membrane in an MEA or ohmic losses in the cathode will render such electrodes useless. O'Hayre *et al.*[73] made an ultra low Pt loaded cathode (0.04 mg_{Pt}/cm^2) by a sputter deposition process in which a 10 nm platinum cathode layer of Pt black particles was directly sputtered onto a Nafion membrane. This MEA produced a maximum power output of 22 mW/cm^2 in dry (non-humidified) O_2/H_2 at room temperature, which was three-fifths of the power of a commercial MEA with ten times the Pt loading (0.4 mg/cm^2). However, these absolute power densities are very low and no results were shown at more practical fuel cell conditions of humidified hydrogen/air.

Another binder-free electrode structure developed by Debe *et al.*[74] worked much better than O'Hayre *et al*'s[73] sputtered electrodes. Debe *et al.*[74] fabricated oriented Pt-coated whisker electrodes on 3M®'s nanostructure thin film (NSTF) support. The resulting fuel cell electrodes produced higher power and exhibited better durability than standard Pt/C catalysts. In an accelerated Pt dissolution test, the NSTF cathode retained ~70% of its initial ECA after 4000 voltage cycles from 0.6 to 1.2 V, while Pt/C only

retained ~30% ECA after 1500 cycles. After the durability test, the 0.15 mg_{Pt}/cm^2 NSTF MEA produced ~460 mW/cm^2 at 0.65 V (~85% of original power), compared to ~230 mW/cm^2 at 0.65 V (~55% of original power) for the 0.40 mg_{Pt}/cm^2 GDE MEA. The NSTF electrodes produced high power at steady-state hot-wet conditions, for example 600 mW/cm^2 at 0.6 V were produced at 80°C, 100% RH, with ambient pressure H_2/air, and a cathode Pt loading of 0.15 mg/cm^2. However, many follow-up studies on the NSTF electrodes showed several operational difficulties. During fast current ramp-up, the ultra-thin NSTF cathode (shown in Figure 1.6) floods easily, which causes severe voltage losses and a delay in power output.[75] This phenomena is especially problematic at cooler temperatures (<60°C) which are present at fuel cell start-up, thus increasing the "key to pedal" time for automotive applications.[76] The thin electrodes have also been shown to be sensitive to contamination, and initially require a 40 hour preconditioning procedure to remove impurities such as chloride and sulfate ions (an unnecessary procedure for conventional electrodes).[77] Additionally, the NSTF electrodes perform poorly in hot-dry conditions. For example, the NSTF electrodes showed a drastic loss of power when operated at 30% RH (a power loss of 70% at 0.65 V as compared to 100% RH operation) due to a decrease in proton conductivity than negatively impacted both the activation and ohmic regions of the polarization curve.[78] Finally, while the NSTF cathodes have shown better resistance to Pt dissolution than Pt/C (and have no corrodible carbon support), they have still shown significant power loss during prolonged testing that has not been fully explained. For example, an MEA with a Pt cathode loading of 0.2 mg/cm^2 lost about 50% of its power at 0.65 V after 1400 hours of testing, which including potential cycling and voltage holds. One hypothesis is that the power loss is

partially due to hydrogen peroxide formation that damages the Pt as well as the membrane close to the cathode.[79]

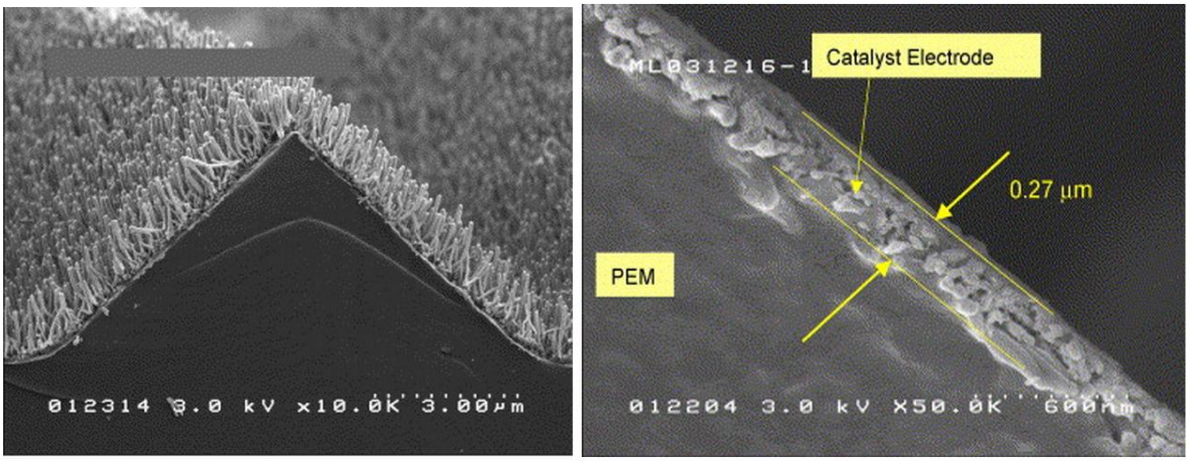

(a) (b)

Figure 1.6. Scanning electron micrographs of typical NSTF catalysts as (a) fabricated on a microstructured catalyst transfer substrate and (b) after transfer to the surface of PEM. Adapted from Debe, M. K., A. K. Schmoeckel, G. D. Vernstrorn, and R. Atanasoski (**2006**) *Journal of Power Sources*, 161, 1002-1011.

Electrode configurations based on carbon nanotubes (CNTs) have also shown some advantages in power output and durability as compared to conventional electrodes, although the production costs of CNTs are much more expensive than Pt/C.[80] Various methods to deposit catalyst particles onto CNTs have been explored, such as impregnation,[81] sputter deposition,[82] precipitation,[83] colloidal,[84] and ion-exchange methods.[85] As an example of the enhanced durability of a Pt/CNT fuel cell catalyst, He *et al.*[86] reported that the electrochemically active surface area was reduced by only 40% of its initial value after 3100 voltages cycles from 0–1.2 V vs. SHE, whereas a similar loss in active area of a conventional Pt/C occurred after only 1400 cycles. High power densities have also been reported with MEAs containing CNT. Tang *et al.*[87]

reported a maximum power density of 595 mW/cm^2 with a cathode Pt loading of 0.4 mg$_{Pt}$/cm^2 for an MEA with CNT with sputter deposited Pt, which was higher than the 435 mW/cm^2 of traditional Pt/C with the same Pt loading and fuel cell operating conditions. The performance and durability of CNTs is very promising, but current synthesis techniques are not suitable for large scale production due to cost limitations.

Other groups grew Pt nanowires, which were mixed or coated with Nafion ionomer. Sun *et al*. grew platinum nanowires on carbon nanospheres by reducing hexachloroplatinic acid (H_2PtCl_6) with formic acid (HCOOH) in an aqueous solution at room temperature (see Figure 1.6 for SEMs of the synthesized nanostructures).[88, 89] When mixed with Nafion ionomer, and evaluated in an RDE experiment, the nanowires produced very high mass activities (0.13 mA/μg, which is ~50% higher than state-of-the-art commercial Pt/C powders) . No MEA H_2/air fuel cell power densities were reported.

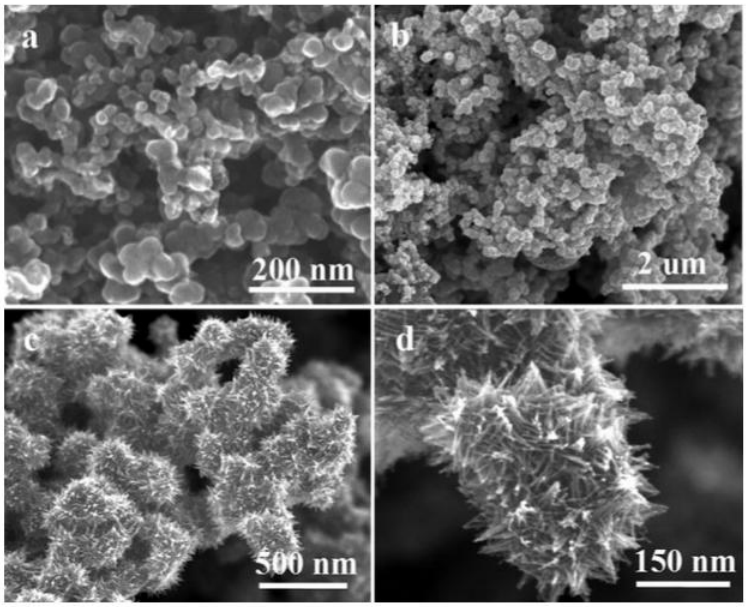

Figure 1.6. a) SEM micrograph of bare carbon nanospheres. b)-d) SEM micrographs of the as-synthesized Pt NW/C (Pt nanowire/carbon) nanostructures, with 60% Pt on carbon, at three different magnifications. Adapted from Sun, S., F. Jaouen, and J.-P. Dodelet (2008) Advanced Materials, 20, 3900-3904.

Lu *et al*.[90] grew, by reduction of $H_2PtCl_6 \cdot 6H_2O$ with formic acid, single crystal Pt nanowires, with a length of 10-20 nm, directly on a carbon gas diffusion layer. These GDEs were then painted with a thin Nafion coating prior to their incorporation into an MEA. With a platinum loading of 0.4 mg/cm^2, the best nanowire electrodes tested produced 10% more power at 0.6 V than an MEA with commercial Pt/C catalyst at the same platinum loading in a PEMFC operated at 75°C with humidified hydrogen/air gas feeds at 2 bar backpressure. The nanowire cathodes lost less electrochemical surface area during an accelerated Pt dissolution voltage cycling test (the nanowires lost 48% of their ECA vs. a 67% loss for a commercial Pt/C catalyst), although fuel cell performance (power densities) after the durability test were not reported. The enhanced durability was attributed to the inherent stability of a platinum structure (wire) over a platinum nanoparticle.

As an alternative to fabricating platinum structures, other research groups have attempted to change the morphology of electrodes created with commercial Pt/C catalysts and ionomer. Several groups, including Baturina *et al*.,[91] Martin *et al*.,[92] Benitez *et al*.[93], and Wang *et al.*[94] have electrosprayed Nafion/catalyst dispersions onto gas diffusion layers in order to decrease the size of catalyst clusters, which were as small as a few hundred nanometers. MEAs were prepared from these cathodes and anodes, where the Nafion content of the electrodes varied from 20-60 wt%. The best power densities from MEAs with electrosprayed electrodes were produced by Baturina *et al*.[91] At cathode Pt loadings of 0.09 mg/cm^2 and 0.36 mg/cm^2, Baturina's MEAs produced a maximum power of 480 and 600 mW/cm^2, respectively, at 80°C with H_2/air at 300 kPa backpressure. The lowest cathode loading (0.0125 mgPt/cm^2) was reported by Martin *et*

al.,[92] but this MEA only produced 40 mW/cm^2 at maximum power when operated at 40°C with non-humidified H_2/O_2 feed gases. No carbon corrosion or Pt dissolution durability data has been reported in the open literature on electrosprayed electrodes.

1.6 Electrospinning Background and PEMFC Applications

Besides spraying small particle clusters ("electrospraying"), a voltage field can also be used to create nanofiber structures from polymer and polymer/particle solutions and melts when appropriate requirements are met. Over the past 20 years, a variety of polymers have been electrospun into nanofibrous materials. Electrospinning (derived from "electrostatic spinning") is a versatile and low-cost method of creating continuous fiber materials with a diameter ranging from several microns to several nanometers.[95] The technique is well-documented for creating various polymeric fibrous structures for lithium battery separators,[96] filtration media,[97-99] medical and pharmacological products,[100, 101] textiles,[102] and sensors[103, 104] both in the laboratory and at the commercial scale by companies such as Freudenberg, Donaldson, Hollingsworth & Vose, KX Industries, Sandler Helsa, Ahlstrom, and Toray.[105]

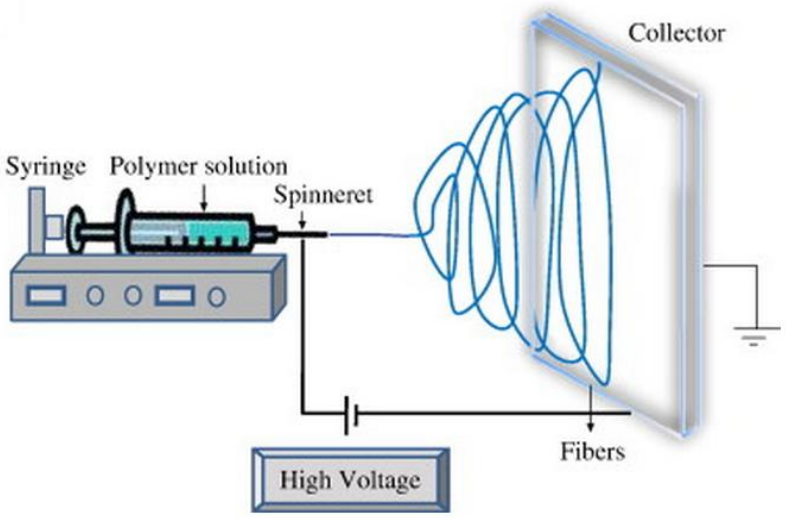

Figure 1.7. Schematic diagram of a typical laboratory electrospinning set-up. Adapted from Bhardwaj, N. and S. C. Kundu (**2010**) *Biotechnology Advances*, 28, 325-347.

A typical laboratory electrospinning setup is shown in Figure 1.7. A high electric field, typically 0.5-5 kV/cm, is applied between the spinneret tip and an electrically grounded collector. The applied voltage induces surface charges on the emerging electrospinning solution/melt. When the applied electric field reaches a critical value, the repulsive electrical forces overcome the surface tension forces and deform the emerging polymer filament into what is known as a Taylor cone.[95, 106] On the way to the grounded counter electrode, the solvent evaporates and solid fibers are precipitated. The fiber jet is thought to accelerate in a whipping motion that coils and elongates the fibers.[107] In order to be electrospun, a polymer solution/melt needs to have proper chain entanglements and viscosity, and appropriate electrospinning conditions must be found (voltage, spinneret to collector distance, relative humidity, and solution flow rate). Nafion forms a micellar dispersion in alcohol/water and organic solvents and it cannot be electrospun into fibers

without the use of a carrier polymer.[108] Nafion has been successfully electrospin with poly(acrylic acid), poly(ethylene oxide), and poly(vinyl alcohol).[109, 110]

Electrospinning has been used to prepare carbon fiber mats that function as a support for catalyst particles. Park *et al.*[111] fabricated 250 nm diameter carbon nanofibers (CNF) by electrospinning a polyacrylonitrile (PAN) solution and carbonizing the resulting nanofiber mat. The carbonized mat was mechanically ground into a powder and was then used as a Pt support. Pt was deposited on the carbon with an H_2PtCl_6 solution in ethylene glycol to form ground Pt-CNF. Electrodes were formed by mixing ground Pt-CNF with a Nafion solution and isopropyl alcohol, and finally spraying this dispersion onto carbon paper to form a GDE. The CNFs provided better electrical conductivity (9.9 S/cm) when compared to commercially available Vulcan carbon (4.5 S/cm) due to the aligned and anisotropic nature of the fibers. When incorporated into an MEA with a cathode Pt loading of 0.5 mg/cm^2, the CNF supported Pt electrodes produced more power than a commercial E-TEK® Pt/C MEA with an H_2/O_2 feed; for example, 775 mW/cm^2 was produced at max power, vs. 425 mW/cm^2 for the Vulcan carbon. No durability results were reported.

Fiberous cathode structures have also been produced by electrospinning in which the polymer is not removed in a post-electrospinning step, but rather the polymer is ionomer and remains in the final electrodes. The first attempt at electrospinning ionomer bound catalyst was published in 2009 by Kotera *et al.*[112], who electrospun a 2-10 micron diameter core-sheath fibers, consisting of an inner core containing Pt-alloy/C catalyst and Flemion™ PFSA ionomer binder and an outer sheath of polyethylene oxide (PEO). In this study, the authors were unable to electrospin fibers composed of just ionomer and

catalyst. Thus, the use of an outer PEO shell was the only way the authors could produce a fiber. The resulting fiber mat was evaluated in a MEA with a conventional Pt/C GDE as the anode, and a 15 μm Flemion membrane at 95°C with H_2/air feed gases and a backpressure of 150 kPa_{abs}. For an MEA with a cathode Pt loading of 0.20 mg/cm^2, about 500 mW/cm^2 of power was produced at 0.65 V.

In 2011, Zhang and Pintauro[17] successfully electrospun a nanofiberous electrode structure by electrospinning Pt/C with a binder of Nafion and poly(acyclic acid) (PAA).

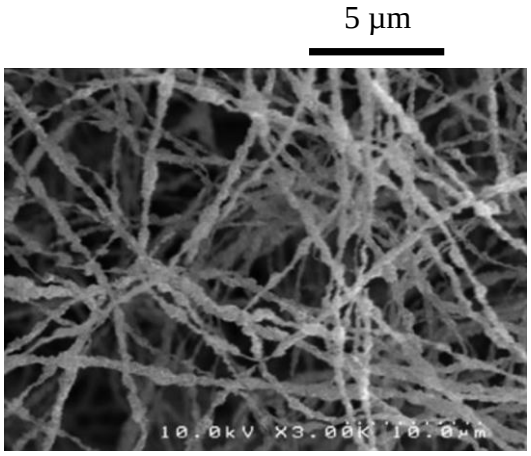

Figure 1.8. Top-down 3,000x SEM image of an electrospun catalyst nanofiber mat. Adapted from Zhang, W. and P. N. Pintauro (**2011**) *ChemSusChem*, 4, 1753-1757.

The electrospun fiber mat was composed of 75 wt% Pt/C (Johnson Matthey HiSpec 4000 40% Pt on Vulcan carbon commercial catalyst), 15 wt% Nafion, and 10 wt% poly(acrylic acid) and had an average fiber diameter of 470 nm (much smaller than the Kotera's 2-10 micron core/sheath fiber structure). A top-down SEM of the nanofiber mat is shown in Figure 1.8. As shown in Figure 1.9, an MEA with 0.4 mg_{Pt}/cm^2 electrospun cathode produced more power than an MEA with a decal cathode of the same Pt loading. Also, an

electrospun cathode at 0.10 mg_{Pt}/cm^2 generated the same power as a decal cathode of 0.4 mg/cm^2. For example, at 0.6 V, the 0.10 mg/cm^2 nanofiber cathode MEA produced 524 mW/cm^2 at 80°C with fully humidified H_2/air feed gases at ambient pressure. Additionally, the nanofiber cathode showed improved durability after an accelerated durability test (1,200 voltage cycles between 0.6 and 1.2 V vs. SHE at 20 mV/s). A nanofiber cathode with a Pt loading of 0.40 mg/cm^2 retained 79% power at 0.6 V compared to only 38% power for the 0.40 mg_{Pt}/cm^2 decal cathode MEA.

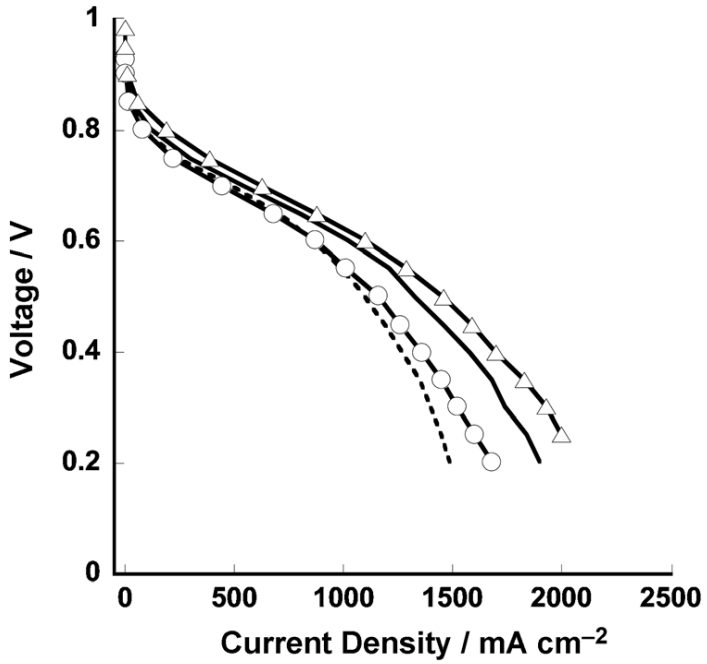

Figure 1.8. Polarization curves for a hydrogen/air fuel cell employing MEAs with an electrospun cathode with the following cathode Pt loadings: (○) 0.1 mg/cm^2 ,(solid line) 0.2 mg/cm^2, and (Δ) 0.4 mg/cm^2 and with a decal cathode (dashed line) of 0.4 mg/cm^2. Adapted from Zhang, W. and P. N. Pintauro (**2011**) *ChemSusChem*, 4, 1753-1757.

This dissertation builds on the preliminary nanofiber electrode work of Zhang and Pintauro[17]. Here, their work is extended by:

- Investigating lower cathode Pt loadings than 0.10 mg/cm^2
- Investigating effects of fuel cell operating conditions on power output
- Optimizing and streamlining MEA fabrication procedures
- Investigating the effect of fiber diameter on power output
- Investigating effects of different cathode binders and catalyst:binder ratios
- Testing cathode durability with accelerated stress tests that simulate automotive-specific load cycling and start/stop cycling behavior

1.7 Remaining Format of Dissertation Chapters

In Chapter II of this dissertation, experimental methods for nanofiber electrode mat electrospinning and for membrane-electrode-assembly (MEA) fabrication are presented. The nanofiber mats contain a commercially available platinum on carbon catalyst with a polymer binder that is a mixture of Nafion and poly(acrylic acid) (henceforth abbreviated as PAA) polymer. The effect of cathode Pt loading on electrochemical performance and fuel cell power densities are discussed, including ultra-low Pt-loaded cathodes with 0.029 mg_{Pt}/cm^2. The performance of MEAs with nanofiber electrodes is compared to a standard MEA in terms of electrochemical surface area, catalyst mass activities, Tafel slopes, and fuel cell power densities. Furthermore, the effects of fuel cell operating conditions on fuel cell power densities, including temperature, back pressure, and feed gas flow rate are shown.

Efforts to optimize and streamline nanofiber electrode MEA fabrication are presented and discussed in Chpater III. Experimental data is presented which shows that thermal annealing of electrospun electrode mats with a Nafion/PAA binder is not

necessary for good electrode performance in a fuel cell. Data is also presented for electrode hot-pressing experiments (hot pressing a nanofiber cathode mat onto a Nafion membrane), where the effects of hot-pressing temperature, time, and pressure on the power output of an MEA are evaluated.

In Chapter IV, the nanofiber electrodes are shown to be robust and produce high power for a wide range of Nafion to catalyst ratios as well as with different fiber diameters. Nanofiber electrode durability is investigated in the second half of the chapter with an emphasis on carbon corrosion of the catalyst support. Here, beginning-of-life and end-of-life performances of nanofiber electrode MEAs are compared with conventional sprayed-coated electrodes.

The performance of polyvinylidene fluoride (PVDF) and blends of Nafion + PVDF as alternative polymeric binders to Nafion/PAA for nanofiber fuel cell cathodes are shown in Chapter V. PVDF is a hydrophobic polymer and its role in slowing carbon corrosion is presented and discussed. Fuel cell power densities are plotted as a function of Nafion/PVDF ratio and as a function of time during accelerated durability testing (carbon corrosion voltage cycling experiments) in order to identify the best cathode composition for stable power output.

1.8 References

(1) Dong, Z., S. J. Kennedy, and Y. Wu (2011) *Journal of Power Sources*, 196, 4886-4904.

(2) Aslani, A. and K. F. V. Wong (2014) *Renew. Energy*, 63, 153-161.

(3) Sims, R. E. H. (2004) *Sol. Energy*, 76, 9-17.

(4) Wagner, F. T., B. Lakshmanan, and M. F. Mathias (2010) *J. Phys. Chem. Lett.*, 1, 2204-2219.

(5) Johnston, B., M. C. Mayo, and A. Khare (2005) *Technovation*, 25, 569-585.

(6) MacLean, H. L. and L. B. Lave (2003) *Progress in Energy and Combustion Science*, 29, 1-69.

(7) Curtin, D. E., R. D. Lousenberg, T. J. Henry, P. C. Tangeman, and M. E. Tisack (2004) *Journal of Power Sources*, 131, 41-48.

(8) Joo, J. B., P. Kim, W. Kim, and J. Yi (2006) *Journal of Electroceramics*, 17, 713-718.

(9) Litster, S. and G. McLean (2004) *Journal of Power Sources*, 130, 61-76.

(10) Neyerlin, K. C., W. B. Gu, J. Jorne, and H. A. Gasteiger (2007) *Journal of the Electrochemical Society*, 154, B631-B635.

(11) Mench, M. M., E. C. Kumbur, and T. N. Veziroglu, *Polymer Electrolyte Fuel Cell Degradation*. 2011: Elsevier Science.

(12) Ralph, T. R. and M. P. Hogarth (2002) *Platinum Metals Review*, 46, 3-14.

(13) Sasikumar, G., J. W. Ihm, and H. Ryu (2004) *Journal of Power Sources*, 132, 11-17.

(14) Gasteiger, H. A., S. S. Kocha, B. Sompalli, and F. T. Wagner (2005) *Applied Catalysis B: Environmental*, 56, 9-35.

(15) Lee, S. J., S. Mukerjee, J. McBreen, Y. W. Rho, Y. T. Kho, and T. H. Lee (1998) *Electrochim. Acta*, 43, 3693-3701.

(16) Antoine, O., Y. Bultel, and R. Durand (2001) *Journal of Electroanalytical Chemistry*, 499, 85-94.

(17) Zhang, W. and P. N. Pintauro (2011) *ChemSusChem*, 4, 1753-1757.

(18) Wilson, M. S., J. A. Valerio, and S. Gottesfeld (1995) *Electrochimica Acta*, 40, 355-363.

(19) Srinivasan, S., M. A. Enayetullah, S. Somasundaram, D. H. Swan, D. Manko, H. Koch, and A. J. Appleby. *Recent advances in solid polymer electrolyte fuel cell technology with low platinum loading electrodes*. in *Energy Conversion Engineering Conference, 1989. IECEC-89., Proceedings of the 24th Intersociety*. 1989.

(20) Warshay, M. and P. R. Prokopius (1990) *Journal of Power Sources*, 29, 193-200.

(21) Hoogers, G., *Fuel Cell Technology Handbook*. 2002: Taylor & Francis.

(22) Srinivasan, S., E. A. Ticianelli, C. R. Derouin, and A. Redondo (1988) *Journal of Power Sources*, 22, 359-375.

(23) Murphy, O. J., G. D. Hitchens, and D. J. Manko (1994) *Journal of Power Sources*, 47, 353-368.

(24) Chun, Y. G., C. S. Kim, D. H. Peck, and D. R. Shin (1998) *Journal of Power Sources*, 71, 174-178.

(25) Uchida, M., Y. Aoyama, N. Eda, and A. Ohta (1995) *J Electrochem Soc*, 142, 4143-4149.

(26) Cheng, X. L., B. L. Yi, M. Han, J. X. Zhang, Y. G. Qiao, and J. R. Yu (1999) *Journal of Power Sources*, 79, 75-81.

(27) Ralph, T. R., G. A. Hards, J. E. Keating, S. A. Campbell, D. P. Wilkinson, M. Davis, J. StPierre, and M. C. Johnson (1997) *Journal of the Electrochemical Society*, 144, 3845-3857.

(28) Wilson, M. S. and S. Gottesfeld (1992) *Journal of Applied Electrochemistry*, 22, 1-7.

(29) Tintula, K. K., A. Jalajakshi, A. K. Sahu, S. Pitchumani, P. Sridhar, and A. K. Shukla (2013) *Fuel Cells*, 13, 158-166.

(30) Kim, H. J., Y. S. Kim, M. H. Seo, S. M. Choi, and W. B. Kim (2009) *Electrochemistry Communications*, 11, 446-449.

(31) Pourbaix, M., *Atlas of electrochemical equilibria in aqueous solutions*. 1966: Pergamon Press.

(32) de Bruijn, F. A., V. A. T. Dam, and G. J. M. Janssen (2008) *Fuel Cells*, 8, 3-22.

(33) Linse, N., L. Gubler, G. G. Scherer, and A. Wokaun (2011) *Electrochimica Acta*, 56, 7541-7549.

(34) Meyers, J. P. and R. M. Darling (2006) *Journal of the Electrochemical Society*, 153, A1432-A1442.

(35) Kulikovsky, A. A. (2011) *Journal of the Electrochemical Society*, 158, B957-B962.

(36) Kocha, S. S., *Chapter 3 - Electrochemical Degradation: Electrocatalyst and Support Durability*, in *Polymer Electrolyte Fuel Cell Degradation*, M.M. Mench, E.C. Kumbur, and T.N. Veziroglu, Editors. 2012, Academic Press: Boston. p. 89-214.

(37) Ferreira, P. J., G. J. la O, Y. Shao-Horn, D. Morgan, R. Makharia, S. Kocha, and H. A. Gasteiger (2005) *Journal of the Electrochemical Society*, 152, A2256-A2271.

(38) Schulenburg, H., B. Schwanitz, J. Krbanjevic, N. Linse, G. G. Scherer, and A. Wokaun (2011) *Electrochem. Commun.*, 13, 921-923.

(39) Matsutani, K., K. Hayakawa, and T. Tada (2010) *Platin. Met. Rev.*, 54, 223-232.

(40) Chun, Y.-G., C.-S. Kim, D.-H. Peck, and D.-R. Shin (1998) *Journal of Power Sources*, 71, 174-178.

(41) Long, N. V., Y. Yang, C. Minh Thi, N. V. Minh, Y. Cao, and M. Nogami (2013) *Nano Energy*, 2, 636-676.

(42) Ma, Y., H. Zhang, H. Zhong, T. Xu, H. Jin, and X. Geng (2010) *Catalysis Communications*, 11, 434-437.

(43) Zhang, J., *PEM Fuel Cell Electrocatalysts and Catalyst Layers: Fundamentals and Applications*. 2008: Springer London.

(44) Beard, B. C. and P. N. Ross (1990) *Journal of the Electrochemical Society*, 137, 3368-3374.

(45) Toda, T., H. Igarashi, H. Uchida, and M. Watanabe (1999) *Journal of the Electrochemical Society*, 146, 3750-3756.

(46) Mukerjee, S., S. Srinivasan, M. P. Soriaga, and J. McBreen (1995) *Journal of the Electrochemical Society*, 142, 1409-1422.

(47) Wan, L.-J., T. Moriyama, M. Ito, H. Uchida, and M. Watanabe (2002) *Chemical Communications*, 58-59.

(48) Yu, P., M. Pemberton, and P. Plasse (2005) *Journal of Power Sources*, 144, 11-20.

(49) Colon-Mercado, H. R., H. Kim, and B. N. Popov (2004) *Electrochem. Commun.*, 6, 795-799.

(50) Antolini, E., J. R. C. Salgado, and E. R. Gonzalez (2006) *Journal of Power Sources*, 160, 957-968.

(51) Colon-Mercado, H. R. and B. N. Popov (2006) *Journal of Power Sources*, 155, 253-263.

(52) Hasche, F., M. Oezaslan, and P. Strasser (2012) *Journal of the Electrochemical Society*, 159, B25-B34.

(53) Serov, A., M. H. Robson, M. Smolnik, and P. Atanassov (2013) *Electrochimica Acta*, 109, 433-439.

(54) Othman, R., A. L. Dicks, and Z. Zhu (2012) *International Journal of Hydrogen Energy*, 37, 357-372.

(55) Maldonado, S. and K. J. Stevenson (2004) *J. Phys. Chem. B*, 108, 11375-11383.

(56) Olson, T. S., K. Chapman, and P. Atanassov (2008) *Journal of Power Sources*, 183, 557-563.

(57) Zhao, D., J. L. Shui, C. Chen, X. Q. Chen, B. M. Reprogle, D. P. Wang, and D. J. Liu (2012) *Chem. Sci.*, 3, 3200-3205.

(58) Bashyam, R. and P. Zelenay (2006) *Nature*, 443, 63-66.

(59) Jaouen, F., J. Herranz, M. Lefevre, J. P. Dodelet, U. I. Kramm, I. Herrmann, P. Bogdanoff, J. Maruyama, T. Nagaoka, A. Garsuch, J. R. Dahn, T. Olson, S. Pylypenko, P. Atanassov, and E. A. Ustinov (2009) *ACS Appl. Mater. Interfaces*, 1, 1623-1639.

(60) Koslowski, U. I., I. Abs-Wurmbach, S. Fiechter, and P. Bogdanoff (2008) *The Journal of Physical Chemistry C*, 112, 15356-15366.

(61) Kramm, U. I., I. Abs-Wurmbach, I. Herrmann-Geppert, J. Radnik, S. Fiechter, and P. Bogdanoff (2011) *Journal of the Electrochemical Society*, 158, B69-B78.

(62) Bouwkamp-Wijnoltz, A. L., W. Visscher, J. A. R. van Veen, E. Boellaard, A. M. van der Kraan, and S. C. Tang (2002) *The Journal of Physical Chemistry B*, 106, 12993-13001.

(63) Faubert, G., G. Lalande, R. Côté, D. Guay, J. P. Dodelet, L. T. Weng, P. Bertrand, and G. Dénès (1996) *Electrochimica Acta*, 41, 1689-1701.

(64) Chen, Z., D. Higgins, A. Yu, L. Zhang, and J. Zhang (2011) *Energy Environ. Sci.*, 4, 3167-3192.

(65) Holdcroft, S. (2014) *Chem. Mat.*, 26, 381-393.

(66) Arico, A. S., A. Di Blasi, G. Brunaccini, F. Sergi, G. Dispenza, L. Andaloro, M. Ferraro, V. Antonucci, P. Asher, S. Buche, D. Fongalland, G. A. Hards, J. D. B. Sharman, A. Bayer, G. Heinz, N. Zandona, R. Zuber, M. Gebert, M. Corasaniti, A. Ghielmi, and D. J. Jones (2010) *Fuel Cells*, 10, 1013-1023.

(67) Park, J.-S., P. Krishnan, S.-H. Park, G.-G. Park, T.-H. Yang, W.-Y. Lee, and C.-S. Kim (2008) *Journal of Power Sources*, 178, 642-650.

(68) Ramani, V., S. Swier, M. T. Shaw, R. A. Weiss, H. R. Kunz, and J. M. Fenton (2008) *Journal of the Electrochemical Society*, 155, B532-B537.

(69) Easton, E. B., T. D. Astill, and S. Holdcroft (2005) *Journal of the Electrochemical Society*, 152, A752-A758.

(70) Muldoon, J., J. Lin, R. Wycisk, N. Takeuchi, H. Hamaguchi, T. Saito, K. Hase, F. F. Stewart, and P. N. Pintauro (2009) *Fuel Cells*, 9, 518-521.

(71) Su, H. N., S. Pasupathi, B. Bladergroen, V. Linkov, and B. G. Pollet (2013) *International Journal of Hydrogen Energy*, 38, 11370-11378.

(72) Ergun, D., Y. Devrim, N. Bac, and I. Eroglu (2012) *Journal of Applied Polymer Science*, 124, E267-E277.

(73) O'Hayre, R., S.-J. Lee, S.-W. Cha, and F. B. Prinz (2002) *Journal of Power Sources*, 109, 483-493.

(74) Debe, M. K., A. K. Schmoeckel, G. D. Vernstrorn, and R. Atanasoski (2006) *Journal of Power Sources*, 161, 1002-1011.

(75) Debe, M. K. and A. J. Steinbach (2007) *ECS Transactions*, 11, 659-673.

(76) Balliet, R. J. and J. Newman (2011) *Journal of the Electrochemical Society*, 158, B1142-B1149.

(77) Steinbach, A. J., C. V. Hamilton, and M. K. Debe (2007) *ECS Transactions*, 11, 889-902.

(78) Sinha, P. K., W. Gu, A. Kongkanand, and E. Thompson (2011) *Journal of the Electrochemical Society*, 158, B831-B840.

(79) Kongkanand, A., J. Zhang, Z. Liu, Y.-H. Lai, P. Sinha, E. L. Thompson, and R. Makharia (2014) *Journal of the Electrochemical Society*, 161, F744-F753.

(80) Sharma, S. and B. G. Pollet (2012) *Journal of Power Sources*, 208, 96-119.

(81) Matsumoto, T., T. Komatsu, K. Arai, T. Yamazaki, M. Kijima, H. Shimizu, Y. Takasawa, and J. Nakamura (2004) *Chemical Communications*, 840-841.

(82) Zacharia, R., S.-u. Rather, S. W. Hwang, and K. S. Nahm (2007) *Chemical Physics Letters*, 434, 286-291.

(83) Satishkumar, B. C., E. M. Vogl, A. Govindaraj, and C. N. R. Rao (1996) *Journal of Physics D-Applied Physics*, 29, 3173-3176.

(84) Guha, A., W. Lu, T. A. Zawodzinski Jr, and D. A. Schiraldi (2007) *Carbon*, 45, 1506-1517.

(85) Yasuda, K. and Y. Nishimura (2003) *Materials Chemistry and Physics*, 82, 921-928.

(86) He, D., C. Zeng, C. Xu, N. Cheng, H. Li, S. Mu, and M. Pan (2011) *Langmuir*, 27, 5582-5588.

(87) Tang, Z., C. K. Poh, K. K. Lee, Z. Tian, D. H. C. Chua, and J. Lin (2010) *Journal of Power Sources*, 195, 155-159.

(88) Sun, S., F. Jaouen, and J.-P. Dodelet (2008) *Advanced Materials*, 20, 3900-3904.

(89) Sun, S., G. Zhang, D. Geng, Y. Chen, R. Li, M. Cai, and X. Sun (2011) *Angewandte Chemie International Edition*, 50, 422-426.

(90) Lu, Y., S. Du, and R. Steinberger-Wilckens (2015) *Applied Catalysis B: Environmental*, 164, 389-395.

(91) Baturina, O. A. and G. E. Wnek (2005) *Electrochem Solid St*, 8, A267-A269.

(92) Martin, S., P. L. Garcia-Ybarra, and J. L. Castillo (2010) *Journal of Power Sources*, 195, 2443-2449.

(93) Benitez, R., J. Soler, and L. Daza (2005) *Journal of Power Sources*, 151, 108-113.

(94) Wang, X. H., F. W. Richey, K. H. Wujcik, and Y. A. Elabd (2014) *Journal of Power Sources*, 264, 42-48.

(95) Bhardwaj, N. and S. C. Kundu (2010) *Biotechnology Advances*, 28, 325-347.

(96) Hwang, K., B. Kwon, and H. Byun (2011) *Journal of Membrane Science*, 378, 111-116.

(97) Qin, X.-H. and S.-Y. Wang (2006) *J Appl Polym Sci*, 102, 1285-1290.

(98) Gopal, R., S. Kaur, Z. Ma, C. Chan, S. Ramakrishna, and T. Matsuura (2006) *J Membrane Sci*, 281, 581-586.

(99) Dotti, F., A. Varesano, A. Montarsolo, A. Aluigi, C. Tonin, and G. Mazzuchetti (2007) *Journal of Industrial Textiles*, 37, 151-162.

(100) Zhang, Y., C. Lim, S. Ramakrishna, and Z.-M. Huang (2005) *Journal of Materials Science: Materials in Medicine*, 16, 933-946.

(101) Lannutti, J., D. Reneker, T. Ma, D. Tomasko, and D. Farson (2007) *Materials Science and Engineering: C*, 27, 504-509.

(102) Lee, S. and S. Kay Obendorf (2006) *Journal of Applied Polymer Science*, 102, 3430-3437.

(103) Sawicka, K., P. Gouma, and S. Simon (2005) *Sensors and Actuators B: Chemical*, 108, 585-588.

(104) Luoh, R. and H. T. Hahn (2006) *Composites Science and Technology*, 66, 2436-2441.

(105) Wendorff, J. H., S. Agarwal, and A. Greiner, *Electrospinning: Materials, Processing, and Applications*. 2012: Wiley.

(106) Chen, H., J. D. Snyder, and Y. A. Elabd (2008) *Macromolecules*, 41, 128-135.

(107) Greiner, A. and J. H. Wendorff (2007) *Angewandte Chemie-International Edition*, 46, 5670-5703.

(108) Ballengee, J. B. and P. N. Pintauro (2011) *Journal of the Electrochemical Society*, 158, B568-B572.

(109) Mollá, S. and V. Compañ (2011) *Journal of Membrane Science*, 372, 191-200.

(110) Ramakrishna, S., Fujihara, K., Teo, W., Lim, T.C., Ma, Z., *An Introduction to Electrospinning and Nanofibers*. 2005, Singapore: World Scientific Publishing.

(111) Park, J.-H., Y.-W. Ju, S.-H. Park, H.-R. Jung, K.-S. Yang, and W.-J. Lee (2009) *Journal of Applied Electrochemistry*, 39, 1229-1236.

(112) Kotera, S., H. Watabe, K. Fujii, I. Terada, C. Matsubara, and H. Uyama (2009) *ECS Transactions*, 25, 821-830.

CHAPTER II

NANOFIBER ELECTRODES WITH LOW PLATINUM LOADING FOR HIGH POWER HYDROGEN/AIR PEM FUEL CELLS

Adapted from Brodt, M., Wycisk, R., and Pintauro, P. N. *Journal of the Electrochemical Society*, **160**, F744-F749 (2013).

2.1 Introduction

The hydrogen/air proton exchange membrane (PEM) fuel cell is a promising candidate for automotive power plants due to its high power output, moderate operating temperature, and quick start-up. Presently, the commercialization of such devices is hindered by the high price and inadequate durability of the platinum catalyst electrodes.[1] Electrode research has focused on reducing catalyst loading and cost by using non-platinum group metals[2], core-shell and platinum alloy catalysts[3], and new support materials such as carbon nanotubes.[4] Efforts have also been directed at more efficient incorporation of platinum into fuel cell electrodes so that high power can be generated at low platinum loadings. Thus, investigators have studied various alternatives to the standard decal (catalyst-coated membrane) and catalyst-coated gas diffusion electrode methods of preparing PEM fuel cell membrane-electrode-assemblies (MEAs)[1, 5-7]. Recently, there have been several reports in the literature where a nanostructured electrode morphology is constructed to maximize catalyst contact with reactant gases while maintaining a sufficiently high protonic and electronic conductivity. These approaches include electrosprayed layers of micron-size catalyst/binder droplets[8] and oriented Pt-coated whisker electrodes.[9]

Electrospinning is a potentially useful technique for creating nanostructured fuel cell electrodes with superior catalyst utilization and long-term durability. The method is well documented for creating various fibrous polymeric materials for lithium battery separators[10], filtration media medical and pharmacological products[11, 12], textiles[13], and sensors[14, 15]. Pintauro and co-workers have used ionomer electrospinning to fabricate a series of proton-exchange and anion-exchange membranes for fuel cell applications with excellent ionic conductivity, moderate water swelling, and good mechanical properties.[16,17]

In the present paper, new results are presented on nanofiber electrode MEAs for hydrogen/air fuel cells. The work is an extension of the very promising results published by Zhang and Pintauro[18], who showed: (1) one can electrospin cathode nanofiber mats composed of Pt/C powder with an ionomer binder, (2) electrospun nanofiber cathodes with a Pt loading of 0.1-0.4 mg/cm^2 performed very well (e.g., a power density of 524 mW/cm^2 at 0.6 V with 0.1 mg_{Pt}/cm^2), and (3) the nanofiber cathode exhibited superior long-term durability, as compared to a traditional decal cathode. In the present study, both cathodes and anodes have been fabricated by electrospinning an alcohol/water suspension of Pt/C catalyst powder with a binder composed of Nafion® polymer and poly(acrylic acid) (PAA). Fuel cell power output was correlated with: (i) the overall Pt loading of a fibrous electrospun cathode and (ii) various operating conditions including different temperatures, backpressures, and gas feed flow rates.

2.2 Experimental

Electrospinning Electrodes - Electrospinning inks were prepared by mixing Johnson Matthey Company HiSpec™ 4000 Pt/C catalyst powder (40% Pt on carbon black), Nafion® ion exchange resin (20% ionomer in alcohol/water from Aldrich), and poly(acrylic acid) (MW=450 kDa from Aldrich) in a water/isopropanol solvent. Nafion forms a micellar solution in alcohol/water mixtures and will electrospray into droplets, unless a suitable carrier polymer is added to the electrospinning solution.[16] In the present study, poly(acrylic acid) (PAA) was used as the carrier, thus providing the required chain entanglements for nanofiber electrospinning. A suspension of Nafion and catalyst was first sonicated for 90 minutes with intermittent mechanical stirring before the addition of poly(acrylic acid). The entire mixture was then stirred for approximately 48 hours. The total polymer and powder content of the spinning suspension was 15 wt%, and the Pt/C:Nafion:PAA weight ratio was 65:23:12. The ink was drawn into a 3 mL syringe and electrospun using a 22-gauge stainless steel needle spinneret, where the needle tip was polarized to a potential of 9 kV relative to a grounded stainless steel rotating drum collector. The spinneret-to-collector distance was fixed at 10 cm and the flow rate of ink was held constant for all experiments at 1.0 mL/h. The Pt loading was controlled by varying the duration of electrospinning time (thus effectively changing the mat thickness). Nanofibers were collected on aluminum foil that was attached to a cylindrical collector drum that rotated at 100 rpm. The drum also oscillated horizontally to improve the uniformity of deposited nanofibers. Electrospinning was performed at room temperature in a custom-built environmental chamber, where the relative humidity was maintained constant at 40%. The resulting fiber mats were annealed at 150^{o}C under

vacuum for 2 hours prior to their incorporation into a MEA (we have since found that this annealing step is not necessary for proper MEA fabrication and operation). It should be noted that the PAA carrier polymer could not be removed from the electrode fibers even after soaking the mats in hot acid (1.0 M H_2SO_4) and boiling them in water.

Membrane-Electrode-Assembly (MEA) Preparation - Nanofiber MEAs were created by hot pressing 5 cm^2 electrospun electrodes (anodes and cathodes) onto the opposing sides of an acid-treated Nafion 212 membrane at 140^oC and 4 MPa for 10 minutes. The Pt loading of a nanofiber mat was calculated from its total weight and the weight-fraction of Pt/C catalyst used in the electrospinning ink. Electrospun anodes were prepared using the same electrospinning procedure, catalyst, and ink composition, as those used to electrospin the cathodes.

A decal MEA was also fabricated with the same Johnson Matthey catalyst as used for electrospinning. Pt/C powder was mixed with a commercial Nafion dispersion (in the tetrabutyl ammonium counterion form) and glycerol. The ink was painted onto a Kapton® sheet followed by thermal drying overnight at 140°C. Electrodes were prepared with a Pt/C to Nafion weight ratio of 77:23 and were hot pressed at 140^oC and 4 MPa for 10 minutes (same conditions as those employed for the electrospun electrodes). A decal-coated membrane was boiled in 1.0 M H_2SO_4 for one hour and then soaked in boiling water for one hour prior to loading in a fuel cell test fixture. 5 cm^2 carbon paper gas diffusion electrodes (Sigracet GDL 25 BC from Ion Power, Inc) were physically pressed onto the MEA's anode and cathode in the test fixture.

Fuel Cell Tests - Fuel cell polarization curves were collected using a Scribner Series 850e test station with mass flow, temperature, and manual backpressure control. The fuel cell test fixture accommodated a 5 cm^2 membrane-electrode-assembly and contained single anode and cathode serpentine flow channels. Experiments in H_2/air were performed at 60°C or 80°C with fully humidified gases at a range of pressures from atmospheric (ambient) pressure to 3 atmospheres and at flow rates from 70 sccm H_2/100 sccm air to 500 sccm H_2/2000 sccm air. Prior to collecting polarization data, the MEAs were pre-conditioned by alternating between two minutes of low current (150 mA/cm^2) and two minutes of low voltage (0.2 V) operation at 80°C. The break-in period lasted for at least four hours, until steady power output from the MEA was achieved. Polarization curves were generated by collecting the current at a given voltage after waiting 60 seconds for system stabilization. Cathode catalyst mass activity measurement data was collected with a current-controlled anodic scan (high current to low current) at 80°C with fully humidified O_2 and H_2 gas feeds at 100 sccm and 1.5 atm (150 kPa_{abs}). For these measurements, the system was given 3 minutes to stabilize at each current density before a voltage reading was taken. Mass activities were determined from a plot of IR-free voltage verse the H_2-crossover corrected current density.

Electrochemical Surface Area (ECA) - In-situ cyclic voltammetry (CV) measurements were performed on 5 cm^2 MEAs at 20 mV/s, where a N_2-purged anode served as both the counter and reference electrodes and the H_2-fed cathode was the working electrode. The fuel cell fixture was operated at 30°C with gas feed streams at dew points of 30°C (fully humidified). The CV was carried out between +0.04 V and

+0.9 V vs. SHE and the electrochemically active surface area was determined from the integrated area above the hydrogen adsorption portion of a voltammogram (corresponding to the voltage range ca. +0.1 to +0.4 V), assuming a charge of 210 $\mu C/cm^2$ to reduce one monolayer of protons on Pt.

2.3 Results and Discussion

A top-down scanning electron micrograph of a cathode nanofiber mat with a Pt loading of 0.065 mg/cm^2 is shown in Figure 2.1a. Prior to imaging, the mat was lightly pressed at room temperature onto conductive SEM tape and then sputter coated with a thin layer of gold to improve contrast. A histogram of the fiber diameter distribution is shown in Figure 2.1b. Using ImageJ software and a sampling of 100 fibers, the average fiber diameter (for a 95% confidence interval) was found to be 589±48 nm. High magnification SEM images of electrospun nanofibers (Figure 2.1c and 2.1d) show porous fibers with a highly roughened surface, offering high Pt surface area exposure to the feed gas, with a uniform distribution of catalyst and ionomer over the fiber length.

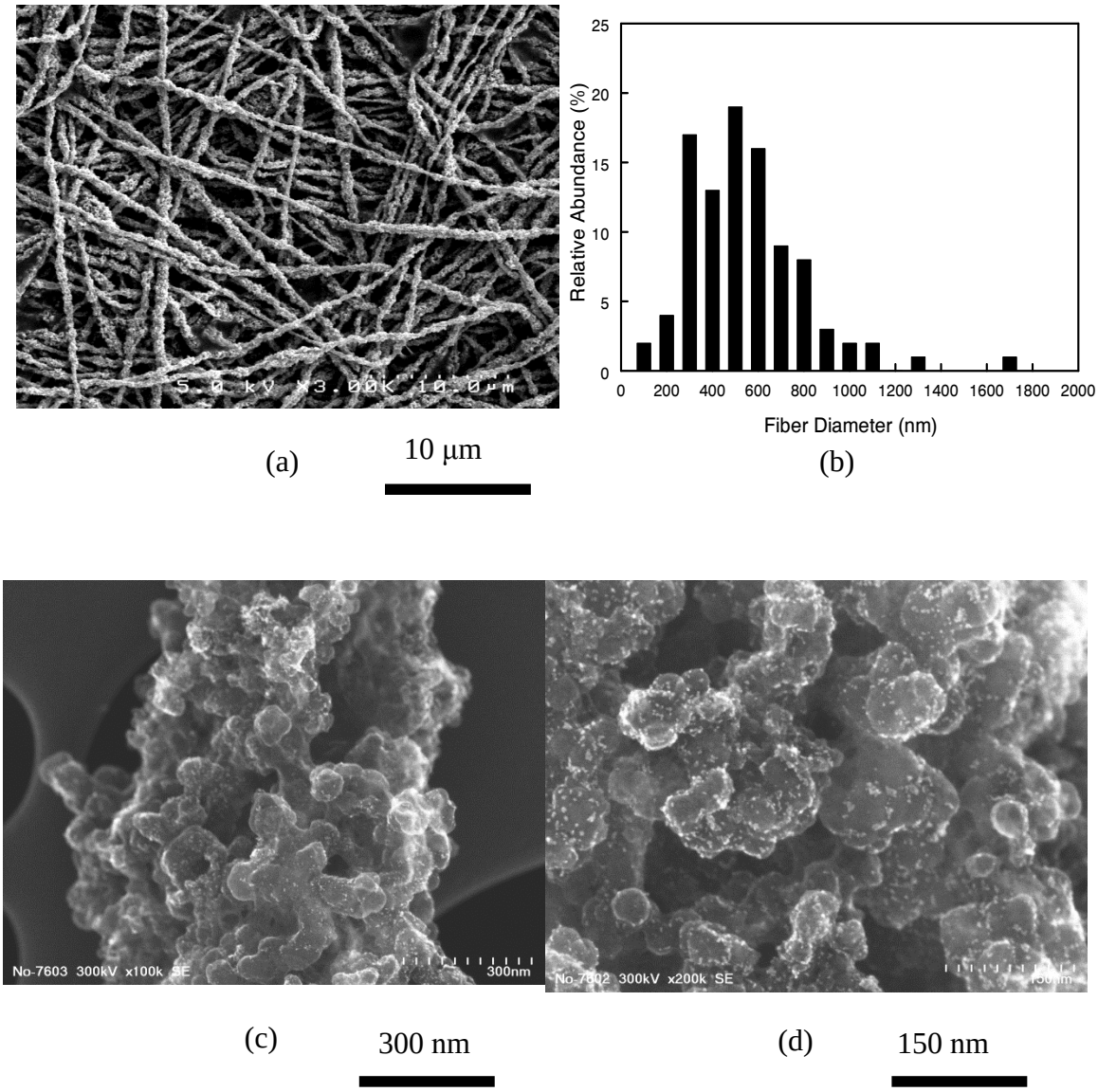

Figure 2.1. (a) Top-down 3,000x SEM image of an electrospun catalyst nanofiber mat; (b) Histogram of the nanofiber diameter distribution for the electrospun mat shown in (a); (c) 100,000x SEM image of a single Pt/C/Nafion/PAA nanofiber; (d) 200,000x SEM image of a Pt/C/Nafion/PAA nanofiber (images (c) and (d) are courtesy of Karren More at Oak Ridge National Laboratory).

Variations in Cathode Nanofiber Pt Loading - The effect of nanofiber cathode platinum loading on fuel cell performance was investigated for Pt loadings of 0.107, 0.065, and 0.029 mg/cm^2. Hydrogen/air fuel cell polarization data were collected at 80^{o}C, 100% RH, and ambient pressure. For the nanofiber MEAs, the anode Pt loading was fixed at 0.1 mg/cm^2. As shown in Figures 2.2a and 2.2b, the nanofiber MEAs perform very well, with a modest drop in power output when the cathode loading was reduced from 0.107 to 0.065 mg/cm^2. Thus, there was a maximum power density loss of only 15% (437 vs. 513 mW/cm^2) when the catalyst loading was decreased by about 40%. Even at a cathode Pt loading of 0.029 mg/cm^2, the observed power densities were reasonable (e.g., 168 mW/cm^2 at 0.65 V with a maximum power density of 306 mW/cm^2). It can also be seen in Figure 2.2 that the performance of the 0.065 mg_{Pt}/cm^2 nanofiber cathode was superior to that of a decal cathode at a Pt loading of 0.104 mg/cm^2. Experimental errors in our fuel cell polarization data are estimated to be ±5-7%; the improvement in nanofiber cathode performance, as compared to the decal electrode MEA, is far greater than this error. The nanofiber cathode at 0.065 mg_{Pt}/cm^2 also out-performs conventional fuel cell MEAs as reported in the open literature. For example, the 0.065 mg_{Pt}/cm^2 nanofiber cathode generated similar power densities (e.g., ~350 mW/cm^2 at 0.65 V) as a 0.4 mg_{Pt}/cm^2 decal cathode that was tested at 2 atm pressure, as reported by Srinivasarao et al.[19]

(a)

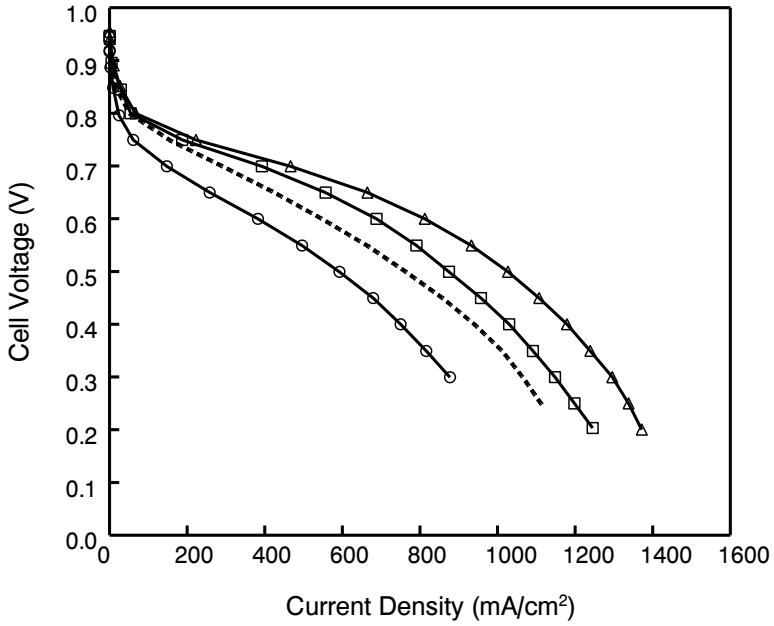

(b)

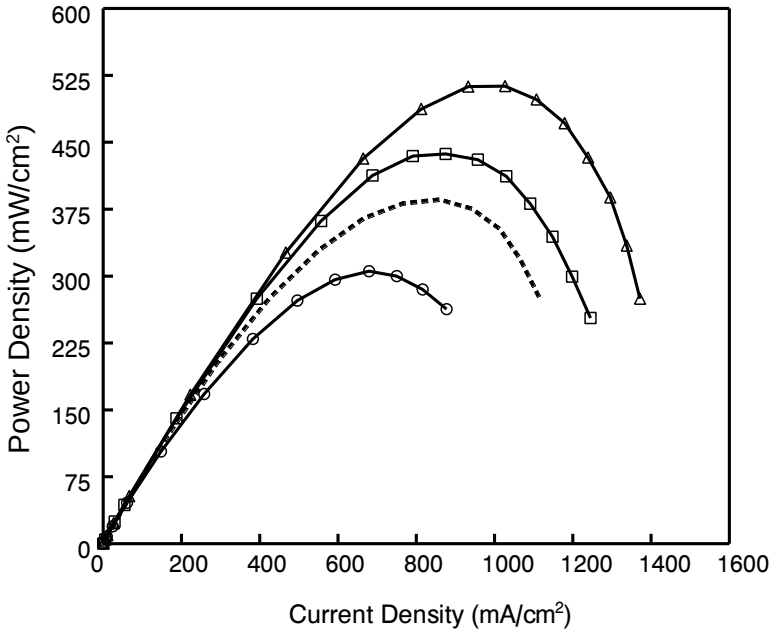

Figure 2.2. (a) Polarization curves and (b) power density vs. current density plots for 5 cm^2 MEAs with a Nafion 212 membrane and Johnson Matthey HiSpec™ 4000 catalyst electrospun cathodes and anodes. The Pt/C:Nafion:PAA weight ratio was fixed at 65:23:12. The anode Pt loading was 0.10 mg/cm^2. The cathode Pt loading was: (Δ) 0.107 mg/cm^2 (□), 0.065 mg/cm^2, and (○) 0.029 mg/cm^2. Also shown is a decal MEA with cathode and anode Pt loadings of 0.104 mg/cm^2 and 0.40 mg/cm^2, respectively (----). Fuel cell operating conditions: 80°C, 100% RH feed gases at ambient pressure, 125 sccm H_2 and 500 sccm air.

To further compare an electrospun and decal cathode and to better understand the effect of cathode loading on fuel cell performance, the electrochemical surface area and mass activity of nanofiber cathodes were determined according to published procedures.[6,9] The results of these experiments are listed in Table 2.1. From the adsorption-limited charging area in the cyclic voltammograms (Figure 2.3), the electrospun cathodes were found to have about 30% more active area than a conventional decal cathode (39-41 m^2/g for electrospun cathode vs. 30 m^2/g for a decal electrode). ECA is a measure of the quality and extent of intimate contact between active catalyst sites, reactants, and both electron and proton conducting pathways; isolated catalyst does not contribute to the electrochemical reaction and is not taken into account during a CV scan. The higher measured area for the electrospun morphology shows better utilization of catalyst, which suggests an improved distribution of carbon-supported Pt powder and binder. The ECA of nanofiber mats was found to be independent of cathode Pt loading, as is typical for conventional thin film electrodes.[6]

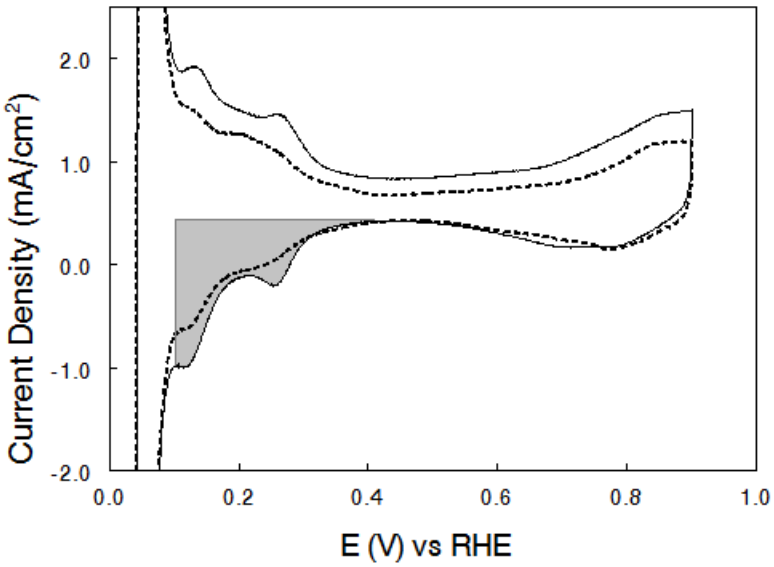

Figure 2.3. In-situ cyclic voltammograms from 0.04 V to 0.9 V taken at 20 mV/s and 30 °C of the MEA with 0.107 mg_{Pt}/cm^2 electrospun cathode (solid line) and the MEA 0.104 mg_{Pt}/cm^2 decal cathode (dashed line). The active electrochemical surface area was calculated using the charge area above the absorption peaks, corresponding to the voltage range ~0.1 to 0.4 V. The integration area for the electrospun cathode is shaded.

The Pt mass activity (listed in Table 2.1) for nanofiber cathodes was also found to be greater than that of an MEA with a decal cathode (0.16-0.17 A/mg_{Pt} vs. 0.11 A/mg_{Pt}) and the activity was independent of cathode fiber Pt loading. The values for ECA and mass activity reported here for our decal cathode are similar to literature values with 40% Pt on Vulcan Carbon catalysts, e.g., Janssen and co-workers[20] reported an ECA of 33 m^2/g and Gasteiger et al.[21] reported an area of 32 m^2/g and compiled a list of literature values for mass activities, ranging from 0.033 to 0.10 A/mg_{Pt}. Zhang and Pintauro

reported higher values of ECA and mass activity for their electrospun fiber cathodes because they used a different voltage range for analyzing CV charging currents and high oxygen pressure for mass activity measurements (150 kPa_g rather than the 150 kPa_{abs} pressure used in the present study).

Table 2.1. Electrochemical Surface Areas (ECA) and Mass Activities at 0.9 V, 150 kPa_{abs}

Electrode Type	Cathode Pt Loading (mg/cm^2)	ECA (m^2/g)	Mass Activity at 0.9 V (A/mg_{Pt})	Tafel slope (mV/dec)
Decal	0.104	30	0.11	64
Electrospun	0.107	41	0.16	66
Electrospun	0.065	41	0.16	69
Electrospun	0.029	39	0.17	66

Values for Pt utilization, with units of $g_{Pt,cathode}/kW$, are listed in Table 2.2 for decal and electrospun cathodes at 0.65 V (fuel cell MEA operating voltages near 0.65 V are often preferred due to high energy conversion efficiency[21]) and at maximum power (which corresponds to maximum catalyst utilization). As expected, Pt is utilized more efficiently in nanofiber cathodes with lower Pt loading, because the low Pt content electrodes are thinner. Thin electrodes reduce overpotential losses, particularly in the high-current region, by providing a shorter oxygen diffusion path, less ohmic resistance, and easier water removal[9, 21, 22]. At 0.65 V, the ultra low 0.029 mg_{Pt}/cm^2 cathode showed the best utilization with 0.17 g_{Pt}/kW; this value was slightly better than the 0.065 electrospun cathode (0.18 g_{Pt}/kW), 32% better than the 0.107 electrospun cathode (0.25 g_{Pt}/kW) and 54% better than the 0.104 decal cathode (0.37 g_{Pt}/kW). These Pt utilizations

are much better than values typically reported with standard/decal cathodes[20] (~0.5 $g_{Pt,cathode}$/kW at 0.65 V for a Pt loading of 0.4 mg_{Pt}/cm^2). The superior performance of the ultra thin 0.029 mg_{Pt}/cm^2 electrospun fiber cathode was further differentiated from a conventional electrode when the MEA was operated at max power, where mass transfer becomes more important. It is noted, however, that the maximum power with the 0.029 mg_{Pt}/cm^2 cathode occurs near 0.4 V, which is not ideal in terms of conversion efficiencies. The thickness of the electrospun cathode layers was measured (from SEMs of freeze-fractured MEAs after a fuel cell test and from a torque-limited micrometer measurement after MEA testing, removal of the carbon paper GDL, and subtracting the measured thickness of the membrane and the estimated thickness of the anode) and found to be 6.2 μm, 3.8 μm, and 1.9 μm for the 0.107, 0.065, and 0.029 mg_{Pt}/cm^2 (as compared to 5.1 μm for a 0.104 mg/cm^2 decal cathode case).

Table 2.2. Pt Utilization at Maximum Power and at 0.65 V

Electrode Type	Cathode Pt Loading (mg/cm^2)	Pt Util. at Max Power ($g_{Pt,cathode}$/kW)	Pt Util. at 0.65 V ($g_{Pt,cathode}$/kW)
Decal	0.104	0.27	0.37
Electrospun	0.107	0.21	0.25
Electrospun	0.065	0.15	0.18
Electrospun	0.029	0.095	0.17

The outstanding performance of the nanofiber cathodes is presently attributed to the unique fiber morphology shown in Figure 2.1, where intra-fiber and inter-fiber porosity leads to a larger electrochemical surface area of accessible Pt, higher Pt mass activity, and better catalyst utilization, as compared to a conventional decal or catalyst coated GDE cathode. Additionally, the electrospun cathode has a larger mass specific double layer capacitance than a decal cathode, as shown in Figure 2.3, which is indicative of excellent ionomer and catalyst dispersion within the nanofibers.[23]

Effects of Temperature, Backpressure, and Feed Gas Flow Rate - For these experiments, the Nafion 212 MEA contained a 0.055 mg_{Pt}/cm^2 nanofiber cathode and a 0.059 mg_{Pt}/cm^2 nanofiber anode. In the first series of experiments, the 5 cm^2 MEA was tested at two temperatures (at 60°C and 80°C) for ambient pressure conditions and two gas feed pressures (1.5 atm and 3 atm, i.e., 150 kPa_{abs} and 300 kPa_{abs}). The hydrogen and air feeds were fully humidified with fixed flow rates of 125 sccm (H_2) and 500 sccm (air). As expected, at a given temperature, an increase in the partial pressure of the reactant gases, i.e., an increase in the feed gas pressure, always increased power generation (see Figure 2). At 80°C and ambient pressure, the maximum power density was 443 mW/cm^2, which increased to 546 mW/cm^2 at 1.5 atm and to 777 mW/cm^2 at 3 atm.

In general, the nanofiber electrode MEA produced higher power at 80°C than 60°C. However, a close examination of Figure 2.4a will show that at low current densities in the ambient pressure case the performance is slightly greater at 60°C than at

80°C. This decrease in performance at a higher temperature, despite faster oxygen-reduction kinetics, has been seen in prior studies and is attributed to lower oxygen and hydrogen partial pressures due to an increase in water vapor pressure with temperature[24,25]. This decrease in partial pressure suggests that a backpressure can mitigate performance losses imposed at a high temperature, and this is indeed shown to be the case in Figure 2.4. As the pressure is increased from ambient to 1.5 atm, the slight disadvantage of fuel cell operation at 80°C and low current densities is eliminated and the advantage of operating at 80°C and higher current densities (e.g. for high power applications) is more pronounced.

(a)

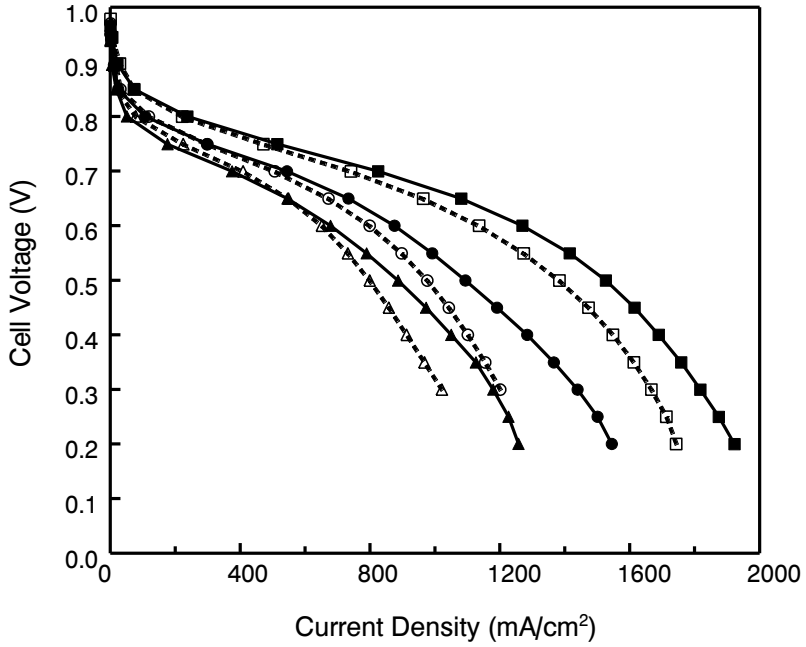

(b)

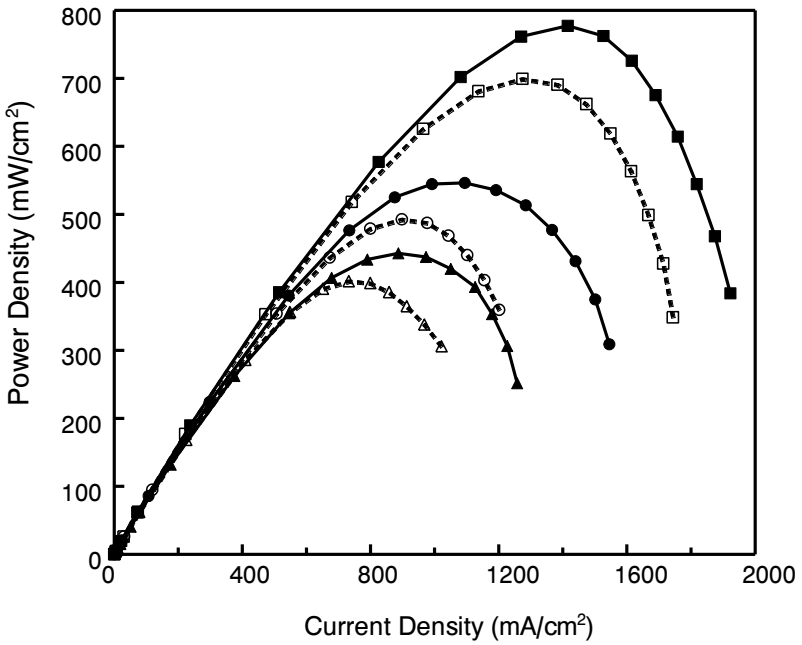

Figure 2.4. (a) Polarization curves and (b) power density vs. current density plots for a 5 cm^2 MEA with a Nafion 212 membrane, an electrospun 0.055 mg_{Pt}/cm^2 cathode, and an electrospun 0.059 mg_{Pt}/cm^2 anode. The Pt/C:Nafion:PAA weight ratio was fixed at 65:23:12. Fuel cell operating conditions: fully humidified 125 sccm H_2 and 500 sccm air, at the following temperatures and pressures: (-▲-) 80°C/1 atm (ambient pressure conditions), (-●-) 80°C/1.5 atm, (-■-) 80°C/3 atm, (-Δ-) 60°C/1 atm, (-○-) 60°C/1.5 atm, and (-□-) 60°C/3 atm.

Using the best conditions from Figure 2.4 (i.e., a temperature of 80°C and a pressure of 3 atm, with a Pt cathode loading of 0.055 mg/cm^2), the effect of feed gas flow rates was assessed, where the gases were fully humidified and the H_2:air flow rate ratio was fixed at 1:4. The minimum H_2 flow rate was 70 sccm in order to avoid being limited by hydrogen stoichiometry. As shown in Figure 2.4, five different flow rates were examined, from a low of 70 sccm H_2/100 sccm air to a maximum of 500 sccm H_2/2000 sccm air. At 1 A/cm^2, these mass flow rates correspond to hydrogen and oxygen stoichiometries of 2 and 1.2, respectively, at the lowest flow rates and 14.3 and 24 at the highest flow rates. At the lowest air flow rate of 100 sccm, the maximum power density was high (595 mW/cm^2) and the power density increased substantially with higher air flow rates. At the two highest air flow rates (1000 and 2000 sccm), there is no indication of a limiting current due to either oxygen mass transfer limitations or water flooding and very high current densities were achieved (2.0-2.5 A/cm^2). The highest power density (906 mW/cm^2) was generated with 2000 sccm air. This power density exceeds that of many/most advanced fuel cell electrode MEAs under investigation today. For example, one can compare the results in Figure 2.5 with the nanostructured thin film (NSTF) catalyst electrodes under development at 3M Company, where a Pt-based NSTF 50 cm^2 MEA with a cathode Pt loading of 0.15 mg/cm^2 produced a maximum power of about 600 mW/cm^2 at 75°C and ambient pressure, with fully humidified feed gases at flow rates of 800 sccm for H_2 and 1800 sccm for air[9]. Based on a power density of 906 mW/cm^2 (the maximum power MEA in Figure 2.4), the total mass of Pt in an 80 KW nanofiber electrode fuel cell stack would be quite modest, only 4.8 g (cathode) + 5.2 g (anode) = 10 g. Even higher power densities are expected when the Nafion 212 membrane in our

MEAs is replaced by a thinner Nafion 211 film (such experiments are currently underway). Electrode durability was not examined in the present study, but prior work by Zhang and Pintauro[18] found that electrospun Pt/C-Nafion-PAA cathodes exhibited less degradation than a traditional decal Pt/C-Nafion cathode in an accelerated voltage cycling durability test.

(a)

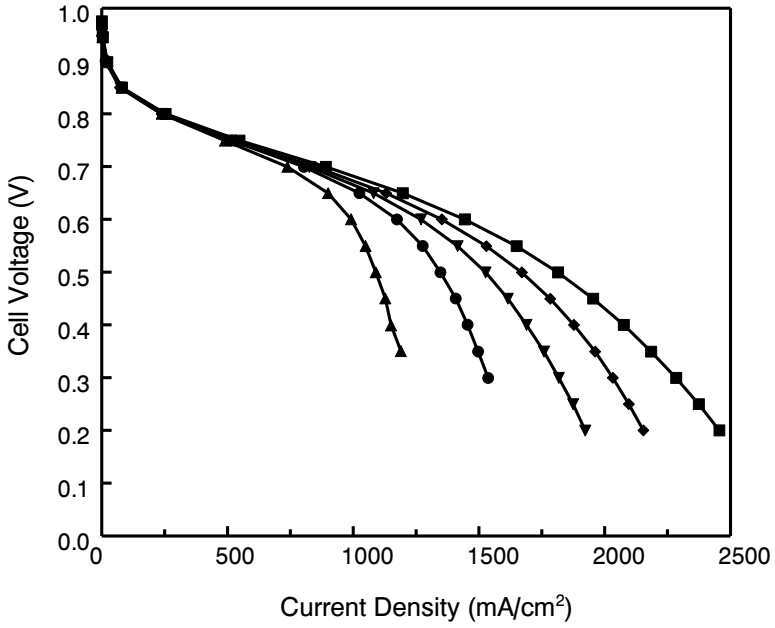

(b)

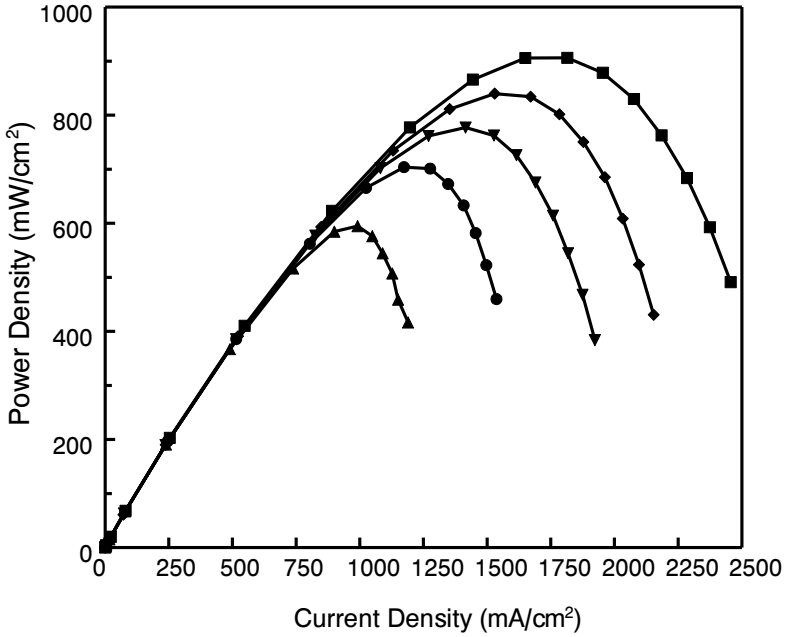

Figure 2.5. (a) Polarization curves and (b) power density vs. current density plots for a 5 cm^2 MEA with a Nafion 212 membrane, an electrospun 0.055 mg_{Pt}/cm^2 cathode, and an electrospun 0.059 mg_{Pt}/cm^2 anode. The Pt/C:Nafion:PAA weight ratio was fixed at 65:23:12. Fuel cell operating conditions: 80°C, 3 atm, and the following fully humidified gas flow rates of H_2/air (in sccm): (▲) 70/100, (●) 70/200, (▼) 125/500, (♦) 250/1000, and (■) 500/2000.

2.4 Conclusions

Electrospinning is a powerful, robust, and effective technique for fabricating high-performance hydrogen/air fuel cell electrodes at low Pt loadings. In a hydrogen/air fuel cell operating at 80^{o}C, an MEA with an electrospun cathode with Johnson Matthey Pt/C powder catalyst at a Pt loading of 0.065 mg/cm^2 and an electrospun anode at 0.10 mg_{Pt}/cm^2 produced more power than a decal MEA with a cathode Pt loadings of 0.104 mg/cm^2 and an anode loading of 0.40 mg/cm^2. At 0.65 V, the difference in MEA performance was significant; where the electrospun cathode generated 360 mW/cm^2 vs 280 mW/cm^2 with a decal cathode (29% more power with nanofibers). An electrospun MEA with a cathode loading of 0.055 mg_{Pt}/cm^2 and anode loading of 0.059 mg/cm^2 produced 906 mW/cm^2 at 80^{o}C with a fully humidified air flow rate of 2000 sccm at 3 atm.

2.5 References

(1) Litster, S. and G. McLean (**2004**) *Journal of Power Sources*, 130, 61-76.

(2) Othman, R., A. L. Dicks, and Z. Zhu (**2012**) *International Journal of Hydrogen Energy*, 37, 357-372.

(3) Ma, Y., H. Zhang, H. Zhong, T. Xu, H. Jin, and X. Geng (**2010**) *Catalysis Communications*, 11, 434-437.

(4) Lv, H., N. Cheng, S. Mu, and M. Pan (**2011**) *Electrochimica Acta*, 58, 736-742.

(5) Wilson, M. S. and S. Gottesfeld (**1992**) *Journal of Applied Electrochemistry*, 22, 1-7.

(6) Ralph, T. R., G. A. Hards, J. E. Keating, S. A. Campbell, D. P. Wilkinson, M. Davis, J. St-Pierre, and M. C. Johnson (**1997**) *J. Electrochem. Soc.*, 144, 3845-3857.

(7) Ren, X., M. S. Wilson, and S. Gottesfeld (**1996**) *J. Electrochem. Soc.*, 143, L12-L15.

(8) Martin, S., P. L. Garcia-Ybarra, and J. L. Castillo (**2010**) *Journal of Power Sources*, 195, 2443-2449.

(9) Debe, M. K., A. K. Schmoeckel, G. D. Vernstrorn, and R. Atanasoski (**2006**) *Journal of Power Sources*, 161, 1002-1011.

(10) Hwang, K., B. Kwon, and H. Byun (**2011**) *Journal of Membrane Science*, 378, 111-116.

(11) Zhang, Y., C. Lim, S. Ramakrishna, and Z.-M. Huang (**2005**) *Journal of Materials Science: Materials in Medicine*, 16, 933-946.

(12) Lannutti, J., D. Reneker, T. Ma, D. Tomasko, and D. Farson (**2007**) *Materials Science and Engineering: C*, 27, 504-509.

(13) Lee, S. and S. Kay Obendorf (**2006**) *Journal of Applied Polymer Science*, 102, 3430-3437.

(14) Sawicka, K., P. Gouma, and S. Simon (**2005**) *Sensors and Actuators B: Chemical*, 108, 585-588.

(15) Luoh, R. and H. T. Hahn (**2006**) *Composites Science and Technology*, 66, 2436-2441.

(16) Ballengee, J. B. and P. N. Pintauro (**2011**) *J. Electrochem. Soc.*, 158, B568-B572.

(17) Park, A. M. and P. N. Pintauro (**2012**) *Electrochem Solid St*, 15, B27-B30.

(18) Zhang, W. and P. N. Pintauro (**2011**) *ChemSusChem*, 4, 1753-1757.

(19) Srinivasarao, M., D. Bhattacharyya, R. Rengaswamy, and S. Narasimhan (**2010**) *International Journal of Hydrogen Energy*, 35, 6356-6365.

(20) Janssen, G. J. M. and E. F. Sitters (**2007**) *Journal of Power Sources*, 171, 8-17.

(21) Gasteiger, H. A., S. S. Kocha, B. Sompalli, and F. T. Wagner (**2005**) *Applied Catalysis B: Environmental*, 56, 9-35.

(22) Ohma, A., T. Mashio, K. Sato, H. Iden, Y. Ono, K. Sakai, K. Akizuki, S. Takaichi, and K. Shinohara (**2011**) *Electrochimica Acta*, 56, 10832-10841.

(23) Marie, J., R. Chenitz, M. Chatenet, S. Berthon-Fabry, N. Cornet, and P. Achard (**2009**) *Journal of Power Sources*, 190, 423-434.

(24) Song, J. M., S. Suzuki, H. Uchida, and M. Watanabe (**2006**) *Langmuir*, 22, 6422-6428.

(25) Adjemian, K. T., S. J. Lee, S. Srinivasan, J. Benziger, and A. B. Bocarsly (**2002**) *J. Electrochem. Soc.*, 149, A256-A261.

CHAPTER III

MEA FABRICATION OPTIMIZATION

3.1 Introduction

The fabrication processing steps for PEM hydrogen/air fuel cell membrane-electrode-assembles (MEAs), have a strong impact on fuel cell performance and require optimization.[1] The conditions for hot-pressing, the step that attaches the anode and cathode to the proton exchange membrane, in particular, has received considerable attention, including careful consideration of the hot-pressing temperature, time, and pressure.[2-5] The hot-pressing step is important as it creates physical contact between the electrodes and the membrane and the hot-pressing conditions can change the porosity of the electrodes, which will affect the transport of gases and water during fuel cell operation.[6] Hot-pressing with improper or too severe conditions can also damage the membrane and cause large parasitic hydrogen crossover currents. The hot-pressing step also serves to anneal the ionomer in the electrodes.[1] When a perfluorosulfonic acid (PFSA) ion exchange polymer, such as DuPont's Nafion®, is solution-cast into a membrane, the material must be annealed to obtain the material's true chemical and mechanical properties.[7] Annealing crystallizes a portion of the PFSA and makes it insoluble in water. Fuel cell electrodes are typically not annealed in a separate step, but are annealed during the hot-pressing step. The hot-pressing temperature is set at or above the α-relaxation glass transition temperature of the PFSA (~100^{o}C for Nafion)[8]. At this temperature, the electrodes are softened, the binder is annealed, and the anode and cathode catalyst/binder layers are adhered to the proton-exchange membrane. Zhang and

Pintauro[9] annealed their electrospun nanofiber electrode mats in a separate step as a precaution to insure the fiber structure was maintained during hot-pressing. In Chapter 2 of this dissertation, the nanofiber mats were annealed separately at well. In this chapter, the annealing process will be investigated to determine if the step is required for proper MEA fabrication with a nanofiber cathode. The hot-pressing temperature, time, and pressure will be systematically investigated and optimized in order to maximize power densities of MEAs with electrospun nanofiber electrodes.

3.2 Experimental

Electrospinning Electrodes - Electrospinning inks were prepared by mixing in an alcohol/water solvent: (a) Tanaka Kikinzoku Kogyo (TKK) TEC10E50E (46.1% Pt on Ketjen Black), a commercial Pt/C catalyst powder, (b) Nafion® ion exchange resin (20% ionomer in alcohol/water from Aldrich), and (c) and poly(acrylic acid) (MW=450 kDa from Aldrich). Nafion forms a micellar solution in alcohol/water mixtures and will electrospray into droplets, unless a suitable carrier polymer is added to the electrospinning solution.[10] In the present study, poly(acrylic acid) (PAA) was used as the carrier, thus providing the required chain entanglements for nanofiber electrospinning. Electrode inks and electrospun cathode mats were prepared in a standard way, identical to the procedure described in Chapter 2 of this dissertation. A suspension of Nafion and catalyst was first sonicated for 90 minutes with intermittent mechanical stirring before the addition of poly(acrylic acid). The entire mixture was then stirred for approximately 48 hours. The total polymer and powder content of the spinning suspension was 15 wt%, and

the Pt/C:Nafion:PAA weight ratio was 63:22:15. The ink was drawn into a 3 mL syringe and electrospun using a 22-gauge stainless steel needle spinneret, where the needle tip was polarized to a potential of 9-11 kV relative to a grounded stainless steel rotating drum collector. The spinneret-to-collector distance was fixed at 10 cm and the flow rate of ink was held constant for all experiments at 1.5 mL/h. Nanofibers were collected on aluminum foil that was attached to a cylindrical collector drum that rotated at 100 rpm. The drum also oscillated horizontally to improve the uniformity of deposited nanofibers. Electrospinning was performed at room temperature in a custom-built environmental chamber, where the relative humidity was maintained constant at 40%.

The resulting fiber mat electrodes (cathodes and anodes) were annealed at 150^{o}C under vacuum for either 15 minutes or 2 hours prior to their incorporation into a MEA. Some anodes and cathodes were not annealed, in which case they were hot-pressed directly after removal from the electrospinning collector drum.

Membrane-Electrode-Assembly (MEA) Preparation – Catalyst Coated Membranes (CCMs) were created by hot pressing 5 cm^2 electrospun electrodes (anodes and cathodes of identical composition) onto the opposing sides of a Nafion 211 membrane at a specified temperature, time, and pressure. Here CCM will refer to an anode-membrane-cathode assembly, whereas an MEA refers to a CCM sandwiched between two gas diffusion layers The platinum loading of a nanofiber mat was calculated from its total electrode weight and the weight-fraction of Pt/C catalyst used in the electrospinning ink. In all experiments, the cathode and cathode Pt loadings were fixed at

0.10 mg/cm^2. 5 cm^2 carbon gas diffusion paper (Sigracet GDL 25 BCH) was physically pressed onto the CCM's anode and cathode in the test fixture to form an MEA. A picture of an MEA is shown below in Figure 3.1

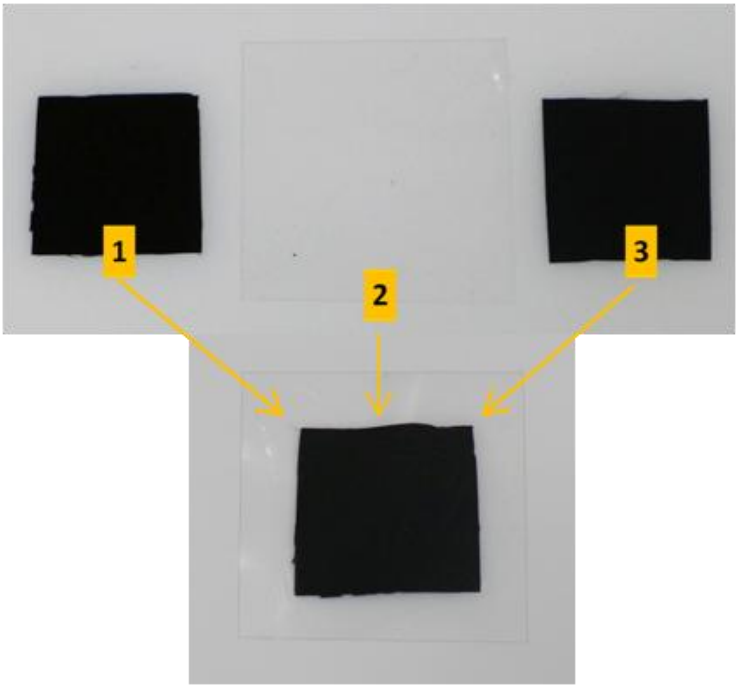

Figure 3.1. Photograph of (1) 5 cm^2 anode, (2) 16 cm^2 Nafion 211 membrane, and (3) 5 cm^2 cathode. These components are physically assembled into a CCM as shown by the arrows, in which the membrane is sandwiched between the anode and cathode.

The hot-pressing pressure was varied between 0-12 MPa, the hot-pressing time was varied between 1 and 6 minutes (always after a 10 minute heating period with no pressure), and the hot-pressing temperature was varied between 100-154°C. A bench top laboratory manual press from Carver, Inc, model number 3851-0 was used for hot-pressing. During hot-pressing, the anode-membrane-cathode were sandwiched between two 6 x 6 cm polytetrafluoroethylene (PTFE) (Teflon) sheets (~300 um thickness each), and were placed between two silicone pads, housed in an aluminum fixture. The pads

help to evenly distribute the pressure across the electrodes. The Carver press has a force gauge and the Teflon sheet area was used to calculate the pressure. A schematic of the hot-pressing set-up is shown in Figure 3.2.

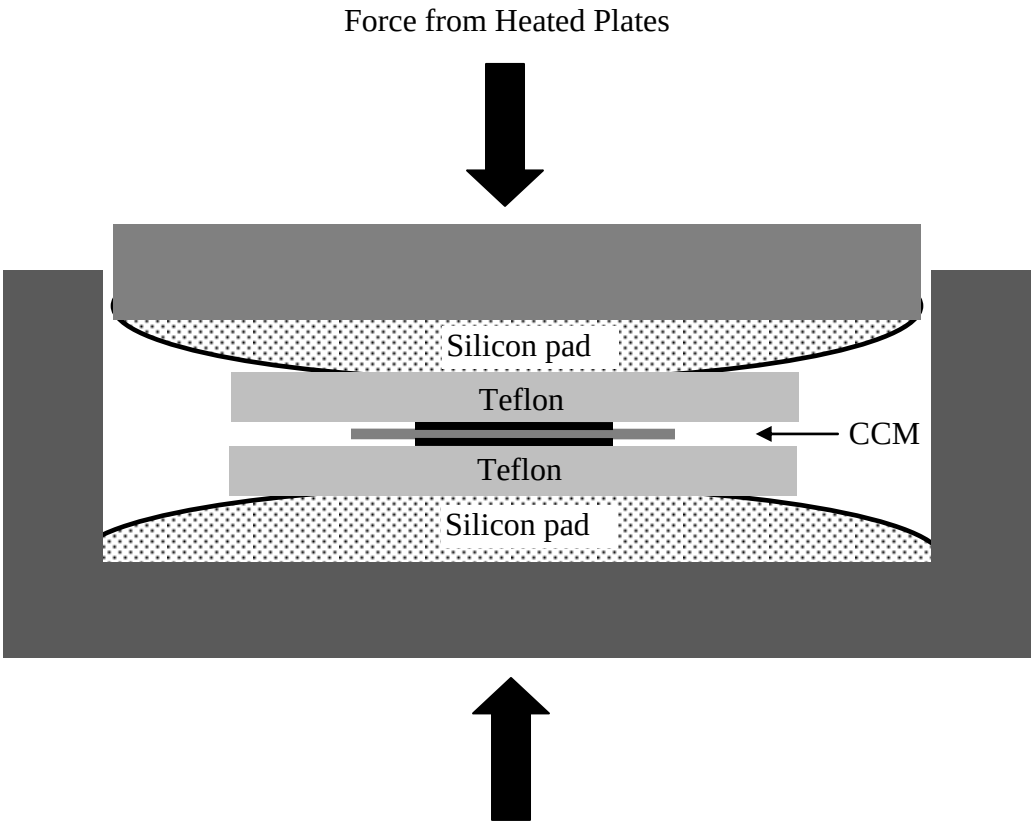

Figure 3.2. Schematic of hot-pressing set-up. Gas diffusion layers are physically pressed onto the hot-pressed CCM later when the CCM is loaded into the fuel cell test fixture.

SEM Imaging of Nanofiber Mat Cathodes – Top-down SEM images of electrospun nanofiber mats were taken with a Hitachi S4200 Scanning Electron Microscope with a 5.0 kV electron beam. Prior to imaging, the mats were lightly pressed at room

temperature onto conductive SEM tape and then sputter coated with a thin layer of gold to improve contrast.

Fuel Cell Tests – Fuel cell polarization curves were collected using a Scribner Series 850e test station with mass flow, temperature, and manual backpressure control. The fuel cell test fixture accommodated a 5 cm^2 membrane-electrode-assembly and contained single anode and cathode serpentine flow channels. Experiments in H_2/air were performed at 80°C with fully humidified gases at atmospheric (ambient) pressure and flow rates of 125 sccm H_2 and 500 sccm air. At 1 A/cm^2, these mass flow rates correspond to hydrogen and oxygen stoichiometries of 3.6 and 6, respectively. This means that at 1 A/cm^2, the air feed contains six times the amount of oxygen that is being consumed in the oxygen reduction reaction at the cathode. Prior to collecting polarization data, the MEAs were pre-conditioned at 80^oC by alternating between a low current (150 mA/cm^2) for two minutes and then a low voltage (0.2 V) for two minutes (where the low voltage corresponds to a high current). The break-in period lasted for at least four hours, until steady power output from the MEA was achieved. Polarization curves were generated by collecting the current at a given voltage after waiting 60 seconds for system stabilization.

3.3 Results and Discussion

The Effect of Nafion Membrane Acid Wash – Often, as a precautionary step, Nafion membranes are boiled in 1 M sulfuric acid and then soaked in water before they are incorporated into an MEA. This pretreatment step is performed to insure that the

membrane is fully in the H^+ form and to remove any impurities.[11] In Chapter 2 of this dissertation, the Nafion membranes were pretreated with an acid wash (1 hour soak in hot 1 M sulfuric acid, followed by 1 hour soak in hot water). However, this pretreatment step is time consuming and may be unnecessary, as the Nafion membranes used in this dissertation are shipped from Ion Power Inc. in the acid form. In order to determine if an acid wash pretreatment step is necessary for proper fuel cell performance, two MEAs with nanofiber electrodes were fabricated and tested in a hydrogen/air fuel cell. One MEA had a membrane that had been pretreated with an acid treatment like in Chapter 2, and the other MEA had a membrane that was used as-received. That is, in the second MEA, the membrane was not washed or processed in any way before being hot-pressed with nanofiber electrodes. Both MEAs used nanofiber electrodes of the same composition and Pt loading (0.10 mg/cm^2 cathode and anode).

Figure 3.3 shows that there was no difference in fuel cell fuel power output between the two MEAs; the polarization curves (collected at 80°C with fully humidified H_2/air feed gases at ambient pressure) were essentially the same. This result indicates that the Nafion membranes can be used as-received and do not require an acid wash pretreatment step for proper performance. In the following dissertation chapters, as well as the remaining sections in the chapter, all Nafion membranes were used as-received.

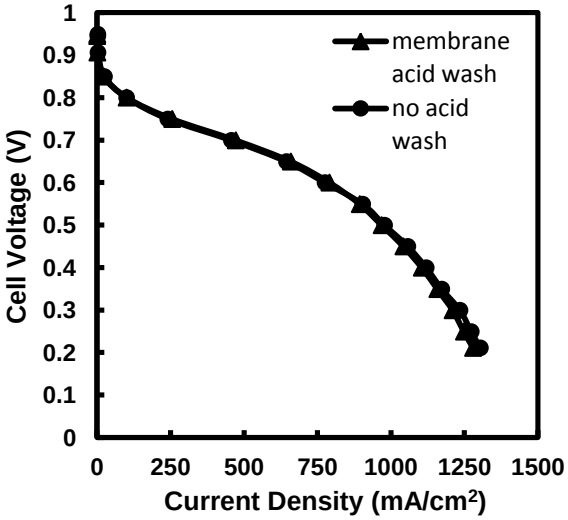

Figure 3.3. Comparison of fuel cell polarization curves for similar MEAs with a Nafion 211 membrane that (▲) was pretreated with a 1 M sulfuric wash, or (●) was *not* pretreated with an acid wash. Fuel cell conditions: hydrogen/air, 80°C, 100% RH, ambient pressure feed gases.

The Effect of Electrode Annealing– Experiments were performed in order to determine if nanofiber electrode thermal annealing is a mandatory processing step for proper MEA operation. First, imaging experiments were performed to make sure the nanofiber structure remained intact after hot-pressing without a prior thermal annealing step without pressure. Electrospun Nafion nanofibers (without particles) have been reported by Ballengee and Pintauro[12] to soften, flow, and weld when subjected to pressure at 150°C. However, Zhang and Pintauro[9] have reported that nanofiber electrode Pt/C/Nafion/PAA mats that were (i) annealed at 150°C under vacuum for 2 hours, and (ii) hot-pressed to a Nafion membrane at 140°C for 10 minutes at a pressure of up to 80 MPa maintained a fiber morphology without any fiber welding. The experiments in this dissertation chapter were performed to confirm that nanofiber electrode mats that have not undergone a prior annealing step also maintain their fiber morphology after hot-pressing. Nanofiber Pt/C/Nafion/PAA electrode mats (cathode and/or anode mats; they

are identical) were hot-pressed onto a Nafion 211 membrane at 4 MPa and either 130°C, 150°C or 170°C for 10 minutes. Another nanofiber mat that was annealed for 2 hours in vacuum at 150°C was also hot-pressed onto a Nafion membrane. As shown in Figure 3.4, no visual differences were found between non-annealed nanofiber mats that were hot-pressed at 130-170°C compared to a hot-pressed nanofiber mat that underwent a prior thermal annealing step without pressure. The nanofiber electrode mats had sufficient mechanical strength to remain intact even without a separate thermal annealing step, when hot-pressed as high as 170°C, which is above the glass transition temperature of Nafion (~100°C)[8] and a higher temperature than standard hot-pressing conditions (100-140°C)[13, 14].

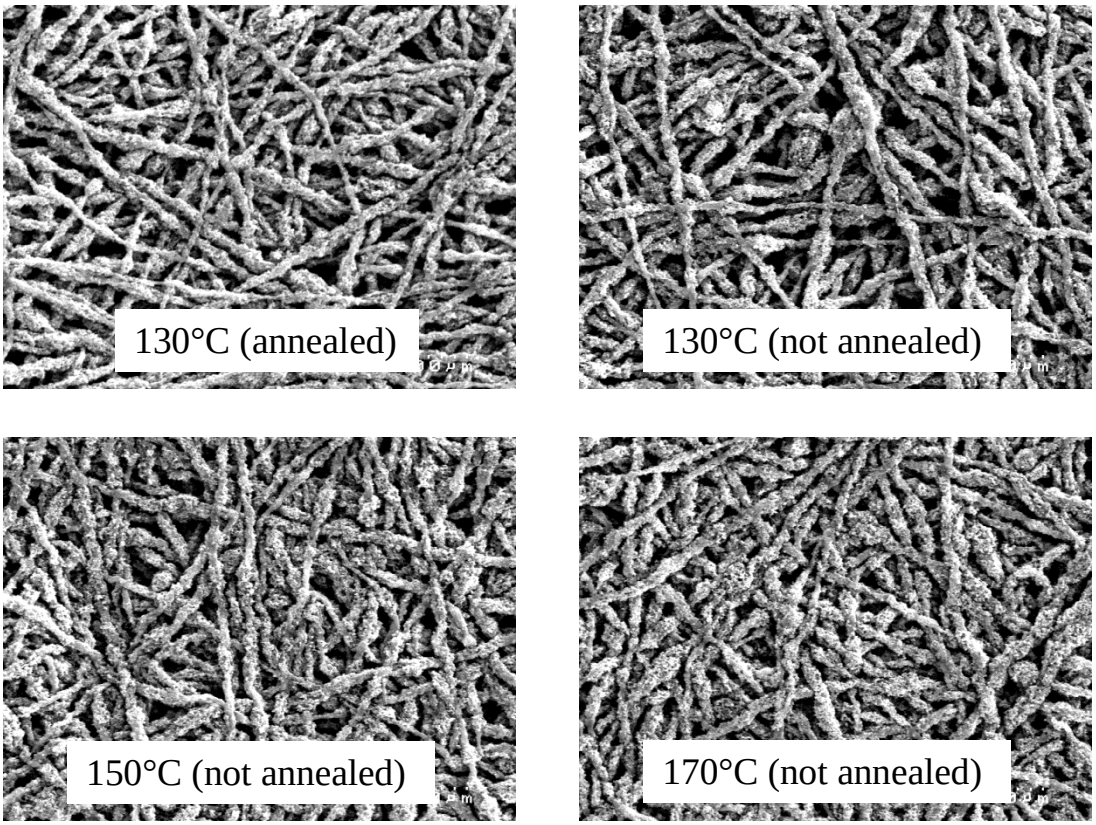

Figure 3.4. Top-down SEMs of Pt/C/Nafion/PAA electrospun mats hot-pressed to a Nafion membrane at different temperatures with and without a prior electrode annealing step.

Fuel cell performance was also investigated with non-annealed electrodes. Two identical CCMs were fabricated where the electrodes were annealed (before hot-pressing) for either 15 minutes or 2 hours at 150^{o}C (in vacuum). A third CCM was prepared where the anode and cathode were not annealed. All three CCMs were hot-pressed at 4 MPa at 140°C for 10 minutes. Gas diffusion layers were physically pressed on to the CCMs in the fuel cell test fixture to create MEAs. Each MEA was tested at 80°C with fully humidified H_2/air gas feeds at 125 sccm/500 sccm at atmospheric pressure. As shown in Figure 3.5, there was essentially no difference in the fuel cell performance for

the MEAs. Therefore, it can be concluded that an electrode annealing step before hot-pressing is not necessary for proper MEA operation with nanofiber cathodes and anodes.

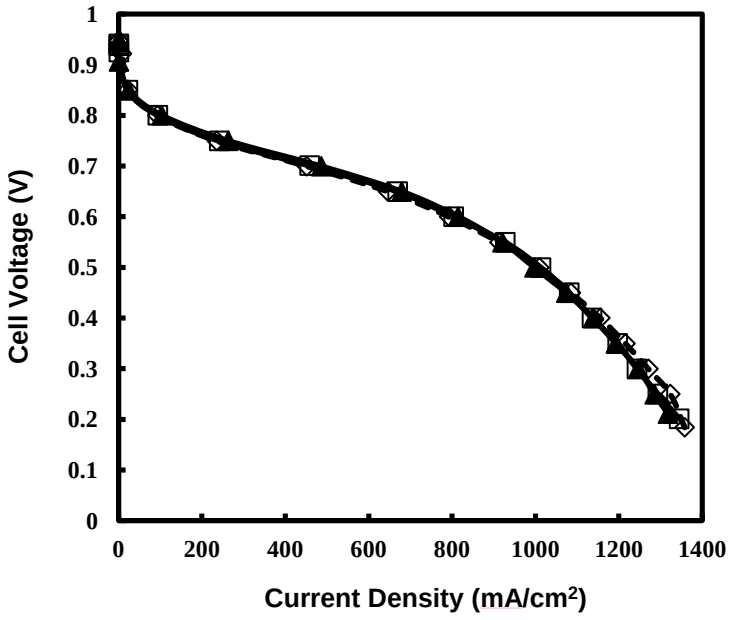

Figure 3.5. Comparison of fuel cell polarization curves for similar MEAs with electrospun electrodes with no annealing (-◊-) or with 15 minute (□) or 2 hr annealing (▲) at 150°C. Fuel cell conditions: hydrogen/air, 80°C, ambient pressure feed gases.

The Effect of Hot-Pressing Conditions on Power Output- The effects of CCM hot-pressing conditions (time, pressure, and temperature) on MEA performance with a Nafion membrane and nanofiber cathodes and anodes were systematically studied with a goal of maximizing fuel cell power density at 0.65 V. The range of hot-pressing conditions were: a pressure between 1 and 4 MPa, a hot-pressing time between 1 and 5 minutes (after a 10 minute heating period with no pressure), and a hot-pressing temperature of 100-140°C. The Minitab Central Composite Response Surface

experimental design program used these input ranges to identify experiments to efficiently find the best combination of hot-pressing pressure, time, and temperature. A central composite design is an effective method to efficiently estimate first and second order terms with systems of three independent variables. It is noted that Minitab suggested some conditions outside of the specified input range, and these experiments (such as 154°C) were also performed when the given value was practically sound (e.g., negative pressures are impossible and this suggestion was ignored). Experiments were performed in random order.

A complete list of experiments with the specified hot-pressing conditions, including the resulting fuel cell power densities at 0.65 V are listed in Table 3.1. The operating conditions for the fuel cell tests were 80°C, 100% RH, and H_2/air geed gases at ambient pressure.

Table 3.1. Hot-Pressing Conditions for CCM Fabrication and Corresponding Power Densities at 0.65 V

Std. Order	Temp (°C)	Pressure (MPa)	Time (min)	Power Density (mW/cm^2)
1	100	1	2	428
2	140	1	2	444
3	100	4	2	489
4	140	4	2	499
5	100	1	5	437
6	140	1	5	462
7	100	4	5	455
8	140	4	5	465
9	154	2.5	3.5	455
10	120	5	3.5	495
11	120	2.5	1	471
12	120	2.5	6	491
13	120	2.5	3.5	471
14	120	2.5	3.5	457
15	120	2.5	3.5	447

Minitab used linear, quadratic, and first-order interaction terms to fit the hot-pressing temperature, pressure, and time to the experimental power densities, according to the following equation:

$$C_1 + C_2\text{Temp} + C_3\text{Pressure} + C_4\text{Time} + C_5\text{Temp}^2 + C_6\text{Presssure}^2 + C_7\text{Time}^2 + C_8\text{Temp*Pressure} + C_9\text{Temp*Time} + C_{10}\text{Pressure*Time} = \text{Power Density} \quad \text{(Eq. 3.1)}$$

Using a least sum of squares algorithm, the regression coefficients of Equation 3.1 were determined. Furthermore, Minitab calculated the standard error for each coefficient which determines whether the contribution of each term is statistically significant. A measure of the significance of each term is expressed quantitatively as a "P-value" in Table 3.2. P-values range from 0 to 1, where a lower P-value indentifies regression coefficients that were statistically significant. Generally only P-values below 0.05 are considered significant.

Table 3.2. Regression Coefficients of Hot-Pressing Variables

Term	Coefficient	P-value
Constant	704.499	0
Temp	9.359	0.392
Pressure	39.573	0.003
Time	-0.984	0.909
Temp*Temp	-3.371	0.771
Press*Press	-12.313	0.233
Time*Time	14.958	0.161
Temp*Press	-4.125	0.713
Temp*Time	1.875	0.867
Press*Time	-18.375	0.137

As shown in Table 3.2, the only regression coefficient with a low P-value (below 0.05) was the linear pressure term. All other terms were considered non significant. As the power densities at 0.65 V were statistically independent of hot-pressing time, the shortest time of 1 min was chosen for convenience. Temperature was also not statistically significant, though a positive temperature coefficient indicated better

performance with increasing temperature, so the upper temperature range of 140°C was chosen. A low P-value for pressure (0.003 in Table 3.2) and a positive coefficient indicates that higher pressures were better. Two additional CCMs were fabricated with larger hot-pressing pressures, 8 MPa and 12 MPa. All of the power densities from Table 3.1 as well as these two high-pressure CCMs are shown in Figure 3.6.

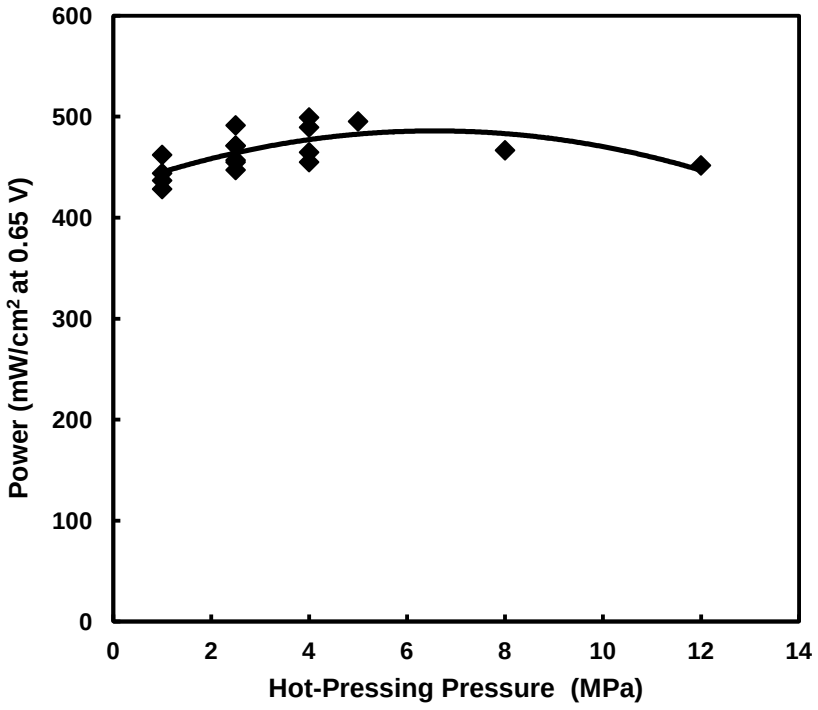

Figure 3.6. The effect of electrode hot-pressing pressure on MEA power density (mW/cm^2) at 0.65 V for 5 cm^2 MEAs with electrospun electrodes with a Pt loading of 0.10 mg/cm^2. Fuel cell conditions: hydrogen/air, 80°C, 100% RH, and ambient pressure feed gases.

Figure 3.6 shows a maximum power is reached about 5 MPa. Thus, hot-pressing conditions that will be used after in the following dissertation chapters will be a 1 minute press (after 10 minute heating) at 5 MPa and 140°C. It is noted, however, that MEAs

perform well over a wide range of hot-pressing conditions. The hot-pressing time, temperature, and pressure were varied from 1-6 minutes, 100°C – 154 °C, and 1-12 MPa, respectively, and the power densities at 0.65 V all fell within 460 mW/cm^2 ± 30 mW/cm^2. To emphasis the point that fuel cell performance was generally insensitive to hot-pressing conditions, polarization curves for two MEAs at two of the most extreme hot-pressing conditions are shown in Figure 3.7. The two polarization curves are very similar, not only at 0.65 V, but along the entire voltage range. For example, there was only about a 10% difference at 0.65 V and a 6% difference at maximum power.

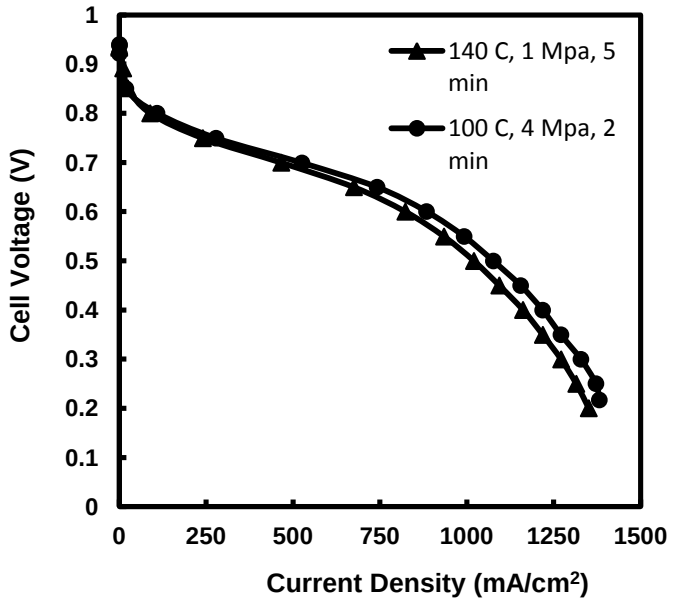

Figure 3.7. Comparison of fuel cell polarization curves for two N211 MEAs with different hot-pressing conditions (▲) 140°C, 1 MPa, and 5 min, or (●) 100°C, 4 MPa, and 2 min. Fuel cell conditions: hydrogen/air, 80°C, 100% RH, ambient pressure feed gases. Cathodes and anodes are nanofiber electrodes with Pt loadings of 0.10 mg/cm^2.

3.4 Conclusions

Work was performed to better understand and optimize the MEA fabrication procedure with nanofiber electrodes. An acid wash membrane pre-treatment step was found to be unnecessary for proper MEA fuel cell performance. The effect of electrode annealing was investigated and it was found that the hot-pressing temperature and time for MEA fabrication was sufficient to anneal the Nafion binder in nanofiber cathodes and anodes. Thus, a separate electrode annealing step, after electrospinning and before hot-pressing electrodes to a Nafion membrane, had no effect on MEA power output and is not needed. Next the effect of hot-pressing temperature, pressure, and time on nanofiber anode/cathode MEA performance in a hydrogen/air fuel cell was assessed and quantified using Minitab central composite experimental design. In general, it was found that fuel cell power output was insensitive to small variations in hot-pressing time and pressure, and only pressure was found to be statistically significant. A pressure of 5 MPa was identified. In the following dissertation chapters, the 5 MPa pressure will be coupled with a hot-pressing temperature of 140°C and a hot-pressing time of 1 min, which was the shortest time investigated.

3.5 References

(1) Frey, T. and M. Linardi (**2004**) *Electrochimica Acta*, 50, 99-105.

(2) Therdthianwong, A., P. Manomayidthikarn, and S. Therdthianwong (**2007**) *Energy*, 32, 2401-2411.

(3) Okur, O., C. I. Karadag, F. G. B. San, E. Okumus, and G. Behmenyar (**2013**) *Energy*, 57, 574-580.

(4) Muruganantham, R., S. Annamalaisundaram, D. Sangeetha, and S. R. Boopathy (**2012**) *J. Fuel Cell Sci. Technol.*, 9.

(5) Glassman, M., A. Omosebi, and R. S. Besser (**2014**) *Journal of Power Sources*, 247, 384-390.

(6) Yim, S. D., Y. J. Sohn, S. H. Park, Y. G. Yoon, G. G. Park, T. H. Yang, and C. S. Kim (**2011**) *Electrochimica Acta*, 56, 9064-9073.

(7) Modestino, M. A., A. Kusoglu, A. Hexemer, A. Z. Weber, and R. A. Segalman (**2012**) *Macromolecules*, 45, 4681-4688.

(8) Osborn, S. J., M. K. Hassan, G. M. Divoux, D. W. Rhoades, K. A. Mauritz, and R. B. Moore (**2007**) *Macromolecules*, 40, 3886-3890.

(9) Zhang, W. and P. N. Pintauro (**2011**) *ChemSusChem*, 4, 1753-1757.

(10) Ballengee, J. B. and P. N. Pintauro (**2011**) *Journal of the Electrochemical Society*, 158, B568-B572.

(11) Mauritz, K. A. and R. B. Moore (**2004**) *Chemical Reviews*, 104, 4535-4585.

(12) Ballengee, J. B. and P. N. Pintauro (**2011**) *Macromolecules*, 44, 7307-7314.

(13) Thanasilp, S. and M. Hunsom (**2010**) *Fuel*, 89, 3847-3852.

(14) Yazdanpour, M., A. Esmaeilifar, and S. Rowshanzamir (**2012**) *International Journal of Hydrogen Energy*, 37, 11290-11298.

Chapter IV

FABRICATION, IN-SITU PERFORMANCE, AND DURABILITY OF NANOFIBER FUEL CELL ELECTRODES

Adapted from Brodt, M., T. Han, N. Dale, E. Niangar, R. Wycisk, and P. Pintauro (**2015**) *Journal of the Electrochemical Society*, 162, F84-F91

4.1 Introduction

The hydrogen/air proton-exchange membrane fuel cell is a promising candidate for emission-free automotive power plants due to its high power output, efficiency of energy conversion, and quick start-up. The successful integration of a sizable fleet of Electric Vehicles into the transportation sector would greatly diminish localized air pollution and alleviate our dependence on depleting oil reserves. Presently, mass commercialization of fuel cell vehicles is challenging due in large part to issues related to the cost and durability of membrane-electrode-assemblies (MEAs)[1].

A principal strategy to reduce the cost of MEAs is to minimize the amount of the platinum catalyst in the electrodes without sacrificing power generation. In this regard, recent R&D efforts have been directed at the investigation of platinum metal alloys[2], core-shell nanostructures[3], and the use of platinum-free metal-nitrogen-carbon catalysts[4,5]. Although these studies have shown some promise in terms of catalytic activity and potential cost savings, they do not currently meet automotive power density and durability targets.

Carbon support corrosion in Pt/C catalysts during fuel cell start-up/shut-down is another ongoing issue that has drawn considerable research attention. In particular, when a hydrogen-air mixture is present in the anode during start-up, the cathode potential spikes as high as 1.5 V vs. SHE, resulting in severe carbon corrosion of the cathode catalyst layer[6]. Researchers have worked to mitigate carbon corrosion at the materials level by investigating catalyst that can better withstand the harsh automotive operating environment. Current efforts are focused on metal oxides and thermally treated carbon supported catalysts[7-10].

Another potential strategy to improve the power density and durability of fuel cell electrodes is to alter the catalyst electrode morphology. Researchers have studied various alternatives to the standard catalyst-coated membrane (CCM) and catalyst-coated gas diffusion electrode (GDE) methods of preparing PEM fuel cell MEAs[1, 11-13]. These new approaches include electrosprayed layers of micron-size catalyst/binder droplets[14] and oriented Pt-coated whisker electrodes[15]. Another promising technique is the electrospinning of particle/polymer (catalyst/ionomer) mixtures into a non-woven nanofiber electrode catalyst mat. Zhang and Pintauro first demonstrated the utility of replacing a conventional MEA cathode with a nanofiber mat where the fibers were composed of Pt/C catalyst with a Nafion/poly(acrylic acid) binder[16]. They found that an MEA with: (i) an electrospun cathode mat (where the average nanofiber diameter was 470 nm), (ii) a Nafion 212 membrane and (iii) a conventional decal anode performed extraordinarily well in a H_2/air fuel cell, producing more than 500 mW/cm^2 without backpressure at 0.6 V and 80^{o}C with a cathode Pt loading of 0.1 mg/cm^2. More recently, Brodt *et. al.* have shown that MEAs with electrospun cathodes containing Johnson

Matthey HiSpec 4000 Pt/Vulcan catalyst produced very high power (up to over 900 mW/cm^2) at an ultra-low cathode platinum loading of 0.055 mg_{Pt}/cm^2 in an H_2/air fuel cell at 80°C and 2 atmospheres back pressure[17]. The excellent performance of nanofiber fuel cell electrodes is attributed to facile oxygen and proton transport to catalytic sites and efficient product water removal, which is a direct consequence of the unique nanofiber electrode morphology, with significant inter-fiber and intra-fiber porosity and a well-mixed dispersion of catalyst powder and ionomer binder.

Herein, we report on new results with nanofiber electrodes that were electrospun with commercially available platinum catalysts supported on either Vulcan carbon (Johnson Matthey catalyst) or high surface area carbon (Tanaka Kikinzoku Kogyo) where the anode and cathode Pt loadings were each fixed at 0.10 mg/cm^2. Experiments focused on: (i) determining the effects of catalyst type, nanofiber catalyst/binder composition, and nanofiber diameter on initial fuel cell power output and (ii) assessing nanofiber electrode durability, in terms of Pt dissolution and carbon corrosion of the catalyst support. For the durability tests, beginning of life and end of life performance of MEAs with nanofiber mat electrodes were compared with MEAs with Nissan Technical Center North America (NTCNA)-sprayed GDE cathodes and commercial GDE anodes.

4.2 Experimental

Electrospinning Electrodes - Electrospinning inks were prepared by mixing the following components in an alcohol/water solvent: (a) a commercial Pt/C catalyst powder, either Johnson Matthey HiSpec™ 4000 (40% Pt on Vulcan carbon), henceforth referred to as JM-Pt(Vulcan), or Tanaka Kikinzoku Kogyo TEC10E50E (46.1% Pt on

high surface area carbon), henceforth referred to as TKK-Pt(HSAC), (b) 1100 EW Nafion® ion exchange resin (20% ionomer in lower aliphatic alcohols and water as received from Aldrich), and (c) poly(acrylic acid) (450 kDa molecular weight from Aldrich). Nafion forms a micellar dispersion in alcohol/water mixtures and will not electrospin into well-formed fibers, unless a suitable carrier polymer is added to the electrospinning solution[18]. In the present study, poly(acrylic acid) (abbreviated as PAA) was used as the carrier. An electrospinning ink was prepared by: (i) wetting 0.15 g catalyst with 0.55 g water, (ii) mixing the wet catalyst with 0.26 g Nafion stock solution and 0.45 g isopropanol, (iii) sonicating the catalyst/Nafion suspension for 90 minutes with intermittent mechanical stirring, (iv) adding 0.24 g of a 15 wt% poly(acrylic acid) solution in 2:1 wt ratio isopropanol:water, and (v) stirring the ink mechanically for approximately 48 hours. This ink recipe was used to fabricate dry electrospun mats with 63 wt% Pt/C, 22 wt% Nafion, and 15 wt% PAA. The amount of catalyst and stock Nafion solution was varied for other inks so the Pt/C:Nafion weight ratio of the resulting dry mat contained 55-72 wt% Pt/C and 13-30 wt% Nafion, where the PAA content was held constant at 15 wt%. An ink was drawn into a 3 mL syringe and electrospun using a 22-gauge stainless steel needle spinneret, where the needle tip was polarized to a potential of 10-12 kV relative to a grounded stainless steel rotating drum collector that was operated at a rotation speed of 100 rpm. The spinneret-to-collector distance was fixed at 10 cm and the flow rate of ink was held constant for all experiments at 1.0 mL/h. Nanofibers were collected on an aluminum foil that was attached to the cylindrical collector drum. The drum oscillated horizontally to improve the uniformity of deposited nanofibers. A schematic diagram of the electrospinning apparatus is shown in Figure 4.1.

Electrospinning was performed at room temperature in a custom-built environmental chamber, where the relative humidity was maintained constant at 40%.

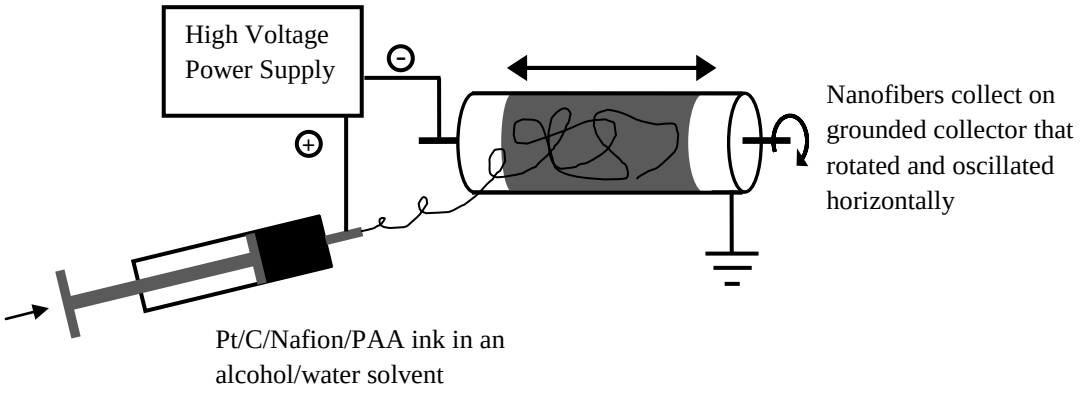

Figure 4.1. Schematic diagram of the electrospinning apparatus for creating a nanofiber mat electrode.

Membrane-Electrode-Assembly (MEA) Preparation - CCMs (Catalyst Coated Membranes) with nanofiber electrodes were fabricated at Vanderbilt University by hot pressing 5 or 25 cm^2 electrospun electrode mats (anodes and cathodes of identical fiber composition) onto the opposing surfaces of a Nafion 211 membrane (henceforth identified as NR211) at 140^oC and 5 MPa for 1 minute, after a 10-minute pre-heating period at 140^oC with no applied pressure. The Pt loading of a nanofiber mat was calculated from the total electrode weight and the weight-fraction of Pt/C catalyst used in the electrospinning ink. Carbon paper gas diffusion layers (GDLs) (Sigracet 25 BCH GDL) were physically pressed onto a CCM's anode and cathode while in the fuel cell test fixture to form an MEA.

Painted gas diffusion electrodes (GDEs) were also fabricated at Vanderbilt University with and without poly(acrylic acid). Pt/C powder was added to the Nafion

dispersion (with and without PAA) and stirred mechanically for 48 hours. The inks were painted in multiple layers directly onto a carbon paper gas diffusion layer (Sigracet GDL 25 BCH) and dried at 70^{o}C for 30 minutes after each painted layer. Painted GDEs with 15 wt% PAA were prepared with 72 wt% TKK-Pt(HSAC) and 13 wt% Nafion (the same composition as some electrospun fiber electrodes). GDEs without PAA were prepared with a composition of 67 wt% TKK-Pt(HSAC) and 33 wt% Nafion. All painted GDEs (5 cm^2 in geometric area) were hot pressed onto NR211 membranes at 140°C and 5 MPa for 1 minute after a 10 minute pre-heating step at 140^{o}C with no applied pressure.

Sprayed GDEs were fabricated at Nissan Technical Center North America (NTCNA). These catalyst inks were made by mixing water, n-propanol, Nafion ionomer dispersion (Ion Power DE2020), and Pt/C powder, either TKK-Pt(HSAC) or JM-Pt(Vulcan) (the same catalysts as the Vanderbilt electrodes). The mass-based ionomer/carbon (I/C) ratio in the ink was kept constant at 0.9. The electrocatalyst cathode layers were formed on gas diffusion layers (GDLs) with microporous layers (SGL Carbon) using an automated robotic spray system. MEAs (25 cm^2) were prepared by hot pressing sprayed cathode GDEs (0.1 mg/cm^2 Pt loading) and commercial Johnson Matthey anode GDEs (with JM-Pt(Vulcan) catalyst at a Pt loading of 0.4 mg/cm^2) onto the opposing surfaces of Nafion® NR211 membranes. The hot-press conditions were 2 MPa pressure for 10 minutes at 130°C.

Fuel Cell Tests - Fuel cell polarization curves were collected at Vanderbilt University and NTCNA. At Vanderbilt, fuel cell tests were performed on 5 cm^2 MEAs, using a Scribner Series 850e test station with mass flow, temperature, and manual backpressure control.

The fuel cell test fixture accommodated a single MEA and contained single anode and cathode serpentine flow channels. Experiments with fully humidified H_2 and air at atmospheric (ambient) pressure were performed at 80°C where the H_2 flow rate was 125 sccm and the airflow rate was 500 sccm. Prior to collecting polarization data, the MEAs were pre-conditioned by operating at 80°C and 1 A/cm^2 for 8 hours. Polarization curves were generated by measuring the current at a given voltage after waiting 60 seconds for system stabilization. The polarization curves were measured in the anodic (positive voltage) direction.

At NTCNA, fuel cell polarization curves were obtained with 25 cm^2 MEAs at 100% and 40% relative humidities at 80°C, using hydrogen and air at a gauge pressure of 1 bar. The current was scanned from low current to high current and the system was given 3 minutes to stabilize at each current density before a voltage reading was recorded. MEAs were pre-conditioned by operating at 1 A/cm^2 at 80°C for 8 hrs. High frequency resistance (HFR) data were recorded in-situ. Performance evaluations were carried out using operating conditions designed to produce meaningful data for automotive applications. The constant gas flow rates used for these evaluations were high: 8 normal liters per minute (NLPM) at the cathode and 4 NLPM at the anode, with no/minimal pressure drop across the flow field. Cathode catalyst mass activity data were collected using a current-controlled anodic scan (high current to low current) at 80°C with fully humidified O_2 and H_2 gas feeds and no back pressure, where the system was allowed to stabilize for three minutes at each data point. Mass activities were determined from a plot of IR-free voltage verse the H_2-crossover corrected current density.

Electrochemical Surface Area (ECA) – In-situ cyclic voltammetry (CV) measurements were performed at NTCNA on 25 cm^2 MEAs with a sweep rate of 20 mV/s, where a H_2-purged anode served as both the counter and reference electrodes and N_2 was fed to the working cathode. The fuel cell test fixture was operated at 30^oC with gas feed streams at a dew point of 30^oC (fully humidified). The CV was carried out between +0.02 V and +0.9 V vs. SHE and the electrochemically active surface area was determined from the integrated area above the hydrogen adsorption portion of a voltammogram (corresponding to a voltage range of approximately +0.1 to +0.4 V), where the charge required to reduce one monolayer of hydrogen atoms on Pt was assumed to be 210 $\mu C/cm^2$.

Durability Tests - MEAs were tested under the Fuel Cell Commercialization Conference of Japan's (FCCJ) standard start-stop potential cycling and load cycling protocols.[19] The goal of these accelerated degradation tests was to generate data for benchmarking and to gain a better understanding of the fundamental mechanisms related to cathode performance loss during fuel cell operation.

Carbon Corrosion (start-stop cycling) - This accelerated durability test simulates start-up and shut-down of a stack without the application of any operational controls that may mitigate fuel cell performance losses. During start-up, if the stack has been shut down for some time, the anode and cathode are filled with ambient air and are pinned to the air-air potential; introducing hydrogen gas causes a hydrogen-air front to move through the anode chamber, with a large shift in the cell potential (to a value as high as 1.5 V). The start-stop durability protocol simulates this event many times by cycling from 1.0 V to 1.5 V at a scan

rate of 500 mV/s (see Figure 4.2). In the present study, 1,000 voltage cycles were performed on a single MEA, where the fuel cell was supplied with H_2 at the anode and N_2 at the cathode (both at 0.5 L/min. and 80°C, with fully humidified feed gases), and the cell potential was cycled using a potentiostat. ECA measurements were made intermittently during a corrosion test and beginning of life (BoL) and end of life (EoL) i-V polarization plots were generated. CO_2 monitoring of the cathode air exhaust, using a non-dispersive infrared detector from CO_2 Meter Inc. (Model No. CM-0052-WP), provided an additional experimental tool for measuring carbon corrosion during the accelerated potential cycling tests. A desiccant moisture trap upstream to the detector inlet removed moisture from the CO_2-containing stream. A detailed description of this monitoring system has been reported elsewhere.[20]

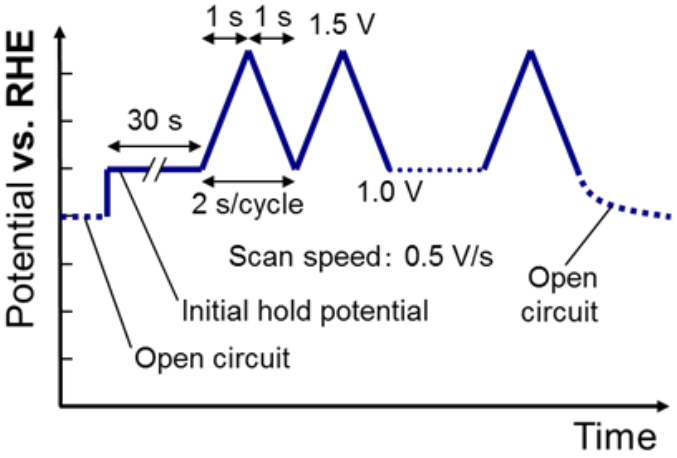

Figure 4.2. Start-stop cycling protocol for accelerated carbon corrosion durability testing.

Pt-Corrosion (load cycling): This accelerated durability test simulates the high load and no load events that typically occur when a fuel cell vehicle is driven at different speeds. In the present study, the MEA was cycled 10,000 times in steps between 0.60 V and 0.95 V

to simulate peak load and OCV/idle (see Figure 4.3). This square wave voltage regimen represents the largest oscillations that may be encountered during normal operation of a fuel cell vehicle stack. Between 0.6 V and 0.95 V, carbon corrosion is insignificant and the major causes for power loss are Pt dissolution, agglomeration, and migration on the support and through the membrane. The temperature, gas flow rate, and humidity operating conditions were the same as in the carbon corrosion tests. Pt degradation was monitored by periodic measurement of the cathode catalyst ECA and by comparing BoL and EoL i-V hydrogen/air fuel cell polarization curves.

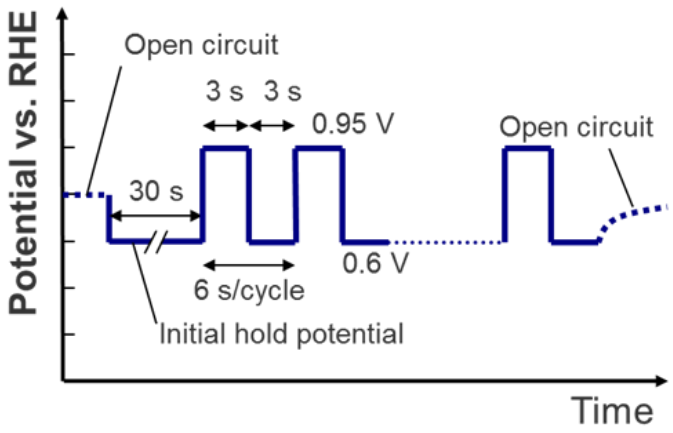

Figure 4.3. Load cycling protocol for accelerated Pt dissolution durability testing.

4.3 Results and Discussion

Effect of Catalyst Type – JM-Pt(Vulcan) and TKK-Pt(HSAC) catalysts were compared to one another in separate nanofiber anode/cathode MEAs, where each electrode had a Pt loading of 0.10 mg/cm^2 and the Pt/C:Nafion:PAA wt ratio composition of the fibers was held constant at 63:22:15. As shown in Figure 4.4, the polarization curves for the two

catalysts were essentially the same. The TKK-Pt(HSAC) showed a modest advantage, but the difference was 10% at most, so there was no clear superiority of one catalyst over the other. The Johnson-Matthey MEA results are similar to those previous published by the Pintauro group[16, 17]. Because of the similarity in catalyst performance in Figure 4.4, JM-Pt(Vulcan) and TKK-Pt(HSAC) were used interchangeably in follow-on electrospinning and MEA experiments.

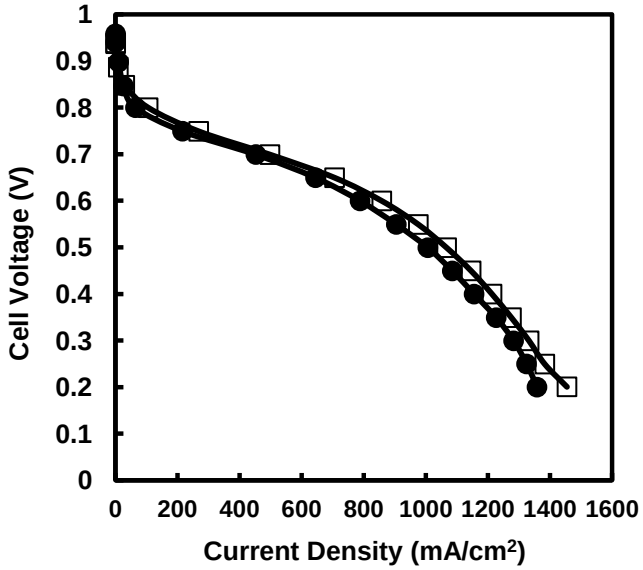

Figure 4.4. Polarization curves for 5 cm^2 MEAs with a Nafion 211 membrane and electrospun nanofiber electrodes with cathode and anode Pt loading of 0.10 ± 0.005 mg/cm^2. Fuel cell operating conditions: 80°C, 100% RH feed gases at ambient pressure, 125 sccm H_2 and 500 sccm air. (□) TKK-Pt(HSAC), and (●) JM-Pt(Vulcan).

Effect of Nanofiber Composition (Catalyst to Ionomer Ratio) - The relative amount of catalyst to proton-conducting Nafion ionomer in electrospun nanofiber mats was varied, while the PAA carrier polymer was maintained constant at 15 wt% and the cathode and anode Pt loadings were fixed at 0.10 mg/cm^2 each. Figure 4.5 shows the fuel cell

performance of TKK-Pt(HSAC) nanofibers for three different catalyst:Nafion:PAA wt ratios: 72:13:15, 63:22:15, and 55:30:15. The fuel cell polarization plots show only marginal differences for the three different MEAs. Top-down SEM images of electrospun nanofiber mats (taken before hot pressing) with the least and greatest amount of Nafion are shown in Figure 4.5b and 5.5c, respectively.

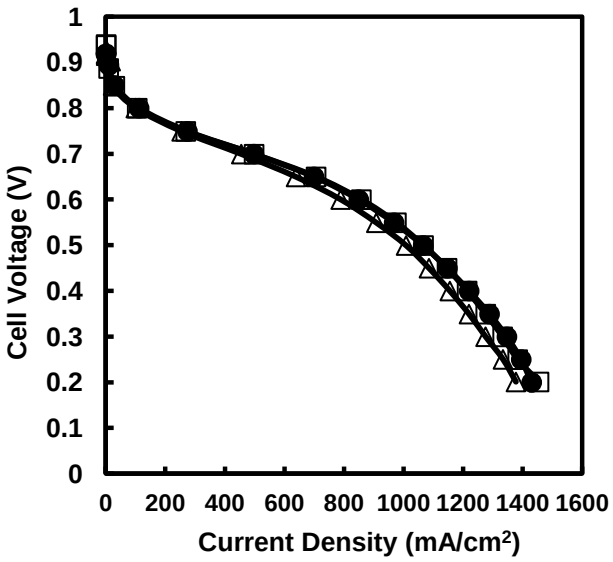

(a)

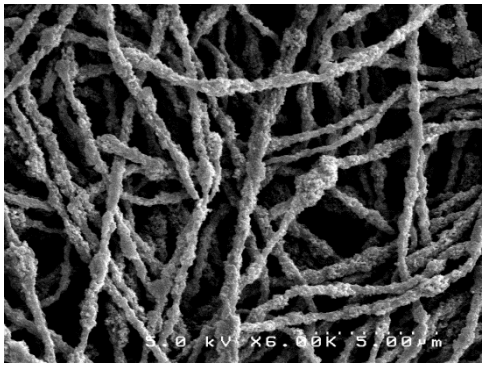

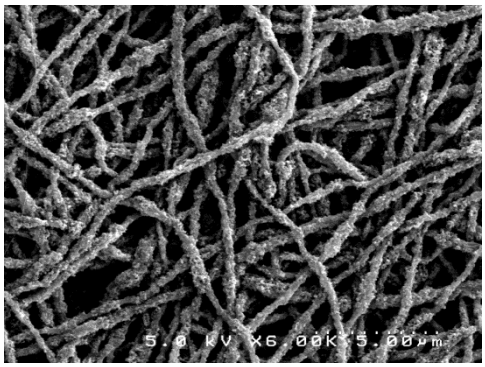

(b) **(c)**

Figure 4.5. (a) Fuel cell polarization curves for 5 cm^2 MEAs with TKK-Pt(HSAC) catalyst and a NR211 membrane operated at 80°C with fully humidified H_2 (125 sccm) and air (500 sccm) at ambient pressure. Cathodes and anodes are electrospun fibers, each having a Pt loading of 0.10 ± 0.005 mg/cm^2, with a catalyst:Nafion:PAA **wt** ratio of: (●) 72:13:15, (□) 63:22:15, and (Δ) 55:30:15. (b) Top-down 6,000x SEM image of a 72:13:15 electrospun nanofiber mat. (c) Top-down 6,000x SEM image of a 55:30:15 electrospun nanofiber mat.

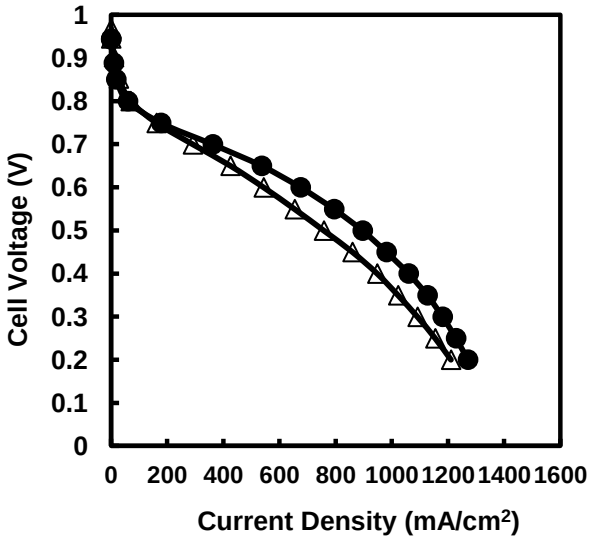

Figure 4.6. Fuel cell polarization curves for 5 cm^2 painted MEAs with TKK-Pt(HSAC) catalyst and a NR211 membrane operated at 80°C with fully humidified H_2 (125 sccm) and air (500 sccm) at ambient pressure. Cathodes and anodes have a Pt loading of 0.10 ± 0.005 mg/cm^2 and are: (●) painted GDE with no PAA and (Δ) painted GDE with PAA.

Effect of PAA - In order to quantify the influence of PAA polymer on cathode performance, two painted MEAs were prepared: one MEA had anode and cathode GDEs with a neat Nafion binder (67 wt% TKK-Pt(HSAC) and 33% Nafion) while the other MEA had GDEs with the same Nafion/PAA binder as a typical nanofiber electrode mat (72 wt% TKK-Pt(HSAC), 13 wt% Nafion, and 15 wt% PAA). The resulting polarization curves, shown in Figure 4.6, indicate that PAA adversely affects fuel cell performance. In a previous study on electrospinning Nafion polymer nanofibers for membrane applications (where the fibers contained PAA but no catalyst powder), it was found that poly(acrylic acid) lowers the proton conductivity of perfluorosulfonic acid polymer.[21] The poor performance of the painted MEA with Nafion/PAA binder in Figure 4.6 is attributed to a similar drop in the ion conductivity of the Nafion.

The results in Figure 4.6 suggest that more power could be generated in a nanofiber electrode MEA if PAA were removed from the Nafion binder after mat preparation. To further investigate this hypothesis, two methods for removing PAA from nanofiber CCMs were evaluated: (1) boiling a CCM for one hour in 1 M H_2SO_4 followed by boiling in DI water for one hour and (2) soaking a CCM in 3% H_2O_2 for one hour at room temperature and then boiling for one hour in DI water. After soaking, GDLs were attached to the CCMs and the resulting MEAs were tested in a fuel cell. After the fuel cell tests, the GDLs were removed and the nanofiber cathodes were imaged by SEM. The polarization curve and cathode SEM after the peroxide wash procedure (the harsher of the two treatments) are shown in Figure 4.7a and 5.7b, respectively. As can be seen, there was no change in MEA performance, as gauged by i-V polarization plots. Additionally, there were no visual differences in the cathode fiber surface morphology, as compared to an untreated cathode. A similar result was found when CCMs were boiled in acid and water. Although this study was unsuccessful in removing PAA, a number of important findings did emerge from the experiments: (a) PAA has a detrimental effect on the performance of painted electrode MEAs in a hydrogen/air fuel cell, (b) at the present time, PAA cannot be removed from the Nafion binder in nanofiber fuel cell electrode mats, (c) the catalyst/Nafion/PAA fibers are chemically and physically robust, and (d) in the future, it might be possible to improve the performance of nanofiber cathodes if a carrier polymer other than PAA were found for Nafion/catalyst nanofiber electrospinning (such experiments were not part of the present study).

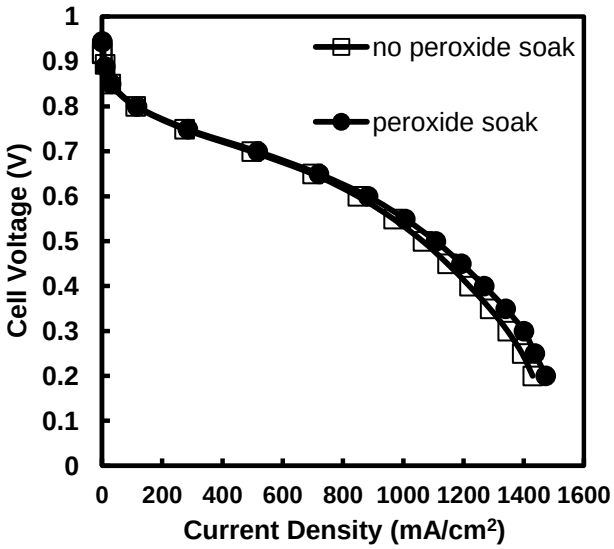

(a)

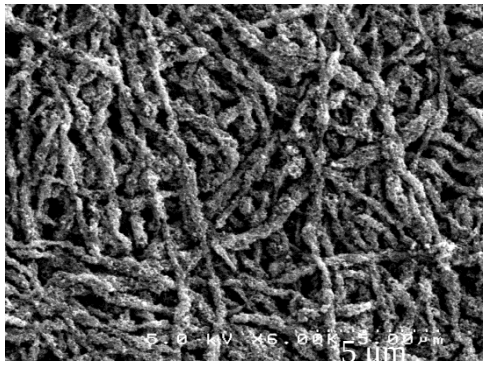

(b)

Figure 4.7. Results from the PAA extraction experiments. (a) Fuel cell polarization curves for 5 cm^2 MEAs with TKK-Pt(HSAC) catalyst with cathode and anode Pt loadings of 0.10 ± 0.005 mg/cm^2 and an NR211 membrane operated at 80°C with fully humidified H_2 (125 sccm) and air (500 sccm) at ambient pressure with or without CCM soaking in 3 wt% hydrogen peroxide and boiled water. (b) Top-down SEM image of an electrospun cathode after soaking in hydrogen peroxide and boiling in water.

Effect of Nanofiber Diameter on Fuel Cell Power Output - In these experiments, the average fiber diameter of an electrospun mat was controlled by altering the solvent content in the electrospinning ink recipe. The results of these experiments, in terms of the ink composition, average fiber diameter of an electrode mat, and the performance of the electrodes in a fuel cell MEA are summarized in Table 4.1. TKK-Pt(HSAC) catalyst powder was used in all of the inks and the diameter of electrospun nanofibers was effectively varied from 250 nm to 520 nm. Figure 4.8 shows two SEM images of an electrode mat surface; Figure 4.8a is a mat with an average fiber diameter of 250 nm, whereas the average fiber diameter in Figure 4.8b is 475 nm (for better imaging, the mats were lightly pressed at room temperature onto conductive SEM tape and sputter coated with a thin layer of gold). For both mats, the general shape and surface roughness of the fibers are the same. The fuel cell performance of the different diameter fiber mat MEAs was essentially the same, as quantified by indistinguishable i-V plots, where the measured power density at 0.65 V was 460 mW/cm^2 ± 7%. This result highlights the superior properties of the nanofiber electrode morphology, where there is sufficient intra-fiber porosity for O_2/Pt-site contact to be independent of fiber diameter and where the binder coating thickness on catalyst particles (the distribution of catalyst and binder in a nanofiber) is independent of fiber size.

Table 4.1. Average Fiber Diameter and MEA Power at 0.65 V for Various Electrospinning Inks (all fibers had a catalyst:Nafion:PAA wt ratio of 63:22:15 and utilized TKK-Pt(HSAC) catalyst)

Solvents added to Electrospinning Ink[1]	Avg. Diameter[2] (nm)	Power Density[3] at 0.65 V (mW/cm^2)
0.85 g n-propanol, 0.85 g water	250	444
0.85 g isopropanol, 0.85 g water	330	462
0.60 g isopropanol, 0.70 g water	380	433
0.40 g ethanol, 0.50 g water	475	475
0.30 g ethanol, 0.40 g water	485	465
0.40 g methanol, 0.50 g water	520	489

[1]This is the amount and composition of solvent added to an ink after mixing catalyst, Nafion stock solution, and PAA solution, as described in the Experimental Section

[2]Fiber electrospinning conditions:10-12 kV for inks containing n-propanol/water and isopropanol/water and 8-10 kV for inks with ethanol/water and methanol/water, ambient temperature air at 40% RH, 10 cm spinneret to collector, 1.0 mL/hr flow rate

[3]Fuel cell operating conditions: 80^{o}C, 100% relative humidity feed gases at ambient pressure, 125 sccm H_2 flow rate, and 500 sccm air flow rate. Pt loading was 0.10 mg_{Pt}/cm^2 for cathode and anode.

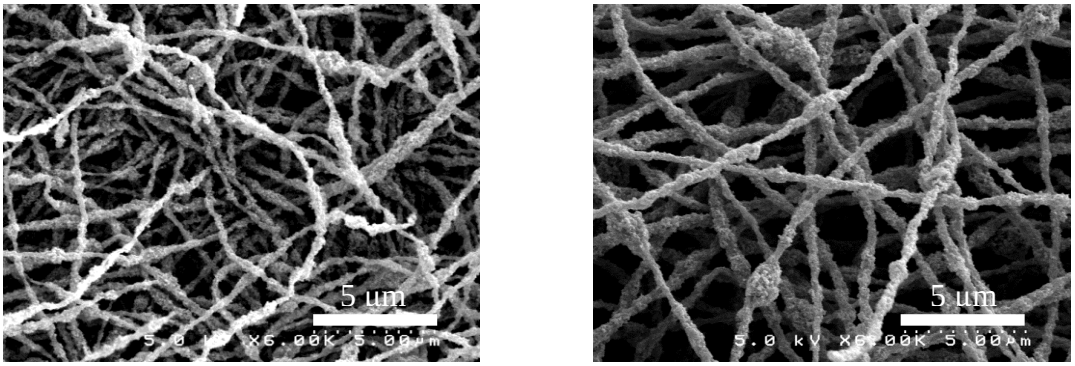

(a) **(b)**

Figure 4.8. Top-down 6,000x SEM images of an electrospun Pt/C/Nafion/PAA nanofiber mat with an average fiber diameter of: (a) 250 nm and (b) 475 nm. The Pt/C catalyst was TKK-Pt(HSAC).

Initial FC Performance of Nanofiber MEAs vs. NTCNA-sprayed MEAs - MEA tests were performed on 25 cm^2 MEAs at NTCNA using nanofiber MEAs that were fabricated at Vanderbilt University and sprayed electrode MEAs that were made at NTCNA. All MEAs were prepared with JM-Pt(Vulcan) catalyst or TKK-Pt(HSAC) catalyst cathodes and anodes, where the Pt loading of each electrode was 0.10 ± 0.005 mg/cm^2. The nanofiber MEAs had a fixed catalyst:Nafion:PAA wt ratio of 72:13:15 and a fixed average fiber diameter of 400 nm (these fiber electrodes produced high power in Vanderbilt University MEA tests). The sprayed cathodes had a catalyst:Nafion wt ratio composition of 67:33.

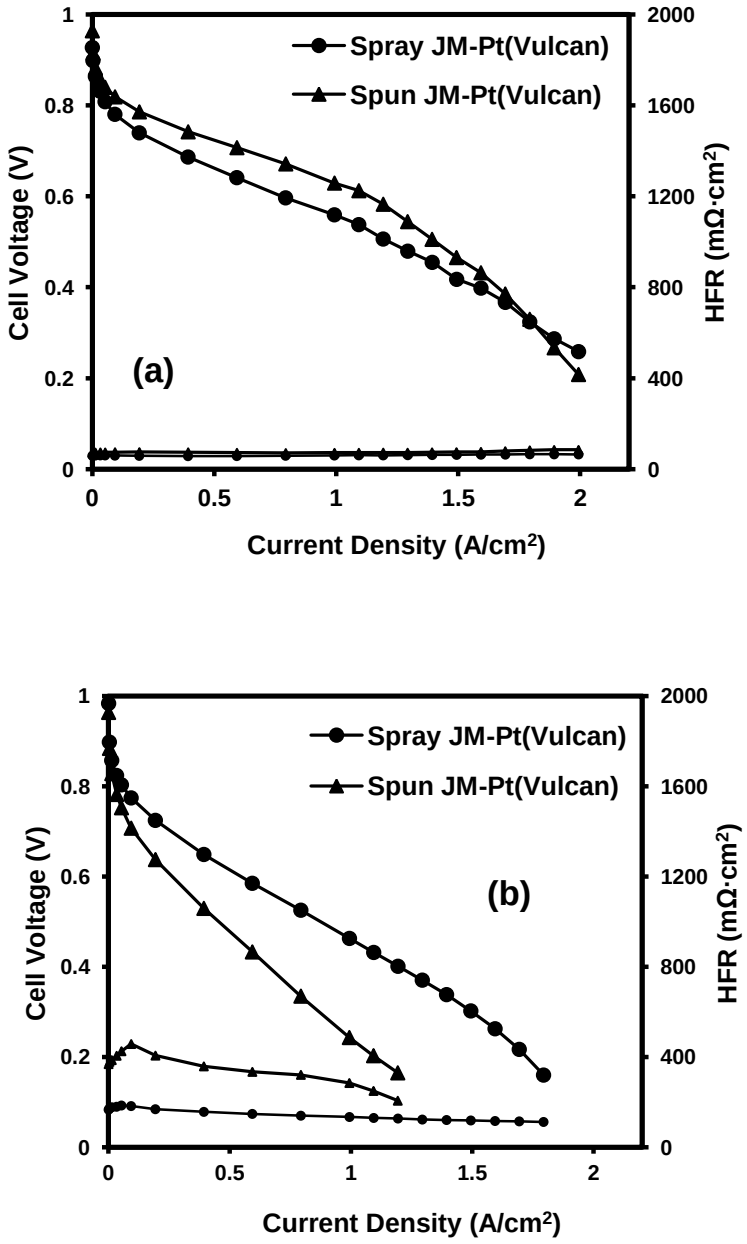

Figure 4.9. Effect of electrode morphology on MEA performance with JM-Pt(Vulcan) catalyst using a nanofiber electrode MEA and NTCNA-sprayed MEA. (a) Fuel cell performance with 100% RH feed gases and (b) fuel cell performance with 40% RH feed gases. Data were recorded at a back pressure of 1 bar with 8 NLPM air and 4 NLPM H_2 at 80°C with a NR211 membrane.

Figure 4.9 shows the effect of electrode structure (nanofibers vs. sprayed) on initial fuel cell performance. At 100% RH conditions, the nanofiber MEA produced more power over essentially the entire voltage range, as compared to the spray-coated MEA (Figure 4.9a). The difference in power densities can be attributed to an increase in the number of active catalyst sites and faster electrode kinetics as shown in Table 4.2, where the nanofiber cathode ECA is 28% higher than the measured values for an MEA with spray-coated Johnson-Matthey catalyst, and the catalytic mass activity of the electrospun fiber cathode is 84% higher than the mass activity of the sprayed MEA. It should be noted that the catalytic activities for the sprayed MEA in Table 4.2, which were measured at ambient pressure, are reasonable but lower than those reported at an elevated oxygen backpressure[22, 23].

Table 4.2. Electrochemical Surface Area, Mass Activity, and Specific Current Density for MEAs with Electrospun or Sprayed Electrodes and JM-Pt(Vulcan) Catalyst Cathodes

Electrode Type	ECA (m^2/g_{Pt})	Mass Activity* (mA/mg_{Pt})	Specific Current Density ($\mu A/cm^2_{Pt}$)
Electrospun	64	81	127
Sprayed	50	44	89

*measurements taken at 0.90 V in O_2 at ambient pressure and 100% RH

The improved performance of the nanofiber cathode is associated with an improvement in the accessibility of air/oxygen to Pt catalyst sites due to a thinner binder (Nafion + PAA) layer covering the catalyst particles and thus, better reactant mass transfer in the electrospun structure. The high sheer stresses at the spinneret tip during nanofiber electrospinning and the elongation of the fiber as it travels from the spinneret to

the collector surface during the electrospinning process thoroughly mixes binder and catalyst on a sub-micron scale and then causes a thinning of the binder coating on catalyst particles. Thus, there is a uniform distribution of binder and catalyst in the nanofibers with little or no catalyst particle agglomeration. There also appears to be better utilization of the catalyst surface area, as the ECA is higher in the electrospun layer, which is associated with more effective electron and/or proton transport to surface Pt sites.

Under low RH conditions, the spray-coated MEA showed significantly better performance than the nanofiber MEA, as shown in Figure 4.9b. This finding is attributed to nanofiber dehydration at the low RH and high feed gas flow rates used in the experiments (8 NLPM at the cathode and 4 NLPM at the anode). There appears to be rapid water expulsion from the electrospun cathode due to the combined effects of a small average fiber diameter and significant interfiber porosity throughout the entire electrode. The high HFR values support this explanation and are indicative of membrane and catalyst binder drying. It is obvious from the results in Figure 4.9 that the very high gas flow rates used in these experiments are not optimal for nanofiber MEA operation at low humidity. Since the present study focused on examining the effect of electrode morphology on durability under automotive-specific start-stop voltage cycling tests, there was no attempt to find the feed gas flow rate conditions that minimized fiber dehydration.

Effect of Load Cycling on i-V Performance (Pt Dissolution Test): The Pt active area/ECA can drop significantly under the load cycle protocol shown in Figure 4.3 due to Pt dissolution/redistribution/agglomeration, but the effect of these cathode changes on i-V performance is not particularly significant. Nonetheless, to be thorough, load cycling durability tests were performed on MEAs with electrospun nanofiber or NTCNA-sprayed electrodes. Both MEAs used TKK-Pt(HSAC) catalyst for the cathode. As shown in Table 4.3, both MEAs showed a high cathode ECA loss (40-50% after 10,000 cycles), but the resulting power loss was minimal (a 5-10% loss at 0.65 V). These results indicate that the nanofiber electrode architecture does not significantly change the way the fuel cell cathode degrades during load cycling. Thus, it can be concluded that there is no effect of electrode morphology on MEA durability for the accelerated Pt dissolution test.

Table 4.3. ECA Loss and EoL/BoL Power Output after 10,000 Load Cycles (Pt Dissolution Test) for TKK-Pt(HSAC) Catalyst

Electrode Structure	ECA Loss (%)	Power at 0.65 V EoL/BoL (100% RH)	Power at 0.65 V EoL/BoL (40% RH)
Spun	49	0.95	0.94
Spray	42	0.91	0.92

Start-Stop Cycling (Cathode Carbon Corrosion Test) - It is known that an accelerated start-stop cycling test for carbon corrosion has a much more severe impact on fuel cell power densities than Pt dissolution load cycling.[7, 20] End-of-life and beginning-of-life polarization curves from carbon corrosion tests with JM-Pt(Vulcan) catalyst are shown in Figures 4.10a and 4.10b for feed gas relative humidities of 100% and 40%, respectively. The spray-coated MEA showed severe performance losses due to carbon corrosion, significantly more than the nanofiber electrode. It should be noted, in particular, that the EoL performance for the nanofiber electrode MEA was close to the BoL performance of the conventional spray-coated MEA.

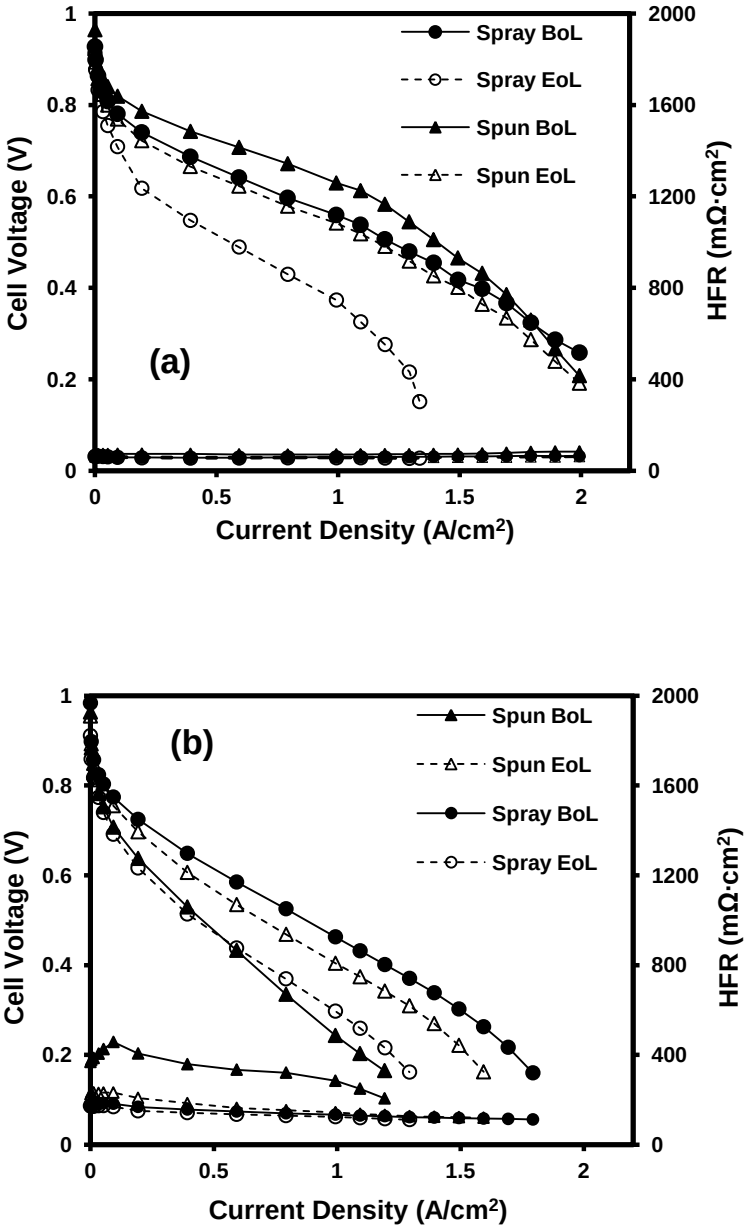

Figure 4.10. Carbon corrosion durability test results, where beginning-of-life (BoL) and end-of-life (EoL) MEA polarization plots are compared for electrospun nanofiber and sprayed electrode MEAs at: (a) 100% RH feed gases and (b) 40% RH feed gases. All data was recorded at a back pressure of 1 bar and 80°C with a NR211 membrane, JM-Pt(Vulcan) catalyst was used for all anodes and cathodes. The hydrogen and air flow rates are 4 NLPM and 8 NLPM, respectively.

The amount of CO_2 detected as a function of time in the air exhaust during the carbon corrosion tests with sprayed and electrospun electrode MEAs is shown in Figures 4.11(a and b). For both electrode morphologies, CO_2 generation increased with the number of voltage cycles, illustrating the aggressive nature of this particular accelerated stress test (repeated potential cycling has been found to be more aggressive than fixed potential hold durability tests[24]).

The cumulative (total) carbon loss for the two MEAs was essentially the same, as shown in Figure 4.11b (17% for the spray-coated electrode MEA and 18% for the nanofiber electrode MEA), suggesting that the mechanism for carbon corrosion is the same for the two electrode morphologies. Additionally, both MEAs underwent a similar BoL to EoL loss in ECA of ~40%, ending at 29 m^2/g_{Pt} for the sprayed cathode and 40 m^2/g_{Pt} for the nanofiber structure. The electrospun electrode started with a higher ECA and maintained its area advantage over the course of the carbon corrosion test.

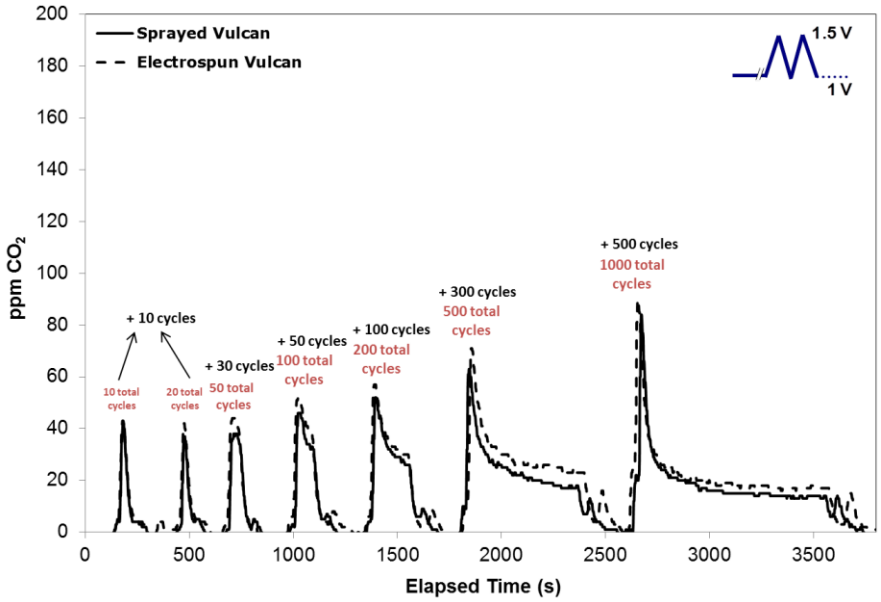

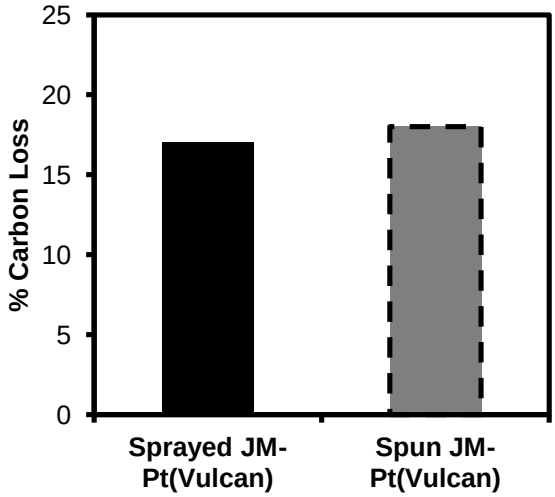

Figure 4.11. Real time measurement of CO_2 in the cathode exhaust during start-stop carbon corrosion potential cycling at 100% RH for a nanofiber and spray-coated MEAs using JM-Pt(Vulcan) catalyst. (a) ppm CO_2 detected in real time in the cathode exhaust (b) integrated total percent carbon loss at the end of the 1,000 cycles (calculated from data in 10a).

The superior EoL performance of the nanofiber MEA at full humidity is attributed to the combined effects of a higher initial ECA, the retention of the nanofiber structure at EoL, and the inter and intra fiber porosity of the nanofiber cathode mat which allows for the rapid expulsion of product water, thus preventing flooding, even when the carbon support has been oxidized and is more hydrophilic. The drop in performance of the spray-coated MEA, on the other hand, is associated with a loss in ECA and a substantial thinning/collapse of the cathode layer, causing severe oxygen mass transport and water flooding issues[25-27] . Performance losses for either MEA at 100% RH are not due to an increase in ohmic resistance, as the HFR remained unchanged before vs. after the corrosion test for both the electrospun and sprayed electrode MEAs.

The performance of the nanofiber MEA is even more impressive after voltage cycling when the power output was measured at 40% RH feed gas conditions. Here, the performance of the electrospun MEA actually *improved* after the carbon corrosion test. Its EoL performance was *significantly better* than its BoL performance, even though there was an 18% loss in carbon mass (as measured by the CO_2 sensor). After voltage cycling (and carbon support oxidation), the nanofibers were more hydrophilic and less prone to drying during fuel cell operation at low RH with the very high feed gas flow rates that were used during the accelerated tests. As expected, the spray-coated MEA showed a similar drop in EoL performance as was observed in the 100% RH results in Figure 4.10a. Better catalyst/binder hydration with the nanofiber electrode after carbon corrosion is supported by the observed decrease in HFR at EoL (there was no change in HFR for the sprayed MEA). It should be noted that the unusual nanofiber corrosion test results at low RH were reproducible, as confirmed by repeated tests with identical MEAs.

Durability experiments were also carried with TKK-Pt(HSAC) nanofiber and sprayed electrode MEAs at 0.10 mg_{Pt}/cm^2. The EoL results were qualitatively similar to those found with JM-Pt(Vulcan) catalyst for the electrospun MEAs at both 100% and 40% RH (e.g., the EoL power output was greater than that at BoL when the feed gas RH was 40%), but the sprayed TKK-Pt(HSAC) MEA exhibited a more dramatic loss in EoL power due to more severe water flooding, as compare to the test with JM-Pt(Vulcan) catalyst. A summary of BoL and EoL MEA performance at 100% and 40% RH is presented in Table 4.4 for sprayed and electrospun electrodes JM and TKK catalyst MEAs.

Table 4.4. EoL/BoL Power Output after 1,000 Start-Stop Cycles (Carbon Corrosion Test)

Humidity	Catalyst	Electrode Structure	Power at 0.65 V EoL/BoL	Max Power EoL/BoL
100%	JM-Pt(Vulcan)	Spun	0.53	0.85
	JM-Pt(Vulcan)	Spray	0.28	0.59
	TKK-Pt(HSAC)	Spun	0.58	0.83
	TKK-Pt(HSAC)	Spray	0.29	0.18
40%	JM-Pt(Vulcan)	Spun	1.71	1.54
	JM-Pt(Vulcan)	Spray	0.51	0.62
	TKK-Pt(HSAC)	Spun	3.14	2.12
	TKK-Pt(HSAC)	Spray	0.27	0.19

4.4 Conclusions

Experimental results have been presented which show that electrospinning is an effective technique for fabricating robust and high performance nanofiber fuel cell electrodes. TKK TEC10E50E catalyst (Pt on HSAC) and JM catalyst (Pt on Vulcan carbon) performed equally well in nanofiber electrode MEAs. The performance of electrospun nanofiber MEAs with TKK-Pt(HSAC) was insensitive to changes in the fiber ionomer content (Nafion 13-30 wt%). Fuel cell performance with TKK-Pt(HSAC) did not change significantly with average fiber diameter, in the range of 250 – 520 nm. Therefore, precise control of nanofiber electrode composition and fiber diameter is not required for optimum fuel cell power output, which should ease scale up and manufacturing.

Nanofiber electrode MEAs (with anode and cathode loadings of 0.1 mg_{Pt}/cm^2 each) exhibited better performance than NTCNA-sprayed MEAs under 100% RH feed gas conditions. It is believed that the nanofiber structure provides more Pt catalyst active sites and these sites are more accessible to oxygen than traditional spray-coated electrodes, due to a thinner Nafion-PAA binder layer on the Pt catalyst particles. At a very high gas feed flow rate and a low RH feed gas condition (40% RH), the electrospun MEA showed significantly higher HFR and poor i-V performance, due to fiber dehydration. Load cycling durability tests on both types of MEAs showed that the electrode structure does not have any significant impact on Pt dissolution durability. On the other hand, the nanofiber electrodes showed significantly better durability as compared to a spray-coated MEA in an automotive start-stop potential cycling test for carbon corrosion. Both sprayed and nanofiber MEAs had comparable CO_2 generation

rates and overall carbon loss (17-18%), but the spray-coated MEA exhibited a more significant performance decline. For 100% RH feed gases, the end-of-life (EoL) i-V performance of an electrospun electrode MEA was essentially the same as the beginning-of-life performance of the spray-coated MEA. This result was attributed to the absence of water flooding in the nanofiber electrodes after the carbon support was oxidized and became more hydrophilic (the morphology of a nanofiber mat promotes water removal). The superior electrode characteristics of the nanofiber structure was even more apparent at 40% RH test conditions, where the EoL performance *improved* and was *significantly better* than the BoL performance after the harsh start-stop potential cycling test even though the MEA had lost 18% of its carbon mass. This results is associated with a more optimal water content/hydration in the nanofiber electrode mat due to the increased hydrophilicity/water retention of the carbon support after start-stop potential cycling. Thus, nanofiber electrode MEAs showed both better initial power output *and* a less severe performance drop after start-stop durability cycling than sprayed electrode MEAs.

4.5 References

(1) Litster, S. and G. McLean (**2004**) *Journal of Power Sources*, 130, 61-76.

(2) Long, N. V., Y. Yang, C. Minh Thi, N. V. Minh, Y. Cao, and M. Nogami (**2013**) *Nano Energy*, 2, 636-676.

(3) Ma, Y., H. Zhang, H. Zhong, T. Xu, H. Jin, and X. Geng (**2010**) *Catalysis Communications*, 11, 434-437.

(4) Serov, A., M. H. Robson, M. Smolnik, and P. Atanassov (**2013**) *Electrochimica Acta*, 109, 433-439.

(5) Othman, R., A. L. Dicks, and Z. Zhu (**2012**) *International Journal of Hydrogen Energy*, 37, 357-372.

(6) Kocha, S. S., *Chapter 3 - Electrochemical Degradation: Electrocatalyst and Support Durability*, in *Polymer Electrolyte Fuel Cell Degradation*, M.M. Mench, E.C. Kumbur, and T.N. Veziroglu, Editors. 2012, Academic Press: Boston. p. 89-214.

(7) Parrondo, J., T. Han, E. Niangar, C. Wang, N. Dale, K. Adjemian, and V. Ramani (**2014**) *Proceedings of the National Academy of Sciences*, 111, 45-50.

(8) Stassi, A., I. Gatto, V. Baglio, E. Passalacqua, and A. S. Aricò (**2013**) *Applied Catalysis B: Environmental*, 142–143, 15-24.

(9) Kumar, A. and V. K. Ramani (**2013**) *Applied Catalysis B: Environmental*, 138–139, 43-50.

(10) Hara, M., M. Lee, C.-H. Liu, B.-H. Chen, Y. Yamashita, M. Uchida, H. Uchida, and M. Watanabe (**2012**) *Electrochimica Acta*, 70, 171-181.

(11) Wilson, M. S. and S. Gottesfeld (**1992**) *Journal of Applied Electrochemistry*, 22, 1-7.

(12) Ralph, T. R., G. A. Hards, J. E. Keating, S. A. Campbell, D. P. Wilkinson, M. Davis, J. St-Pierre, and M. C. Johnson (**1997**) *J. Electrochem. Soc.*, 144, 3845-3857.

(13) Ren, X., M. S. Wilson, and S. Gottesfeld (**1996**) *J. Electrochem. Soc.*, 143, L12-L15.

(14) Martin, S., P. L. Garcia-Ybarra, and J. L. Castillo (**2010**) *Journal of Power Sources*, 195, 2443-2449.

(15) Debe, M. K., A. K. Schmoeckel, G. D. Vernstrorn, and R. Atanasoski (**2006**) *Journal of Power Sources*, 161, 1002-1011.

(16) Zhang, W. and P. N. Pintauro (**2011**) *ChemSusChem*, 4, 1753-1757.

(17) Brodt, M., R. Wycisk, and P. N. Pintauro (**2013**) *J. Electrochem. Soc.*, 160, F744-F749.

(18) Ballengee, J. B. and P. N. Pintauro (**2011**) *J. Electrochem. Soc.*, 158, B568-B572.

(19) Ohma, A., K. Shinohara, A. Iiyama, T. Yoshida, and A. Daimaru (**2011**) *ECS Transactions*, 41, 775-784.

(20) Niangar, E., T. Han, N. Dale, and K. Adjemian (**2013**) *ECS Transactions*, 50, 1599-1606.

(21) Chen, H., J. D. Snyder, and Y. A. Elabd (**2007**) *Macromolecules*, 41, 128-135.

(22) Gasteiger, H. A., S. S. Kocha, B. Sompalli, and F. T. Wagner (**2005**) *Applied Catalysis B: Environmental*, 56, 9-35.

(23) Liu, Y., M. W. Murphy, D. R. Baker, W. Gu, C. Ji, J. Jorne, and H. A. Gasteiger (**2009**) *J. Electrochem. Soc.*, 156, B970-B980.

(24) Shao, Y., J. Wang, R. Kou, M. Engelhard, J. Liu, Y. Wang, and Y. Lin (**2009**) *Electrochimica Acta*, 54, 3109-3114.

(25) Hashimasa, Y., T. Shimizu, Y. Matsuda, D. Imamura, and M. Akai (**2013**) *ECS Transactions*, 50, 723-732.

(26) Meyers, J. P. and R. M. Darling (**2006**) *J. Electrochem. Soc.*, 153, A1432-A1442.

(27) Young, A. P., J. Stumper, and E. Gyenge (**2009**) *J. Electrochem. Soc.*, 156, B913-B922.

Chapter V

POWER OUTPUT AND DURABILITY OF NANOFIBER CATHODES WITH PVDF AND NAFION/PVDF CATALYST BINDERS IN HYDROGEN/AIR FUEL CELLS

5.1 Introduction

The hydrogen/air proton-exchange membrane fuel cell is an efficient energy conversion device with high power output at moderate operating temperatures. It is a promising candidate for emission-free automotive power plants, but issues remain regarding the high cost and problematic durability of membrane-electrode-assemblies (MEAs)[1]. For commercialization, the Pt loading of fuel cell MEAs (particularly the cathode) must be reduced while maintaining high power output and the catalytic activity of the cathode for electrochemical oxygen reduction must be maintained for long-term operation with various power cycles and numerous stack start-ups and shut-downs.[2]

In a series of previous papers, Pintauro and coworkers have shown that an electrospun nanofiber cathode, composed of Pt/C particles and a binder of Nafion + poly(acrylic acid) (abbreviated as PAA) performs remarkably well in a hydrogen/air proton exchange membrane fuel cell.[3-5] For example, a nanofiber electrode MEA with a 0.055 mg_{Pt}/cm^2 cathode and 0.059 mg_{Pt}/cm^2 anode produced more than 900 mW/cm^2 at maximum power in a H_2/air fuel cell at 80°C, 100% RH, and high feed gas flow rates at 2 atm backpressure. In a recent collaborative study between Vanderbilt University and Nissan Technical Center North America, Brodt *et al.*[5] showed that MEAs with an electrospun particle/polymer cathode generated high beginning-of-life power and also exhibited excellent durability, as determined from end-of-life polarization curves after an

accelerated start-stop voltage cycling (carbon corrosion) test. Thus, after 1,000 simulated start-stop cycles, a nanofiber MEA with Johnson Matthey Pt/C catalyst and a binder of Nafion + PAA maintained 53% of its initial power at 0.65 V and 85% of its maximum power, as compared to a 28% power retention at 0.65 V and 58% maximum power for a sprayed electrode MEA. The excellent initial performance of nanofiber fuel cell electrodes was attributed to the unique nanofiber electrode morphology, with inter-fiber and intra-fiber porosity which results in better accessibility of oxygen to Pt catalyst sites and efficient removal of product water. The superior end-of-life performance of the nanofiber MEA after a carbon corrosion test was attributed to the combined effects of a high initial electrochemical cathode surface area, the retention of the nanofiber structure after testing (no collapse of the cathode, as confirmed by SEM imaging), and the rapid/effective expulsion of product water from the cathode which minimizes/eliminates flooding.

In the present paper, we present new results on the initial power and carbon corrosion durability of nanofiber cathode MEAs with different cathode binders. Experiments focused on finding binder compositions that minimize carbon corrosion of the cathode catalyst layer of an MEA. Cathode carbon corrosion occurs in a hydrogen/air fuel cell stack when a hydrogen-air mixture is present in the anode during start-up. The resulting spike in the cathode voltage to a potential of about 1.5 V vs. SHE produces severe corrosion of the carbon support material of the cathode catalyst, with associated damage by electrode layer thinning and disintegration, platinum nanoparticle agglomeration, and the loss of catalytically active platinum surface area.[6, 7] Surface oxides may also form, making the cathode layer more hydrophilic and prone to water

flooding, which drastically reduces oxygen access to active catalytic sites.[8] System control strategies have been sought to minimize these voltage spikes, but no practical solutions have emerged to eliminate the problem.[9] At the materials level, researchers have been investigating new catalyst supports that are not susceptible to corrosion, including metal oxides and thermally treated carbon supported catalysts.[10-13] Another approach is the complete removal of all Pt support material from the cathode layer, as is the case with 3M Company's nanostructure thin film structured Pt whisker electrodes.[14]

The approach taken in the present study was to focus on the role of water during cathode carbon corrosion and to minimize/alter the concentration of water at the surface of Pt/C particles. Since water is directly involved in the electrochemical oxidation of the carbon support material in a fuel cell cathode[14] (via Equation 1), it is expected that the introduction of a hydrophobic polymer, such as poly(vinylidene fluoride) (henceforth abbreviated as PVDF) into the cathode catalyst binder will slow carbon corrosion rates.

$$C + 2H_2O \rightarrow CO_2 + 4H^+ + 4e^- \qquad \text{(Eq. 1)}$$

The use of a PVDF electrode binder, however, is challenging because it does not conduct protons and its oxygen permeability is low. Nevertheless, it has been used with some success as the electrode binder in PBI-based hydrogen/air fuel cell electrodes.[15] In the present study both PVDF and Nafion/PVDF blended binders have been investigated, where the presence of some Nafion improves proton conductivity and oxygen transport rates. It is well known that Nafion and PVDF are incompatible/immiscible polymers which phase-separate when solution cast into thin film membranes.[16] We have found that well-mixed PVDF/Nafion blends with nm-domains, can be prepared by electrospinning

Nafion + PVDF mixtures.[17] The present chapter does not deal with the chemistry/morphology of Nafion/PVDF blended fibers, but only on the use of these blends as binders in hydrogen/air fuel cell cathodes. Oh *et al.*[18] wrote that the hydrophobicity of the catalyst carbon surface is a critical factor in determining its corrosion resistance in an MEA fuel cell. This chapter will investigate if the corrosion resistance of carbon based cathodes can also be improved by using a more hydrophobic catalyst binder, rather than changing the catalyst support.

To investigate the hypothesis that one can affect the corrosion resistance of fuel cell cathodes by adjusting the hydrophobicity/hydrophilicity of the cathode binder, a series of electrospun nanofiber MEAs were prepared and evaluated, where the cathode fiber mat binder was either neat PVDF or various Nafion/PVDF blends with weight ratios ranging from 20/80 to 80/20. Methods for electrospinning high Pt/C content nanofibers with these new binders were identified and MEAs were fabricated with the resulting nanofiber mat electrodes. Fuel cell test focused on comparing beginning-of-life (BoL) and end-of-life (EoL) fuel cell power output after a carbon corrosion voltage cycling experiment for various nanofiber cathode MEAs and for MEAs with conventional painted GDE cathodes of the same binder composition and Pt loading.

5.2 Experimental

5.2.1. *Materials*

Johnson Matthey HiSpec® 4000 (40% Pt on Vulcan carbon) catalyst was used for all electrodes. 450 kDa molecular weight poly(acrylic acid) (PAA) was purchased from Sigma Aldrich, from which a 15 wt% stock solution was created in 2:1 (w:w) isopropanol

(IPA):water solvent. Kynar® HSV 900 polyvinylidene fluoride (Arkema, Inc.) was used to prepare a 10 wt% stock solution in 7:3 (w:w) dimethylformamide (DMF):acetone. 1100 EW Nafion® ion resin (purchased from Ion Power®) was dried to solid crystals and used to make two different stock solutions: (1) a 20 wt% Nafion solution in 2:1 (w:w) n-propanol:water, for inks containing PAA and (2) a 20 wt% Nafion solution in 7:3 (w:w) DMF:acetone for inks made with PVDF.

5.2.2 Electrospinning Electrodes - Table 5.1 lists the compositions for each cathode electrospinning ink and final dry nanofiber cathode. Inks were prepared using the following sequence: (i) wetting catalyst with water (ink 1 in Table 5.1) or DMF (inks 2-7), (ii) adding the appropriate amount of isopropanol (IPA) (ink 1), tetrahydrofuran (THF) (inks 2-6), or acetone (ink 7), (iii) adding the appropriate weight of Nafion via stock solutions A or B (defined in Table 5.1), (iv) sonicating the suspension for 90 minutes with intermittent mechanical stirring, (v) adding PAA (stock solution C for ink 1) or PVDF (stock solution D for inks 2-7), and (vi) stirring the ink mechanically for 12 hours. The final inks contained catalyst powder with (i) Nafion and PAA in alcohol/water solvent, (ii) PVDF in DMF/acetone, or (iii) Nafion + PVDF in a solvent of DMF/THF/acetone. Nafion lacks the necessary chain entanglements and will not electrospin into well-formed fibers unless a suitable carrier polymer is added to the electrospinning solution[19]. In the present study, PAA or PVDF acted as the carrier.

Table 5.1. Electrospinning Ink Composition and Final Dry Nanofiber Composition of Electrospun Cathodes

Ink	Ink Composition (g)	Dry Electrode Composition Wt%
1	0.20 g catalyst, 0.80 g water, 0.53 g IPA, 0.37 g stock solution A[1], 0.25 g stock solution C[3]	64 catalyst, 24 Nafion, 12 PAA
2	0.20 g catalyst, 0.27 g DMF, 0.80 g THF, 0.34 g stock solution B[2], 0.173 g stock solution D[4]	70 catalyst, 24 Nafion, 6 PVDF
3	0.20 g catalyst, 0.67 g DMF, 0.60 g THF, 0.29 g stock solution B, 0.29 g stock solution D	70 catalyst, 20 Nafion, 10 PVDF
4	0.20 g catalyst, 0.52 g DMF, 0.52 g THF, 0.214 g stock Solution B, 0.43 g stock solution D	70 catalyst, 15 Nafion, 15 PVDF
5	0.20 g catalyst, 0.78 g DMF, 0.68 g THF, 0.145 g stock solution B , 0.57 g stock solution D	70 catalyst, 10 Nafion, 20 PVDF
6	0.20 g catalyst, 0.85 g DMF, 0.75 g THF, 0.09 g stock solution B, 0.70 g stock solution D	70 catalyst, 6 Nafion, 24 PVDF
7	0.20 g catalyst, 0.30 g DMF, 1.6 g acetone, 0.87 g stock solution D	70 catalyst, 30 PVDF

[1]Stock Solution A: 20 wt% Nafion in 2:1 n-propanol:water w:w

[2]Stock Solution B: 20 wt% Nafion, in 7:3 DMF:acetone w:w

[3]Stock Solution C: 15 wt% PAA in 2:1 IPA:water w:w

[4]Stock Solution D: 10 wt% PVDF in 7:3 DMF:acetone w:w

Electrospinning was performed at room temperature in a custom-built environmental chamber with relative humidity control.[18] An ink was drawn into a 3 mL syringe and electrospun using a single 22-gauge stainless steel single orifice needle

spinneret, where the needle tip was polarized to a high positive potential relative to a grounded stainless steel rotating drum collector. The spinneret-to-collector distance was fixed at 10 cm and the flow rate of ink was held constant for all experiments at 1.0 mL/h. Nanofibers were collected on aluminum foil that was attached to the collector drum,. The drum rotated at a speed of 100 rpm and oscillated horizontally to improve the uniformity of a deposited nanofiber mat. The voltage was in the 12-15 kV range for all ink recipes. Ink 1 (Table 5.1) was electrospun at 40% RH and inks 2-7 were electrospun at 50-70% RH.

5.2.3 SEM Imaging of Nanofiber Mats – Top-down SEM images of electrospun nanofiber mats were taken with a Hitachi S4200 Scanning Electron Microscope with a 5.0 kV electron beam. Prior to imaging, the mats were lightly pressed at room temperature onto conductive SEM tape and then sputter coated with a thin layer of gold to improve contrast.

5.2.4 Membrane-Electrode-Assembly (MEA) Preparation - CCMs (Catalyst Coated Membranes) with nanofiber electrodes were fabricated by hot pressing 5 cm^2 electrospun particle/polymer nanofiber mats onto the opposing surfaces of a Nafion 211 membrane at 140^oC and 5 MPa for 1 minute, after a 10-minute pre-heating period at 140^oC with no applied pressure. The Pt loading of a nanofiber mat was calculated from the total electrode weight and the weight-fraction of Pt/C catalyst used in the electrospinning ink.

Carbon paper gas diffusion layers (GDLs) (Sigracet 25 BC GDL) were physically pressed onto a CCM's anode and cathode while in the fuel cell test fixture to form an MEA.

Painted gas diffusion electrodes (GDEs) were also fabricated. Catalyst/PVDF or catalyst/Nafion/PVDF inks were painted in multiple layers directly onto a carbon paper gas diffusion layer (Sigracet GDL 25 BC) and dried at 70^{o}C for 30 minutes after depositing each layer. The same Nafion/PVDF ink recipes (inks 2-7 in Table 5.1) were used for the painted GDEs, except an additional 1.0 g of DMF and 1.0 g of acetone was added to each ink, in order to decrease the ink viscosity so that thin layers could be easily spread onto the carbon paper. Conventional cathode GDEs were also prepared with a composition of 70 wt% catalyst and 30% Nafion, using n-propanol/water as the solvent. All painted GDEs (5 cm^2 in geometric area) were hot pressed onto Nafion 211 membranes at 140°C and 5 MPa for 1 minute after a 10 minute pre-heating step at 140^{o}C with no applied pressure (same conditions as the nanofiber electrodes).

The Pt loading of both nanofiber and GDE cathodes was fixed at 0.10 mg/cm^2. All nanofiber and GDE cathode MEAs contained a nanofiber anode with Nafion/PAA binder (electrospinning ink 1 from Table 5.1) at a Pt loading of 0.10 mg/cm^2.

5.2.5 Fuel Cell Tests - Fuel cell tests were performed on 5 cm^2 MEAs, using a Scribner Series 850e test station with mass flow, temperature, and manual backpressure control. The fuel cell test fixture accommodated a single MEA and contained single anode and cathode serpentine flow channels. Experiments with fully humidified H_2 and air at atmospheric (ambient) pressure were performed at 80°C where the H_2 flow rate was 125 sccm and the airflow rate was 500 sccm. Prior to collecting polarization data, MEAs

were pre-conditioned at 80°C with fully humidified air and hydrogen by alternating every 2 minutes between operation at 150 mA/cm^2 and 0.2 V. This break-in process was continued until steady-state was achieved (typically ~4 hours, but as long as 12 hours for cathodes with a neat PVDF binder). Polarization curves were generated by measuring the voltage at a given current in the anodic (positive voltage) direction after waiting two minutes for system stabilization. High frequency resistance (HFR) data were collected at 6000 Hz.

5.2.6 Electrochemical Surface Area (ECA) – In-situ cyclic voltammetry (CV) measurements were performed on 5 cm^2 MEAs, with a sweep rate of 20 mV/s, where a H_2-purged anode served as both counter and reference electrodes and N_2 was fed to the working cathode. The fuel cell test fixture was operated at 30^{o}C with gas feed streams at a dew point of 30^{o}C (fully humidified). A cyclic voltammogram was generated between +0.04 V and +0.9 V vs. SHE and the electrochemically active surface area was determined from the integrated area above the hydrogen adsorption portion of the curve (corresponding to a voltage range of approximately +0.1 to +0.4 V), where the charge required to reduce one monolayer of hydrogen atoms on Pt was assumed to be 210 μC/cm^2.

5.2.7 Durability Tests - MEAs were tested under the Fuel Cell Commercialization Conference of Japan's (FCCJ) standard start-stop potential cycling protocol.[20] For a carbon corrosion accelerated durability test, the voltage at the cathode was cycled between 1.0 and 1.5 V at a scan rate 500 mV/s with a triangular wave. 1,000 total voltage cycles were performed on a single MEA, where the fuel cell was supplied with 125 sccm H_2

at the anode and 250 sccm N_2 at the cathode (both feed gases were fully humidified at ambient pressure). Beginning-of-life (BoL) and end-of-life (EoL) polarization curves were collected as well as intermittent polarization curves at cycle number 100, 250, and 500. This accelerated durability test simulates start-up and shut-down of a stack without the application of any operational controls that may mitigate fuel cell performance losses. CO_2 monitoring of the cathode exhaust, using a non-dispersive infrared CO_2 detector from CO2 Meter Inc. (Model No. CM-0152), provided an additional experimental tool for measuring carbon corrosion during the accelerated potential cycling tests. Nafion tubing and a water-trap upstream to the detector inlet removed moisture from the CO_2-containing stream. The highly selective and semi-permeable Nafion tubing allowed water vapor transfer from the cathode exhaust stream to the drier ambient air, but it did not allow transfer of CO_2.

5.3 Results and Discussion

5.3.1 Analysis of Nanofiber Cathodes with Nafion/PAA, Nafion/PVDF or neat PVDF Binder – It was shown in Chapter 4 of this dissertation that MEAs with nanofiber mat cathodes composed of Pt/C powder and Nafion/poly(acrylic acid) (abbreviated as PAA) as the catalyst binder produce higher power at beginning-of-life (BoL) and have better durability after an accelerated carbon corrosion test, as compared to MEAs with a conventional GDE slurry cathode.[5] In this new set of experiments, polyvinylidene fluoride (PVDF) was investigated as: (1) a carrier polymer for Nafion fiber electrospinning (an alternative to PAA) and (2) the sole binder or a blending agent with Nafion that will increase the hydrophobicity of the cathode. Initial MEA fuel cell tests were performed with two limiting case PVDF-containing binders: (1) neat PVDF and (2)

80/20 wt% Nafion/PVDF, which represents the minimum PVDF content required to electrospin well-formed electrode fibers with Nafion and Pt/C powder. The final (dry) cathode fiber composition for these two cases is 70 wt% Pt/C and 30 wt% PVDF for the neat PVDF mat case and 70 wt% Pt/C, 24 wt% Nafion, and 6 wt% PVDF for the 80/20 Nafion/PVDF mat. As shown by the SEM images in Figure 5.1, electrospun catalyst mats with PVDF and Nafion/PVDF binders appear to be highly porous with a roughened surface. The overall fiber/mat morphology is nearly identical to catalyst fibers electrospun with Nafion/PAA binder as reported previously[4], although 80/20 Nafion/PVDF fibers had more variability along the fiber length. The mat with a neat PVDF binder had an average fiber diameter of 620 nm and the average fiber diameter for the 80/20 Nafion/PVDF mat was 450 nm. We have reported previously that such differences in fiber diameter (for cathodes with a Nafion + PAA binder) have no effect on fuel cell performance.[5]

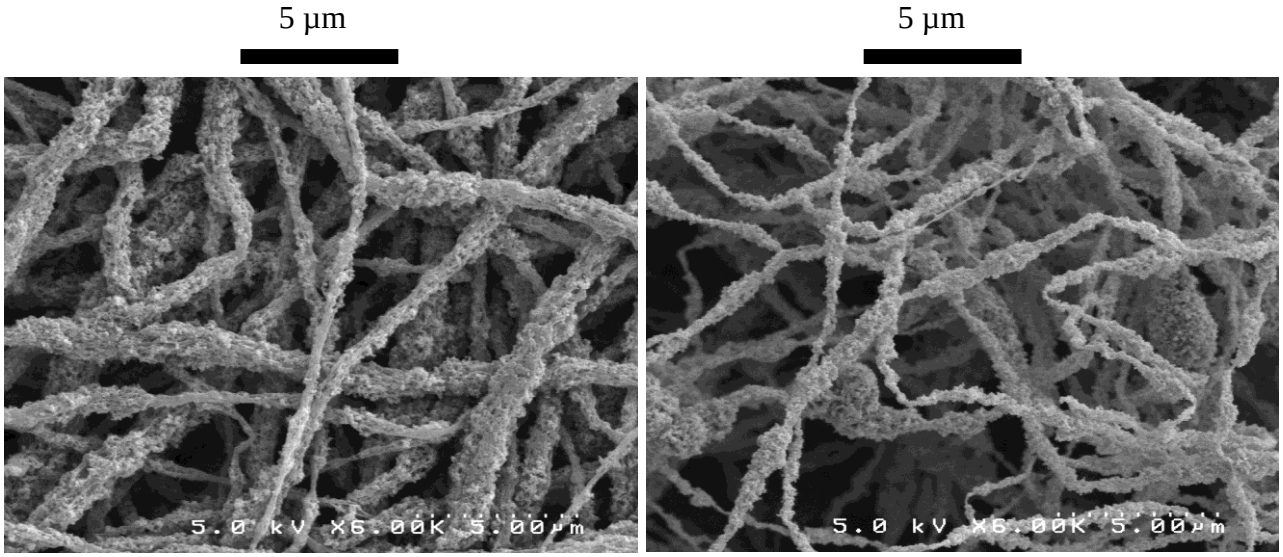

Figure 5.1. Top-down 6,000x SEM images of: (a) an electrospun Pt/C-PVDF nanofiber mat (fiber composition: 70 wt% Pt/C powder and 30 wt% PVDF) and (b) an electrospun Pt/C-Nafion/PVDF nanofiber mat with a binder of 80/20 Nafion/PVDF w/w (fiber composition: 70 wt% Pt/C powder, 24 wt% Nafion, and 6 wt% PVDF).

In Figure 5.2, hydrogen/air fuel cell polarization curves are shown for MEAs with cathodes containing Nafion/PVDF (80/20 wt%) and neat PVDF binders at a cathode Pt loading of 0.10 mg/cm^2. For comparison, V-i data are also presented for a 0. 10 mg/cm^2 nanofiber cathode with a binder of Nafion/PAA (ink 1 in Table 5.1) where the fiber composition is 64 wt% Pt/C, 24 wt% Nafion, and 12 wt% PAA. Data were collected at 80°C with air and hydrogen at ambient pressure and 100% relative humidity (RH). The Nafion/PVDF and Nafion/PAA cathode MEAs generated similar polarization curves, with the Nafion/PVDF cathode MEA having slightly higher current densities at voltages < 0.65 V and slightly smaller current densities at voltages > 0.65 V. The neat PVDF cathode MEA, with no proton conducting ionomer in the cathode binder, worked surprisingly well (current densities > 1 A/cm^2 were achieved), but not at the same

performance level as the MEAs with Nafion/PVDF or Nafion/PAA binder. It should be noted that for all MEAs in this chapter, the nanofiber anode was of the same composition and morphology, so any changes in MEA power output could be attributed to the functioning of the cathode.

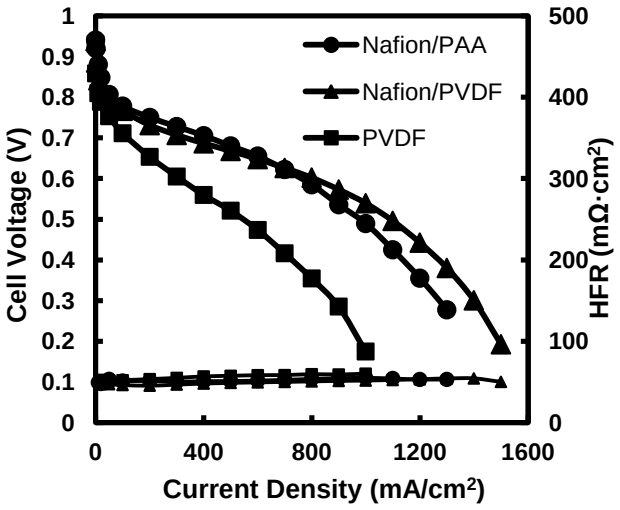

Figure 5.2. Beginning-of-life polarization curves for 5 cm^2 MEAs with a Nafion 211 membrane, a 0.10 mg_{Pt}/cm^2 electrospun cathode and a 0.10 mg_{Pt}/cm^2 electrospun anode. Fuel cell operating conditions: 80°C, 125 sccm H_2 and 500 sccm air at ambient pressure and 100% RH. The cathode binder (w/w) is : (●) Nafion/PAA (67/33), (▲) Nafion/PVDF (80/20), or (■) PVDF.

The greater activation overpotentials and slightly lower power in the high voltage region of the V-i curve for the Nafion/PVDF MEA as compared to the Nafion/PAA MEA is associated with differences in the electrocatalytic activity of the Pt/C cathode catalyst.

The reduction in catalyst activity of the Nafion/PVDF cathode could be due to either a lower concentration of oxygen at the catalyst surface, because the oxygen permeability in PVDF is low (~0.09 barrers,[21] which is about two orders of magnitude lower than that in wet Nafion[22]) or due to less water at the catalyst surface (water is needed for fast ORR kinetics[23]). The slopes of the fuel cell polarization curves for the Nafion/PAA and Nafion/PVDF binders were essentially identical in the ohmic region, suggesting that there is sufficient Nafion in the Nafion/PVDF binder for proton conduction. Despite the low oxygen permeability of PVDF, the Nafion/PVDF cathode MEA had smaller voltage losses than the Nafion/PAA in the mass transfer (high current) region of the polarization curve, indicating that the addition of PVDF to the Nafion is aiding rather than hindering mass transfer. The Nafion/PVDF cathode MEA produced 13% higher maximum power than the MEA with a Nafion/PAA binder cathode (545 vs. 484 mW/cm^2). The presence of PVDF makes Nafion binder more hydrophobic and this hydrophobicity appears to aid in repelling product water from the cathode. Thus, an improvement in water expulsion in the high current region of the polarization curve in Figure 5.2 due to the hydrophobicity of PVDF outweighs any detrimental effects of PVDF on oxygen permeability. Thus, an 80/20 wt% Nafion/PVDF cathode binder is an acceptable alternative to a Nafion/PAA binder and might be preferable for high power operation. An improvement in cathode mass transfer due to an increase in binder hydrophobicity has been reported previously by Song *et al.*[24] who found that an MEA with a cathode binder composed of 5 wt% polytetrafluoroethylene (PTFE) and 95% Nafion had lower ORR catalytic activity, but produced more power during fuel cell operation (e.g. ~20% more power at 0.4 V), as compared to a standard Nafion binder MEA. The authors concluded that the addition of

hydrophobic PTFE to Nafion improved water removal and thus indirectly assisted in oxygen access to catalytic sites.

While the addition of 20 wt% PVDF to the Nafion cathode binder was found to be acceptable and even beneficial in the high current region, the use of a neat PVDF cathode binder resulted in much lower fuel cell performance. The kinetic region of the neat PVDF polarization curve showed higher activation/kinetic losses than the Nafion/PVDF and Nafion/PAA binder cases. The HFR of the neat PVDF MEA was not significantly different than the Nafion/PAA and Nafion/PVDF MEAs, but this measurement is more reflective of the membrane/electrode contact resistance[25] and is not an indicator of the binder's proton conductivity. In the ohmic region of the polarization curve, the neat PVDF MEA exhibited significantly higher voltage losses, as expected since this polymer does not conduct protons. Proton conduction in ionomer-free fuel cell cathodes has been observed and associated with Pt/C catalyst surface oxides and the presence of water at the Pt/C catalyst surface, but the general phenomenon is not well understood[26-27] and it is not known if such surface oxide species are affecting cathode performance in the present study.

5.3.2. The Effect of Binder Composition (Nafion/PVDF Weight Ratio) on Nanofiber Cathode Performance and Comparison to a Conventional Nafion GDE– These tests expanded on the preliminary studies, above, to investigate Nafion/PVDF binder compositions with a PVDF content wt% between 20 and 100%, i.e., nanofiber cathode MEAs were also fabricated with Nafion/PVDF ratios of 67/33, 50/50, 33/67, and 20/80. The purpose of these experiments was to determine the effect of Nafion/PVDF ratio on

initial fuel cell performance as well as the cathode durability after an accelerated carbon corrosion test, where the results are compared to a conventional painted GDE cathode MEA with a Nafion binder. For all cathodes, the Pt loading was fixed at 0.10 mg/cm^2 and the total binder content was constant relative to the amount of catalyst at 30 wt% binder.

Figure 5.3a compares the beginning-of-life (BoL) polarization curves of the nanofiber Nafion/PVDF cathode MEAs with six different Nafion/PVDF ratios to a conventional Nafion GDE MEA (with no PVDF and no PAA in the cathode binder). Figure 5.83b shows the end-of-life (EoL) polarization curves of the same MEAs after 1,000 voltage cycles between 1.0-1.5 V vs. SHE (an accelerated carbon corrosion test experiment that simulates start/stop cycling). The polarization curves of the nanofiber Nafion/PVDF MEAs are shown as solid, unbroken lines and a conventional GDE MEA with 70% Pt/C and 30 wt% Nafion in the cathode binder is shown as a dashed line. A nanofiber anode (0.1 mg/cm^2 Pt loading with a binder of Nafion/PAA) was employed for all MEAs.

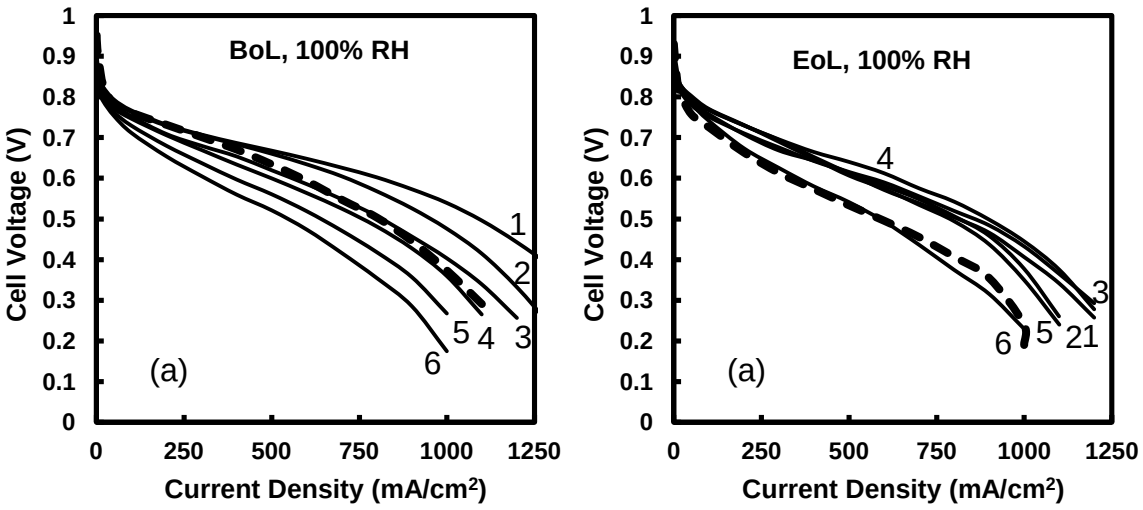

Figure 5.3. Polarization curves for MEAs with electrospun Nafion/PVDF cathodes (unbroken lines) and an MEA with a conventional painted GDE cathode with 70 wt% Pt/C and 30 wt% Nafion (dashed line). The electrospun cathode Nafion/PVDF w/w are: (1) 80/20, (2) 67/33, (3) 50/50, (4) 33/67, (5) 20/80, and (6) 0/100. All MEAs are 5 cm^2 and contain a Nafion 211 membrane and 0.10 mg_{Pt}/cm^2 at the cathode and anode. Fuel cell operating conditions are 80°C, 125 sccm H_2 and 500 sccm air at ambient pressure and 100% RH. (a) BoL data, (b) EoL data.

As shown in Figure 5.3a, as the PVDF cathode binder content was increased from 20 wt% to 100 wt%, the initial fuel cell performance decreased throughout the entire voltage range. Also, the conventional cathode MEA produced similar current densities as a nanofiber 80/20 and 67/33 Nafion/PVDF cathode MEAs in the kinetic region, up to ~0.7 V (i.e., these MEAs have similar overpotenial losses). The Nafion GDE MEA performed better than nanofiber Nafion/PVDF MEAs with more than 33% PVDF binder at voltages over 0.7 V. At lower voltages (higher current densities), where water removal is more important, the nanofiber Nafion/PVDF cathode MEAs with 20-50 wt% PVDF worked significantly better than the conventional GDE MEA. The nanofiber structure

with inter-fiber and intra-fiber porosity, with some hydrophobic PVDF present seems to prevent water accumulation in the cathode, thus increasing oxygen mass transfer to active Pt sites. Nanofiber Nafion/PVDF MEAs with the highest PVDF content (67, 80, and 100 wt%) did not work particularly well, with smaller current densities at all voltages, as compared to the conventional cathode MEA due to higher activation losses and higher ohmic losses.

After the carbon corrosion test, at EoL (Figure 5.3b), there was a much smaller difference in power output among the Nafion/PVDF nanofiber cathode MEAs. MEAs with less than 50 wt% PVDF content in the cathode binder exhibited a decrease in power density, as expected, but MEAs with a PVDF content greater than 50 wt% showed an increase in power after the accelerated corrosion test. This is a new and unexpected result. After the corrosion test, all Nafion/PVDF nanofiber cathode MEAs work significantly better than the conventional Nafion GDE MEA. At EoL, the polarization curves for the conventional MEA and the neat PVDF cathode binder nanofiber MEA were similar, another surprising and important result.

5.3.3. Comparison of Nanofiber and Painted GDE Nafion/PVDF Cathode MEAs at BoL and EoL– In order to decouple the effects of nanofiber morphology and Nafion/PVDF binder compositions, painted GDEs were created and tested with the same binder as the nanofibers in Figure 5.3. The MEA polarization curves with nanofiber cathodes are compared to MEAs with painted GDE cathodes of the same composition in Figure 5.4. Each plot shows one binder composition for nanofiber and GDE cathode MEAs at BoL and EoL. HFR data are not shown because: (1) there was no significant difference in

HFR for nanofiber or painted cathode GDEs at all cathode binder compositions, for both BoL and EoL and (2) the BoL HFR data were consistent with numbers in the literature,[27] e.g., at 100% RH and 40% RH the HFR was 50 ± 5 $m\Omega \cdot cm^2$ and 220 ± 20 $m\Omega \cdot cm^2$, respectively. The similarity in HFR values for the different electrodes at EoL and BoL indicates good membrane/electrode adhesion and no membrane degradation or increase in resistance at the membrane-electrode interface during a voltage cycling test[28, 29] so all differences in fuel cell power output at BoL and EoL are due to changes at the cathode.

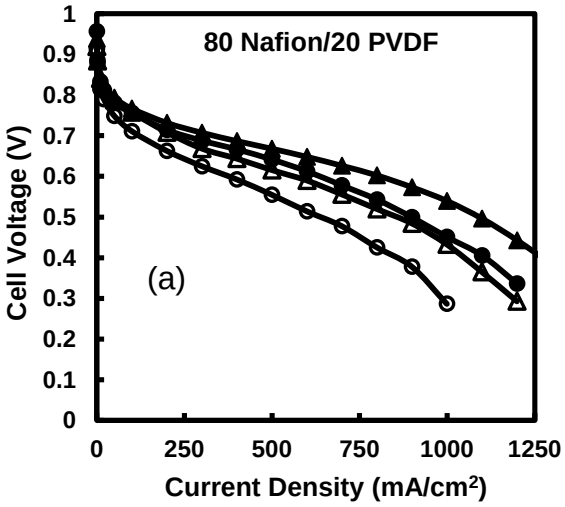
80 Nafion/20 PVDF
(a)
Cell Voltage (V)
Current Density (mA/cm²)
0
0.1
0.2
0.3
0.4
0.5
0.6
0.7
0.8
0.9
1
0
250
500
750
1000
1250

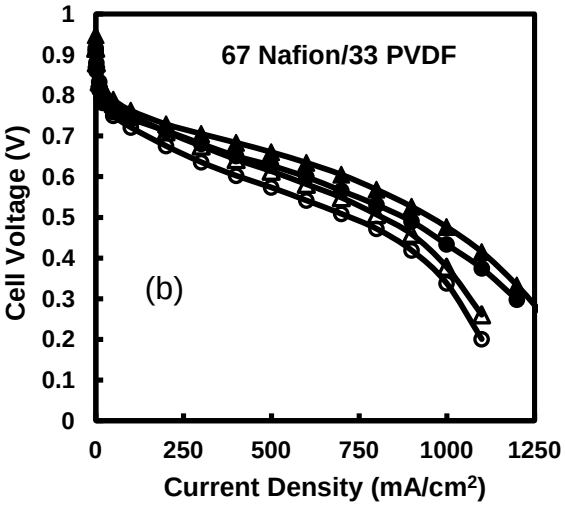
67 Nafion/33 PVDF
(b)
Cell Voltage (V)
Current Density (mA/cm²)
0
0.1
0.2
0.3
0.4
0.5
0.6
0.7
0.8
0.9
1
0
250
500
750
1000
1250

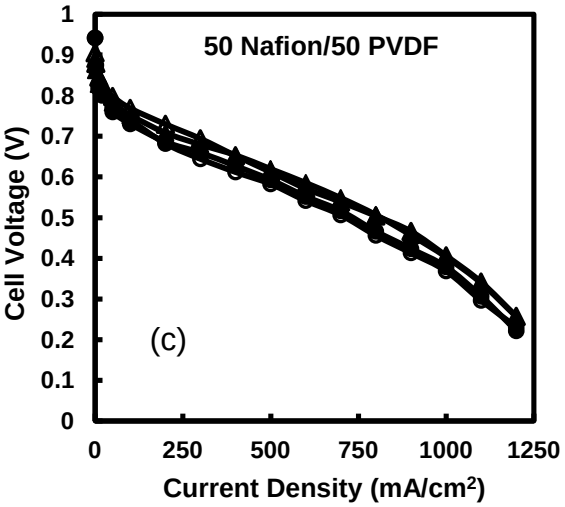
50 Nafion/50 PVDF
(c)
Cell Voltage (V)
Current Density (mA/cm²)
0
0.1
0.2
0.3
0.4
0.5
0.6
0.7
0.8
0.9
1
0
250
500
750
1000
1250

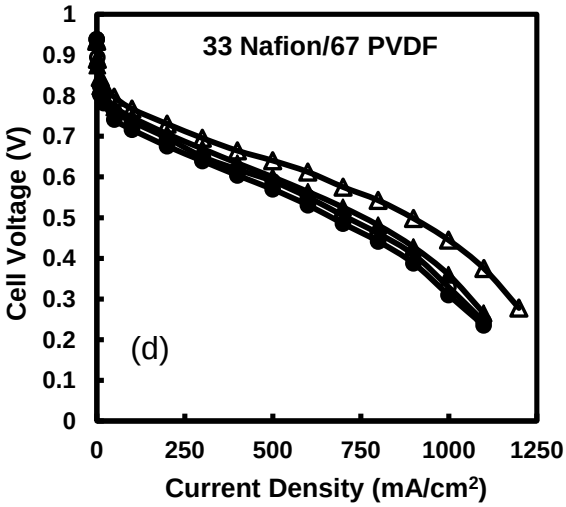
33 Nafion/67 PVDF
(d)
Cell Voltage (V)
Current Density (mA/cm²)
0
0.1
0.2
0.3
0.4
0.5
0.6
0.7
0.8
0.9
1
0
250
500
750
1000
1250

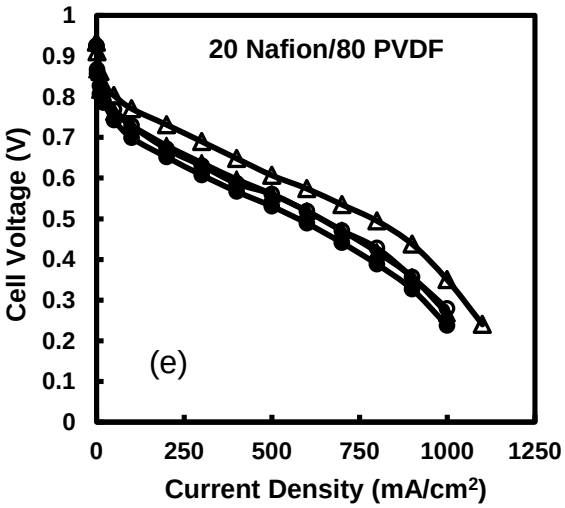
20 Nafion/80 PVDF
(e)
Cell Voltage (V)
Current Density (mA/cm²)
0
0.1
0.2
0.3
0.4
0.5
0.6
0.7
0.8
0.9
1
0
250
500
750
1000
1250

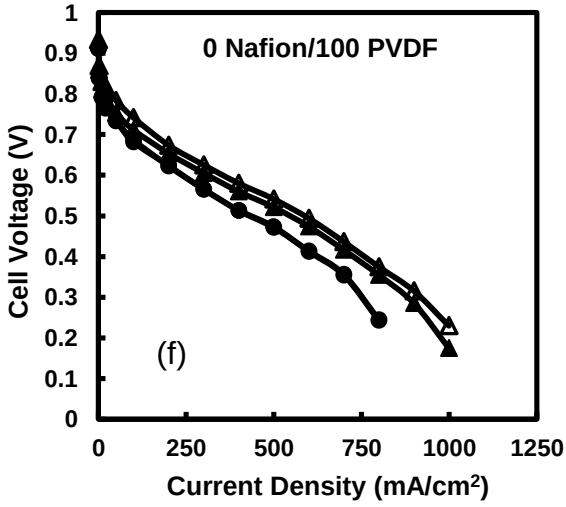
0 Nafion/100 PVDF
(f)
Cell Voltage (V)
Current Density (mA/cm²)
0
0.1
0.2
0.3
0.4
0.5
0.6
0.7
0.8
0.9
1
0
250
500
750
1000
1250

Figure 5.4. BoL (solid symbols) and EoL (open symbols) polarization curves for 5 cm^2 MEAs with a Nafion 211 membrane and 0.10 mg_{Pt}/cm^2 cathode and anode after 1,000 voltage cycles. Fuel cell operating conditions: 80°C, 100% RH, 125 sccm H_2 and 500 sccm air at ambient pressure. Each plot shows data for an MEA with a nanofiber cathode (triangles) and an MEA with a painted GDE cathode (circles) with the same Nafion/PVDF cathode composition: (a) 80/20, (b) 67/33, or (c) 50/50, (d) 33/67, (e) 20/80, or (f) 0/100.

The polarization curves in Figure 5.4 show the nanofiber cathode MEAs produced higher current densities than their analogous painted GDE MEAs at BoL and EoL for all voltages. At BoL, the nanofiber MEAs showed smaller activation overpotential losses in the kinetic (high voltage) region of the polarization curves and similar ohmic losses as compared to the GDE MEAs. Also, the nanofiber 80/20 Nafion/PVDF MEA (Figure 5.4a) showed smaller mass transfer losses than the 80/20 GDE cathode MEA. With 80% Nafion, the cathode is still primarily composed of a hydrophilic binder, and the nanofiber structure, with inter-fiber and intra-fiber porosity, provided superior water removal and better oxygen access to catalyst sites at high current density. The nanofiber Nafion/PVDF MEAs with a higher PVDF content did not show this advantage in mass transfer as compared to their GDE cathode analogues.

The Nafion/PVDF GDE cathode MEAs showed two similar trends as the nanofiber cathode MEAs: (1) MEAs with a Nafion/PVDF cathode binder with < 50 wt% PVDF generated less power after the corrosion cost and (2) GDE and nanofiber cathode MEAs with a cathode Nafion/PVDF binder with >50% PVDF generated more power after the corrosion test. For example, both 80/20 Nafion/PVDF cathode MEAs generated less power after the voltage cycling (i.e., a smaller current was generated at a given

voltage), but the painted cathode MEA lost 48% of its initial power at 0.65 V and 26% of its maximum power, as compared to a 38% power loss at 0.65 V and 20% power loss at maximum power for the nanofiber cathode MEA. The largest relative increase in fuel cell performance (between BoL and EoL) was seen with 20/80 Nafion/PVDF MEAs, i.e., the mixed polymer binder with the least amount of Nafion. At 0.65 V, the power density of the 20/80 MEAs increased by 36% for the nanofiber MEA and 20% for the GDE 20/80 MEA. Thus, the unusual result in which fuel cell performance increased after a harsh voltage cycling test was also exhibited by both the painted GDE and nanofiber cathode MEAs, but only at a high PVDF cathode binder content. It should be noted, however, this phenomena, in which the corrosion test seems to function as an activation procedure, was much more pronounced with nanofiber cathode MEAs.

5.3.4. Electrochemical Surface Area and Kinetic Parameter Measurements– In this section, electrochemical surface area (ECA) and kinetic parameters (mass activity and Tafel slope) are presented for nanofiber and GDE cathode MEAs of various binder compositions. The important data, listed in Table 5.2 and discussed below help explain the fuel cell polarization curves shown previously in this chapter.

Table 5.2. Beginning and End-of-Life Electrochemical Surface Area, Mass Activity Data, and Tafel Slopes for MEAs with Electrospun or Painted GDE Cathodes

Electrospun Cathodes

Cathode Pt/C Binder (w/w)	ECA (m^2/g_{Pt})		Mass Act* (A/mg_{Pt})		Tafel Slope (mV/decade)	
	BoL	EoL	BoL	EoL	BoL	EoL
Neat PVDF	29	23	0.051	0.082	82	79
20 Nafion/80 PVDF	44	32	0.067	0.12	77	78
33 Nafion/67 PVDF	45	33	0.071	0.12	82	76
50 Nafion/50 PVDF	44	30	0.093	0.11	75	74
67 Nafion/33 PVDF	45	30	0.11	0.11	75	77
80 Nafion/20 PVDF	45	30	0.12	0.11	80	84
67 Nafion/33 PAA	45	28	0.16	0.14	70	78

Painted GDE Cathodes

Cathode Pt/C Binder (w/w)	ECA (m^2/g_{Pt})		Mass Act* (A/mg_{Pt})		Tafel Slope (mV/decade)	
	BoL	EoL	BoL	EoL	BoL	EoL
Neat PVDF	25	21	0.035	0.053	72	73
20 Nafion/80 PVDF	35	25	0.044	0.084	75	75
33 Nafion/67 PVDF	34	25	0.053	0.079	84	79
50 Nafion/50 PVDF	36	24	0.067	0.077	79	81
67 Nafion/33 PVDF	36	23	0.081	0.073	84	82
80 Nafion/20 PVDF	35	23	0.083	0.072	79	81
100 Nafion	36	21	0.11	0.080	73	77

*measurements taken at 0.90 V in O_2 at 7 psi_g and 100% RH

The BoL ECAs for nanofiber MEAs were independent of the Nafion/PVDF binder ratio and essentially identical to that for a Nafion/PAA cathode binder. This was true for both nanofiber MEAs with an ECA of 44-45 m^2/g and GDE cathodes, with an ECA of 34-36 m^2/g. Thus, one can conclude that the addition of PVDF to Nafion binder does not change the number of active Pt sites in a fuel cell cathode (nanofiber or conventional GDE). The BoL ECA of the neat PVDF cathode MEA, however, was quite low (25 m^2/g which is only 65% of that for a Nafion/PAA or Nafion/PVDF binder); Pt

sites are inactive presumably due to the absence of mobile protons. It should be noted that the ECA data in Table 5.2 for the Nafion GDE cathode is similar to that reported in the literature for painted and decal cathodes with 40% Pt/Vulcan catalyst. For example, Janssen *et al.*[30] reported an ECA of 33 m^2/g and Gasteiger *et al.*[2] reported an area of 32 m^2/g. The higher Pt reaction site surface area for the nanofiber cathodes is attributed to the better distribution of catalyst powder and binder. During the electrospinning process a better mixing of catalyst and binder is achieved due to the very high sheer stresses at the spinneret tip (the presence of a Taylor cone) followed by fiber elongation between the Taylor cone and collector surface. Rapid solvent evaporation and drying "freezes in" a well-mixed particle/polymer morphology (no agglomeration of particles) with significant intra-fiber voids and a very thin coating of binder on all catalyst particles. A higher ECA provides more accessible catalyst sites to protons and oxygen and a higher concentration of oxygen at catalyst sites thus improving fuel cell performance in the kinetically-controlled high voltage region of the polarization curve.

The measured cathode mass activities at BoL increased with increasing Nafion content in a Nafion/PVDF binder. The mass activity of the nanofiber cathode with neat PVDF binder was 0.051 A/mg_{Pt}. Replacing 20-33% of the PVDF binder with Nafion increased the mass activity to about 0.07 A/mg_{Pt}, and increasing the Nafion content to 67-80% of the total cathode binder further increased the mass activity to about 0.12 A/mg_{Pt}. Thus, while the addition of PVDF does not alter the ECA, it does appear to slow the kinetics of the oxygen reduction reaction. The GDE cathode mass activities were ~40% lower than those for a nanofiber cathode, but followed the same general trend with regards to Nafion and PVDF content.

The decrease in cathode activity with the addition of high PVDF is attributed to less water at the cathode surface (due to the hydrophobic nature of PVDF). Ogasawara *et al*.[31] have reported that water promotes the ORR reaction, in particular the mechanistic step where adsorbed oxygen atoms react with an adsorbed water molecule to form two adsorbed OH, while too high a water concentration hinders the ORR step by blocking (flooding) Pt adsorption sites where molecular oxygen dissociates. The results in Table 5.2, where the ECAs of nanofiber and GDE cathode were independent of binder composition but the ORR mass activity increased with increasing Nafion/PVDF weight ratio is an entirely new finding that has not been observed before for hydrogen/air PEM fuel cells. The cathodic oxygen reduction reaction Tafel slopes for all MEA (nanofiber and GDE) were between 70-84 mV/dec and showed no trends with regards to binder composition, so it can be concluded that there is no change in the ORR reaction mechanism with a change in binder composition or a change in cathode morphology.

Changes in cathode hydrophilicity due to binder composition can explain not only the differences in BoL catalyst activity for Nafion/PVDF MEAs, but also the unusual increase in power densities (and mass activities) of some cathodes after the carbon corrosion durability test. During an accelerated carbon corrosion voltage cycling test, the cathode layer degrades, including the loss of carbon support material and an associated decrease in the Pt ECA as Pt detaches from corroded carbon regions and either agglomerates into large Pt particles or migrates into the membrane and become inactive.[32] The associated decrease in catalyst activity with this loss of ECA generally leads to a decrease in fuel cell power densities. During a carbon corrosion voltage cycling test, it is also known that there is also an increase in the catalyst surface

concentration of carbon oxidation species, such as C-OH and C=O, which makes the catalyst more hydrophilic.[8] This increase in cathode hydrophilicity is usually deleterious to MEA performance because it promotes excessive water retention in the cathode (e.g., flooding) during current flow which inhibits O_2 access to catalyst sites. An increase in hydrophilicity of a hydrophobic Nafion/PVDF binder cathode, however, may be beneficial for fuel cell operation. Thus, for all cathodes tested here, the significant loss in ECA at EoL was not accompanied by a similar drop in mass activity. On the contrary, for most Nafion/PVDF binders, the mass activity at EoL either remained the same or increased viz-a-viz the BoL activity. So at EoL, there was less Pt present (smaller ECA), but the remaining Pt was more activite for ORR. While an increase in specific activity (based on the measured ECA) has been reported after a durability test[33], there has never been an increase in mass activity (based on the initial Pt) for Pt/C catalysts after an accelerated start/stop carbon corrosion voltage cycling experiment. This unexpected increase in catalyst activity accounts for the unprecedented increase in power densities of the high PVDF content MEAs after the carbon corrosion voltage cycling experiments.

5.3.5. Low Humidity Operation– Polarization curves with Nafion/PVDF MEAs were also collected with H_2/air feed gases at 40% RH. These experiments were analogous to the polarization curves in Figure 5.3 and were performed to determine if there is any fundamental differences in power output at low vs. high humidity and to see how Nafion/PVDF cathode MEAs compare to a traditional Nafion MEA with low relative humidity feed gases (ECA and ORR kinetic parameters were not measured at low

humidity). BoL and EoL polarization curves are reported at 40% RH, but the corrosion tests were performed under standard conditions, with fully humidified feed gases.

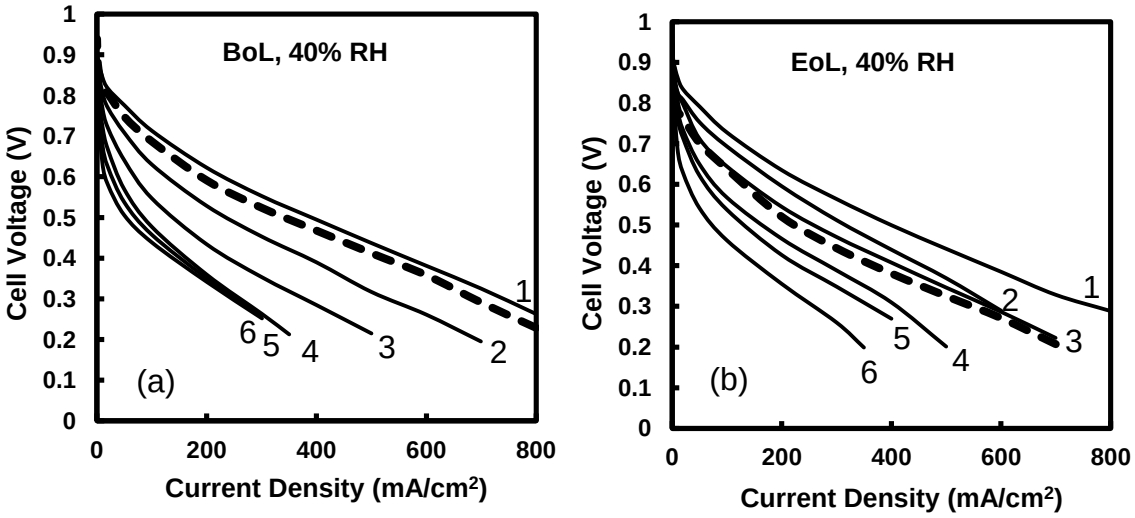

Figure 5.5. Polarization curves for MEAs with electrospun Nafion/PVDF cathodes (unbroken lines) and an MEA with a conventional GDE cathode with 70 wt% Pt/C and 30 wt% Nafion (dashed line). The electrospun cathode Nafion/PVDF w/w are: (1) 80/20, (2) 67/33, (3) 50/50, (4) 33/67, (5) 20/80, and (6) 0/100. All MEAs are 5 cm^2 and contain a Nafion 211 membrane and 0.10 mg_{Pt}/cm^2 at the cathode and anode. Fuel cell operating conditions are 80°C, 40% RH, 125 sccm H_2 and 500 sccm air at ambient pressure. (a) BoL data, (b) EoL data

When operated at 40% RH, the performance of the Nafion/PVDF cathode binder MEAs was inversely proportional to the binder PVDF content, i.e., less current (less power) was generated over the entire voltage range as the PVDF content increased, as shown in Figure 5.5a. This was the same trend seen with fully humidified feed gases, although the activation/kinetic and ohmic losses with increasing PVDF content were more severe at low humidity. It is expected that the cathode drying effect due to a more hydrophobic cathode binder would be exacerbated with drier feed gases. The

performance of MEAs with little or no Nafion in the cathode (0 wt% Nafion and 20 wt% Nafion) were particularly poor. For example, the neat PVDF MEA only produced 7 mW/cm^2 at 0.65 V and 76 mW/cm^2 at maximum power. These results were not unexpected. 3M Company's NSTF cathodes with platinum whiskers (and no hydrophilic ionomer binder) also showed a drastic loss of power at low humidity conditions (e.g., ~70% power loss occurred at 0.8 V, as determined from HFR-corrected voltage, when going from 100% RH to 50% RH with anode/cathode H_2/O_2 gas feeds), which was attributed to a severe decrease in proton conductivity that negatively impacted both the activation and ohmic regions of a polarization curve.[26] The authors of the 3M study concluded that the conductivity decrease of the cathode not only reduced proton transport, but also decreased the catalytic activity of the cathode as the current density distribution shifted towards that part of the cathode closest to the membrane surface, leaving Pt farther from the membrane inactive. For these reasons, the authors of reference [26] recommended high humidity operating conditions for ionomer-free cathodes. The same situation holds for high PVDF content Pt/C powder nanofibers.

At BoL, only the nanofiber Nafion/PVDF with the smallest amount of PVDF (20 wt% of the cathode binder) worked better than a conventional Nafion GDE, as seen in Figure 5.5a. Conventional MEAs with Nafion binders have been reported to produce less power at low humidities due to a reduction in ORR kinetics and a decrease in proton activity due to dehydration of Nafion binder acidic groups.[34] It makes sense that such power losses would be move severe in binders that are more hydrophobic and have fewer acid groups. One would expect that these power losses could be mitigated if the hydrophilicity of the cathode were increased and this appears to be the case at EoL, as

shown in Figure 5.5b. Indeed, after the voltage cycling corrosion test, there is an increase in hydrophilic carbon oxidation species on the cathode catalyst support material and the nanofiber Nafion/PVDF polarization curves shift upward to a higher performance. When operated at 100% RH, only MEAs with a cathode PVDF binder content >50 wt% exhibited an increase in performance, but at 40% RH this unusual increase in power output after voltage cycling was extended across the entire PVDF range. At EoL (Figure 5.5b), the conventional Nafion GDE cathode MEA generated less power (a lower current density for a given voltage) than nanofiber PVDF/Nafion binder cathode MEAs with a PVDF content less than 50 wt.%.

5.3.6. Summary of Power Output for all MEAs – Figure 5.6 summarizes the power output (at 0.65 V) for all nanofiber cathode MEAs (Nafion/PAA, Nafion/PVDF, and PVDF) and GDE cathode MEAs (Nafion, Nafion/PVDF, PVDF). This data was taken from Figures 5.2-5.5 as well GDE polarization curves collected with 40% RH feed gases that were not explicitly shown above, but which are listed in Appendix A of this dissertation.

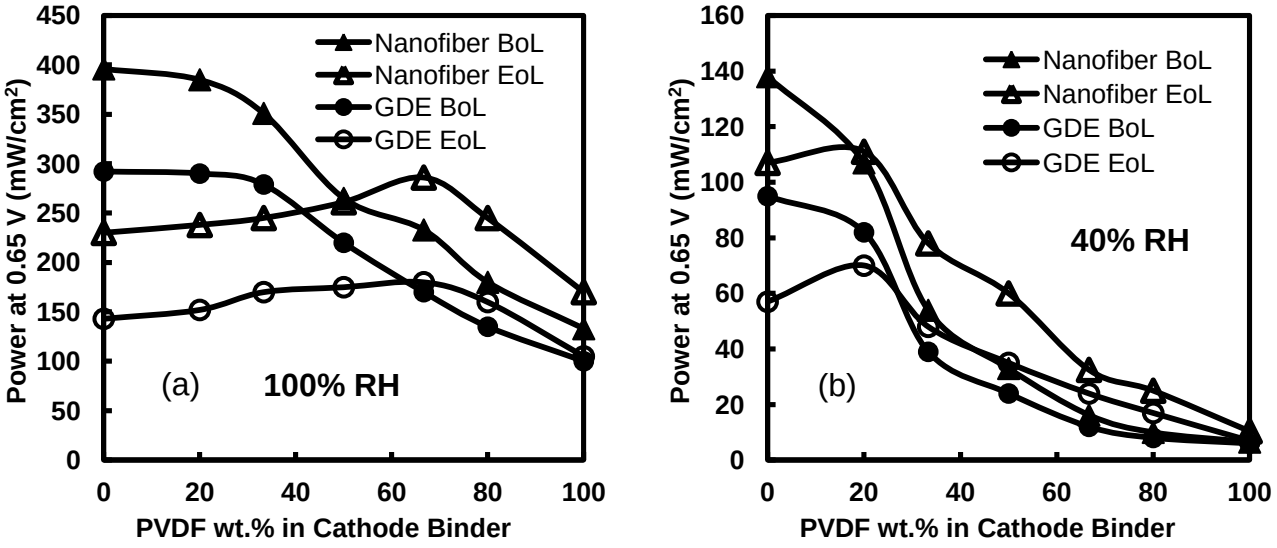

Figure 5.6. Power densities at 0.65 V at BoL (solid symbols) and EoL (open symbols) of MEAs as a function of PVDF wt% in the cathode binder (the remaining wt% is Nafion, except in the nanofiber case at 0% PVDF, where the binder is 67 wt.% Nafion and 33 wt.% PAA). The cathodes have a Pt loading of 0.10 mg/cm^2 and are either electrospun (triangles) or painted GDEs (circles). For all MEAs, a nanofiber 0.10 mg/cm^2 anode was used with a 67 wt% Nafion and 33 wt% PAA binder. Fuel cell operating conditions: 80°, 125 sccm H_2 and 500 sccm air at ambient pressure at either (a) 100% RH, or (b) 40% RH.

The data in Figure 5.6a highlights the benefit of a nanofiber morphology with Nafion/PVDF binders. Recall that in Figure 5.3a, the nanofiber Nafion/PVDF cathode MEAs with less than 50 wt% PVDF outperformed a GDE MEA with Nafion only. BoL power densities in Figure 5.6 show that nanofiber PVDF/Nafion MEAs also outperform their respective GDE MEAs (with the same binder). Furthermore, at EoL with fully humidified feed gases, all nanofiber cathode MEAs work better than all GDE cathode MEAs, regardless of binder type (i.e. the effect of morphology is much more important than the effect of Nafion/PVDF ratio at EoL). Initially, the best nanofiber cathode contained a binder of either 67 wt% Nafion and 33 wt% PAA binder or 80 wt% Nafion

and 20 wt% PVDF. The best binder at EoL, after a decrease in performance of low PVDF content cathode MEAs and an increase in performance in high PVDF content cathode MEAs, was 33 wt% Nafion and 67 wt% PVDF. This 33/67 Nafion/PVDF nanofiber cathode MEA produced 79% more power at 0.65 V than the best GDE cathode MEA at EoL (which was also 33/67 Nafion/PVDF).

The results in Figure 5.6b, with 40% RH feed gases, look much different than 5.6a. All the data at BoL and EoL show the same downward trend in power as the PVDF content is increased for binders with more than 20% PVDF. At EoL only the Nafion/PAA and 80/20 Nafion/PVDF binders worked well. For binders with more than 20% PVDF, cathode morphology (nanofiber vs. painted) had less effect on power output than at 100% RH. At 20-67 wt% PVDF content, the nanofiber cathode MEAs outperformed the GDE cathode MEAs, but at 80 and 100% PVDF the EoL performance at 40% RH was essentially independent of cathode morphology. In general, cathodes with high PVDF content worked poorly at low humidity regardless of cathode morphology.

Intermittent polarization curves at 100% RH were collected during the corrosion tests to determine how power densities varied with cycle number. These results for nanofiber cathode MEAs are shown in Figure 5.7a and painted GDE cathode MEAs are shown in Figure 5.7b, where the measured power density at 0.65 V is plotted vs. voltage cycle number. This data compliments the data in Figure 5.6a, by showing not only starting and ending power densities, but also how the power changed over the 1,000 voltage cycle test.

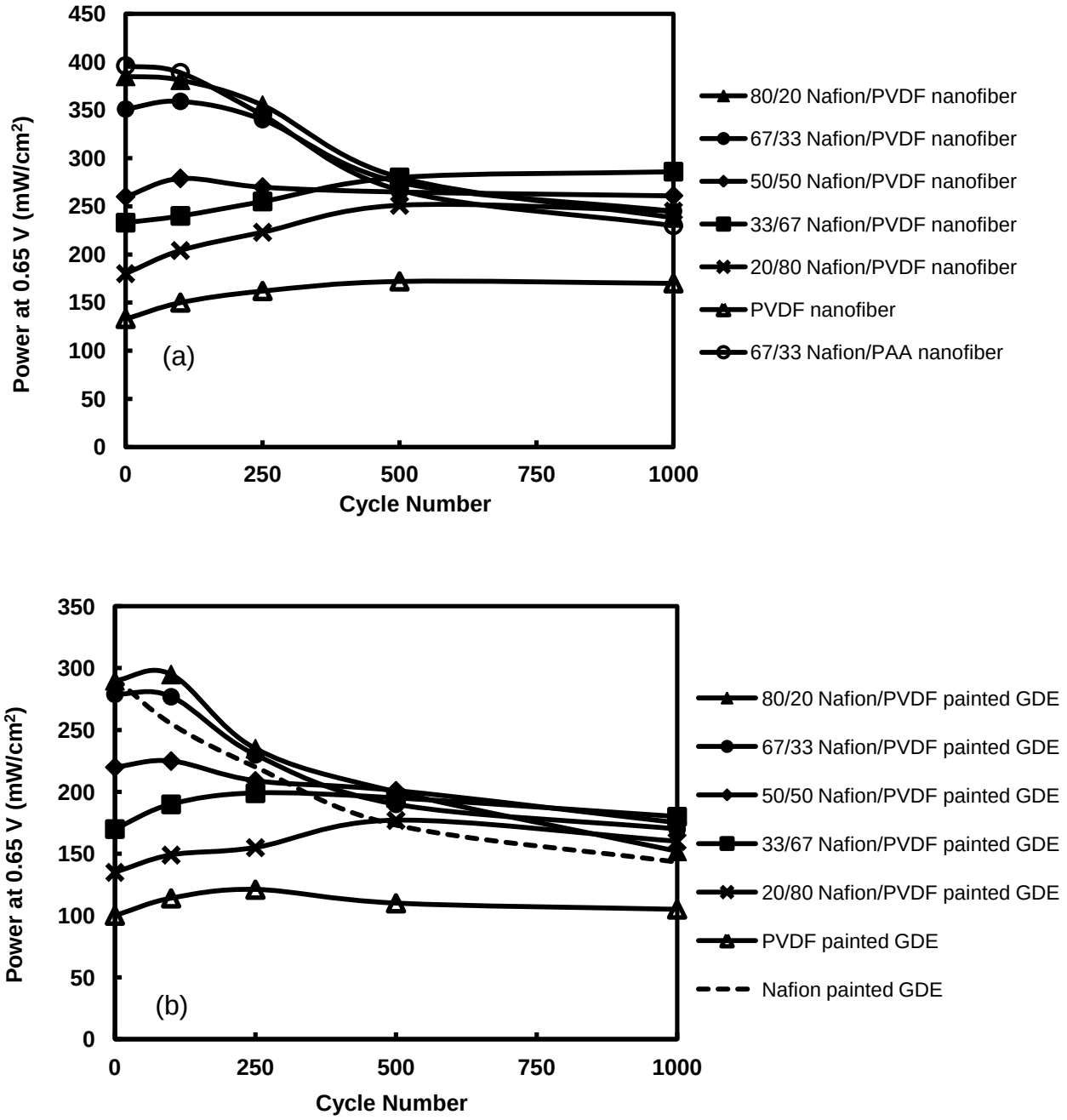

Figure 5.7. Power densities at 0.65 V for MEAs with either an electrospun cathode (a) or a painted GDE cathode (b) as a function of voltage cycle number. MEAs have 0.10 mg_{Pt}/cm^2 cathodes and anodes. Fuel cell operating conditions: 80°, fully humidified 125 sccm H_2 and 500 sccm air at ambient pressure.

The rates at which the MEA power densities changed were affected by both binder composition and cathode morphology. In general, the power density changes were faster initially and became more moderate (stable) as the cycle number increased. Most of the power loss or gain occurred in the first 500 voltage cycles. The slope of the power density changes of the nanofiber 50/50 and 33/67 Nafion/PVDF cathode MEAs at 1,000 cycles was very flat. This result was different than seen with the painted GDE cathode MEAs of the same composition, which showed continued power loss between 500 and 1,000 cycles. This promising results suggest that such nanofiber Nafion/PVDF cathodes with high PVDF binder content might maintain steady performance if voltage cycling was continued past 1,000 cycles and continue to outperform painted GDE cathode MEAs. Such experiments were not performed in the present study.

5.3.7 Analysis of In-Situ CO_2 Emissions in Cathode Exhaust During Carbon Corrosion Durability Testing– In an attempt to better understand how the presence of PVDF is affecting carbon corrosion and to distinguish between the role that cathode morphology and binder composition are having on fuel cell power output and durability, the cathode carbon loss was measured during the accelerated durability testing. Figure 5.8 shows the CO_2 concentration levels vs. time in the cathode exhaust for three Nafion/PVDF electrospun cathode MEAs (Figure 5.8 a), a Nafion GDE cathode MEA (Figure 5.8b), and a Nafion/PVDF GDE cathode MEA (Figure 5.8b) during a carbon corrosion voltage cycling experiment. The shape of these CO_2 production rate vs. time curves are similar to those collected at Nissan Technical Center North America (NTCNA) and reported in Chapter 4 of this dissertation as well as others in the literature[35] i.e., a sharp spike in

concentration when the voltage cycling test is initiated followed by a steady decrease in the CO_2 generation. The initial spike in CO_2 is attributed to the rapid decomposition of accumulated surface oxide species on the Pt carbon support material.[36] In these experiments, the voltage cycling was stopped intermittently during the 1,000 cycle test in order to collect H_2/air polarization curves, which explains the breaks in CO_2 production in Figures 5.8a and 5.8b. It is immediately obvious that the carbon corrosion rates were significantly slower for cathodes with a higher fraction of PVDF in the Nafion/PVDF binder.

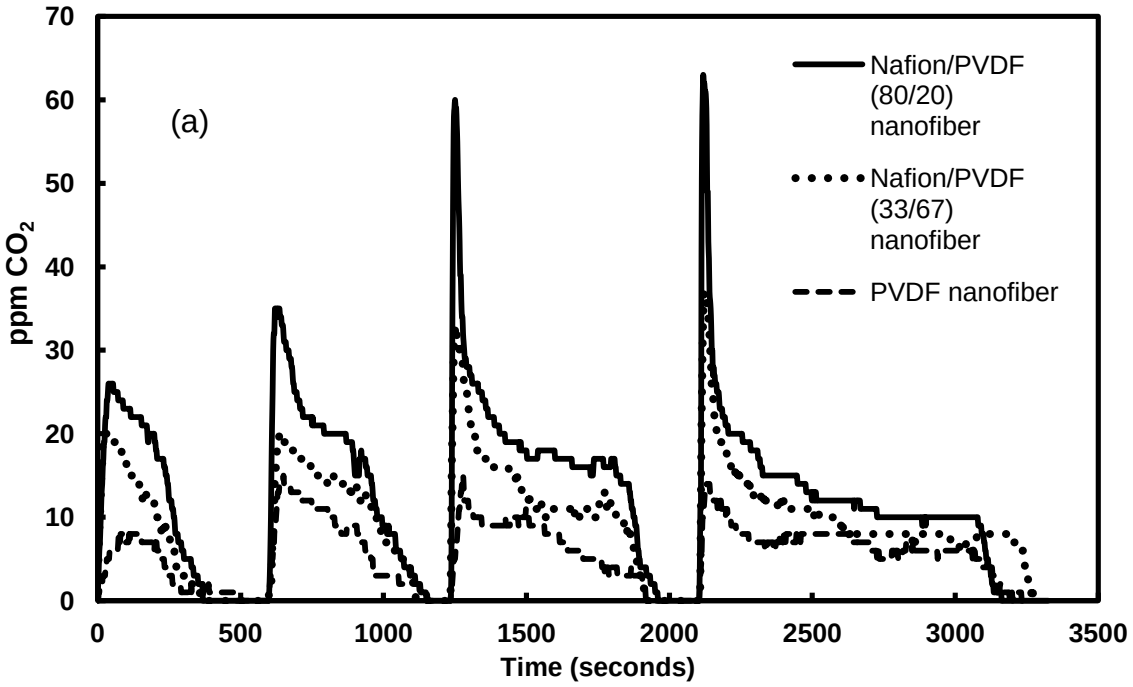

Cycle number: (H_2/air polarization curves were collected after 0,100, 250, 500, and 1,000 cycles)

0-100	101-250	251-500	501-1000 voltage cycles

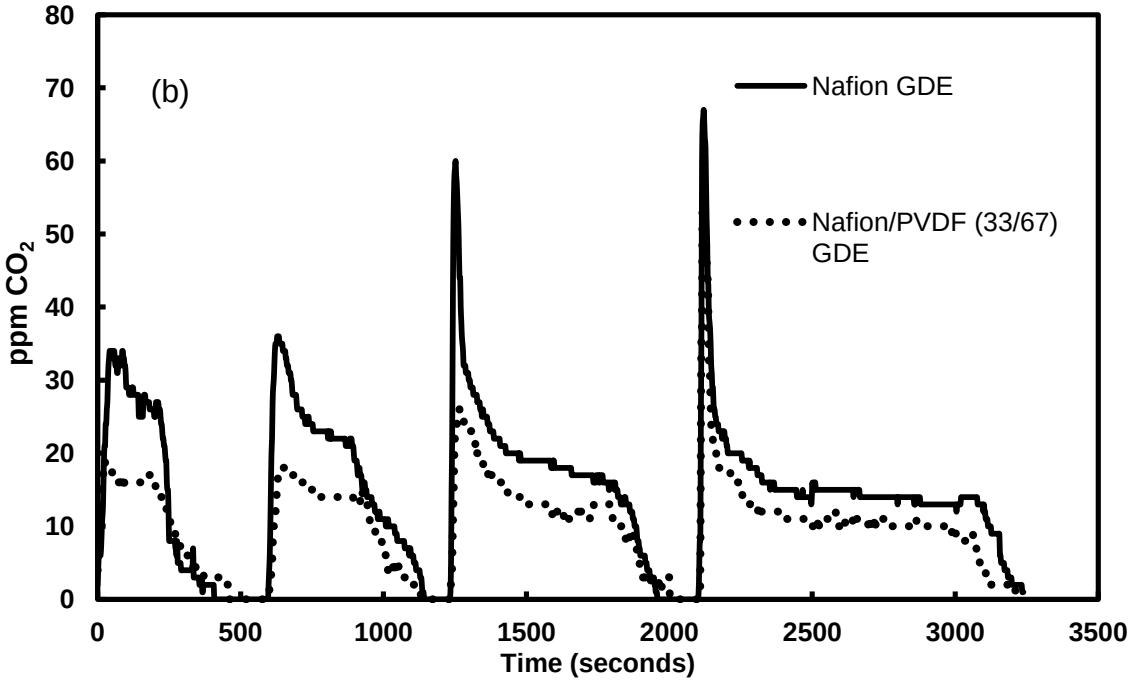

Cycle number: (H_2/air polarization curves were collected after 0,100, 250, 500, and 1,000 cycles)

0-100	101-250	251-500	501-1000 voltage cycles

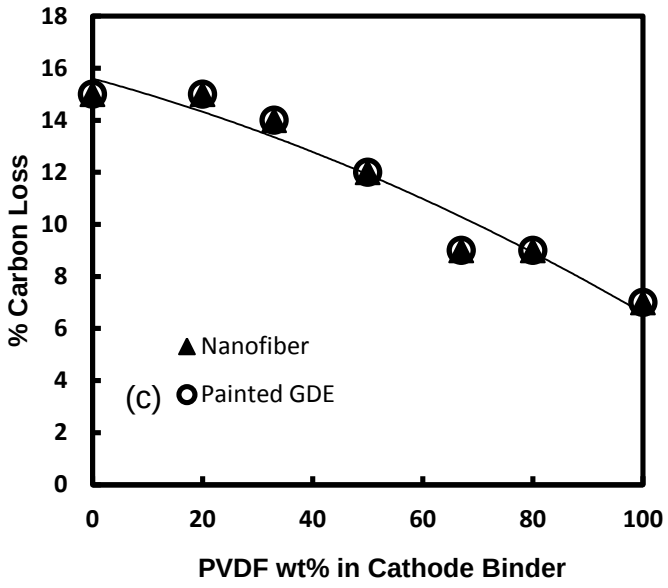

Figure 5.8. Real time measurement of CO_2 in the cathode exhaust during a carbon corrosion potential cycling experiment at 100% RH. (a) ppm CO_2 detected in real time in the cathode exhaust for three nanofiber MEAs (b) ppm CO_2 detected in real time in the cathode exhaust for a Nafion GDE MEA and a Nafion/PVDF MEA (c) Cumulative cathode carbon loss after 1,000 cycles for nanofiber and painted GDE MEAs as a function of PVDF wt% in the cathode binder as calculated from real time CO_2 data (such data for some MEAs is shown in Figure 5.8a and b). The remaining binder wt% is Nafion, except in the nanofiber case at 0% PVDF, which has a Nafion/PAA binder.

The cumulative carbon loss for all cathodes after 1,000 voltage cycles is shown in Figure 5.8c for both nanofiber and GDE cathodes. The extent of carbon support corrosion was strongly dependent on the amount of PVDF in the cathode binder and not on the cathode morphology (nanofiber vs. painted). For example, at the extremes, cathodes with no PVDF lost 15 wt% carbon and the neat PVDF cathodes lost 6-7 wt% carbon. This result for the cathodes with no PVDF is very similar to the data collected in the NTCNA lab[5] in which an electrospun Nafion/PAA MEA was reported to lose 18% cathode carbon as compared to 17% for a conventional sprayed electrode MEA after 1,000 cycles. In this

previous collaboration with Nissan, the 1,000 cycles were divided up slightly differently (with additional interruptions), which could account for the small difference between the two labs (~15 wt% loss at Vanderbilt compared to ~17 wt% loss at NTCNA), as the CO_2 levels peak when the voltage cycling is re-initiated. The lower CO_2 concentrations (less carbon corrosion) for binders with higher PVDF content is attributed to their being less water present at the Pt/C cathode power surface. Maass *et al.*[37] and Kreitmeier *et al.*[38] found that carbon corrosion rates directly correlated with the humidity level of the cathode feed gases such that wetter cathodes generated more CO_2.

In order to determine if the mitigation of carbon corrosion in PVDF-based cathodes also correlates with a mitigation of ECA loss as has been reported previously for traditional cathodes, cathode ECA loss has been plotted vs. carbon loss for the MEA data in this chapter and compared to reports in the literature (Figure 5.9). It is noted that despite different corrosion tests (for example this work and the NTCNA tests performed voltage cycling from 1-1.5 V at 500 mV/s, while the others did a voltage hold at either 1.3 or 1.4 V), the data in Figure 5.9 shows a strong correlation with carbon loss and ECA loss. Thus there is nothing special about the overall carbon loss in nanofiber or GDE cathodes that contain PVDF. The presence of PVDF is slowing carbon corrosion *and* ECA loss, as expected, with a correlation that matches literature data.

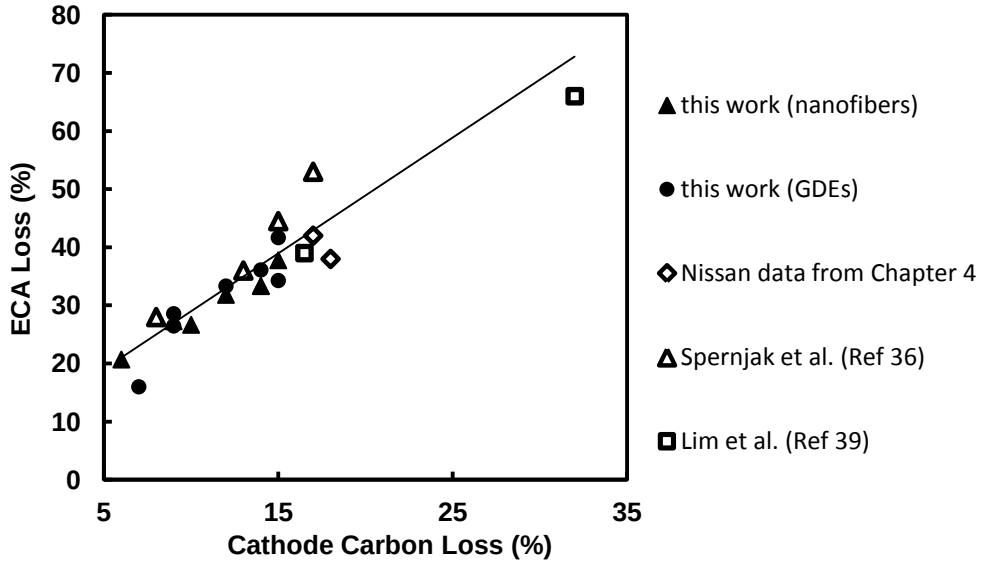

Figure 5.9. Cathode ECA loss plotted vs. cathode carbon loss after accelerated carbon corrosion tests for this work and others in the literature.

Therefore, the initial hypothesis that increasing the hydrophobicity of the cathode by adding PVDF will slow carbon corrosion is confirmed. However, the relationship between EoL power densities and corrosion is less clear and straightforward. While the extent of carbon corrosion was controlled by the binder (Nafion/PVDF ratio) and unaffected by cathode structure, the power retention was a strong function of cathode structure and binder composition (as was shown in Figure 5.6) and did not directly correlate with corrosion (the best EoL power was not produced by the cathode with the least corrosion and some cathodes exhibited an increase in performance despite losing ECA). The relative MEA power retention after a carbon corrosion test as a function of ECA loss is displayed in Figure 5.10 for the MEAs in this chapter and compared to data taken from H_2/air polarization curves before/after carbon corrosion tests in the literature.

A dotted line connects 100% power at no ECA loss with complete loss of power and total ECA loss, the two limiting extremes. This plot essentially shows the power density per geometric area vs. the change in active Pt in that area and highlights the unusual result in which the Pt activity increases (higher power output with less Pt).

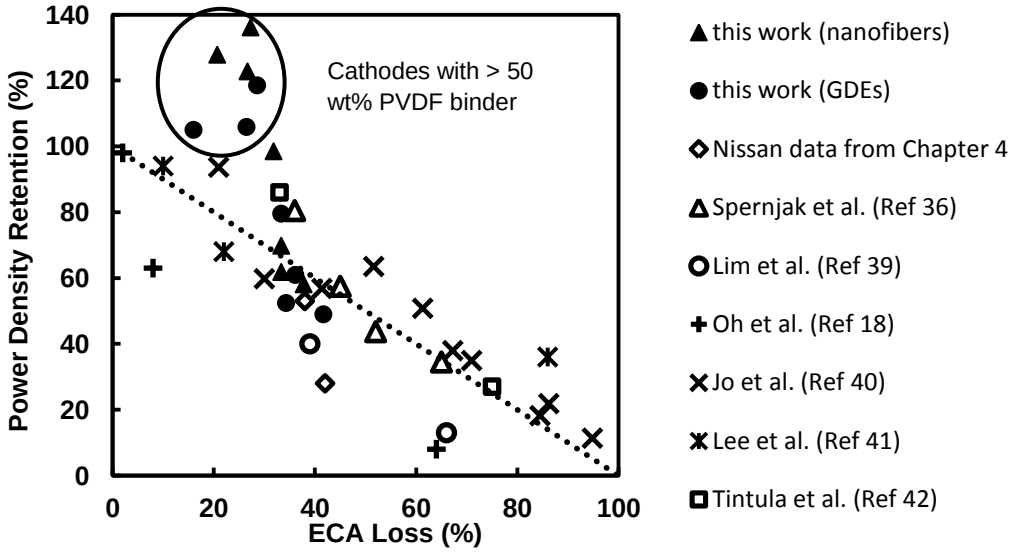

Figure 5.10. Power retention at 0.65 V for MEAs with H_2/air feed gases plotted vs. % ECA loss after accelerated carbon corrosion tests for this work and others in the literature.

Considering the fact that Figure 5.10 contains many MEAs with different operating parameters, testing conditions, catalyst loadings, etc, the data still shows a clear trend with power density and ECA loss, albeit with some spread. All points generally follow the same trend except for the cathodes with a PVDF content > 50 wt% which show an increase of power density at 0.65 V after an accelerated corrosion test. Other groups

synthesized novel carbon catalyst supports that were shown to be much more durable (in terms of ECA and power retention) than traditional amorphous carbon supports, however none of these resulting catalysts showed an increase in mass activity/power density as seen with the Nafion/PVDF cathodes. There seems to be a fundamental difference in changing the catalyst binder as compared to changing the carbon/catalyst. For example, Lee *et al.*[41] synthesized a carbon nanotube supported Pt catalyst which was shown to have better carbon corrosion durability in an MEA than traditional amorphous carbon catalysts (due to a higher degree of carbon graphitization and hydrophobicity), though there was no increase in mass activity or power densities in H_2/air polarization curves after a carbon corrosion test. The increase in Pt activity after a carbon corrosion test seems to be unique with hydrophobic binders or at least with PVDF, where the catalyst becomes more activated during the corrosion test in comparison to its initial state.

Many important conclusions can be drawn about the use of mixed Nafion/PVDF cathode binders when considering the 100% RH polarization curve data, ECA and mass activity, and carbon corrosion data together: (i) the replacement of a portion of the Nafion cathode binder with PVDF does not affect the amount of available Pt sites, but it does hinder the ORR activity, (ii) the addition of (a small amount of) PVDF enhances the mass transfer region compared to cathodes with a fully hydrophilic binder, (iii) the addition of PVDF slows carbon corrosion, and (iv) the mass activity and fuel cell power densities of MEAs with a high cathode PVDF content that are low initially improve after an accelerated carbon corrosion durability test due to an increase in carbon hydrophilicity and Pt activity. These results were seen to some extent with both nanofiber and GDE cathode MEAs. Perhaps most interesting, though, were the differences between the two

cathode morphologies. The corrosion rates (as measured by carbon and % ECA loss) in Nafion/PVDF cathodes are independent of cathode morphology and only depend on binder composition (Nafion/PVDF ratio). However, the 100% RH BoL vs. EoL results in Figure 5.6 show that morphology and binder composition both have an effect on EoL power output; the nanofibers start at a higher power and then lose a smaller percent of initial power (or gain more power in the case of the cathodes > 50 wt% PVDF) to perform much better at EoL. It is clear that carbon corrosion is having less of a detrimental effect on power output in a nanofiber structure as compared to a painted GDE, though at this time it is not clear exactly why. The absolute values of ECA are higher at EoL for nanofibers, but the relative change between BoL and EoL was the same as the GDEs, so this cannot explain the smaller percent in power loss. One explanation is GDE MEAs have been shown to undergo extreme cathode thinning and structural collapse during carbon corrosion tests which leads to reduced fuel cell performance.[38, 43] Such SEM-cross sectional analysis was not performed in the present study. Also, local corrosion rates in the cathode are based on local conditions,[44] such as concentrations of water/humidity levels. Another possible explanation as to why the effects of carbon corrosion are less severe with a nanofiber cathode is that there is more uniform corrosion of the carbon support throughout the entire electrode, due to a better distribution of hydrophilic binder and/or water.

5.4 Conclusions

Electrospun nanofiber mats were fabricated with 70% Pt/C catalyst and 30% Nafion/PVDF binder, where the PVDF binder content was varied from 20% to 100%. The mats were used as the cathode in MEAs for hydrogen/air fuel cells. The 80/20 Nafion/PVDF binder cathode MEA had lower catalyst activity in comparison to a Nafion/PAA binder cathode MEA, but produced higher power densities at low voltages due to excellent water removal. Thus, a very high power of 545 mW/cm^2 was produced with the highest Nafion/PVDF ratio at 100% RH, which was 13% higher than the nanofiber MEA with a Nafion/PAA binder and 35% higher than a conventional Nafion GDE cathode MEA. Increasing the PVDF cathode binder content >20 wt% decreased the initial power output of MEAs when operated at both 100% and 40% RH due to a reduction of ORR kinetics and an increase in the ohmic resistance of the binder. The decrease in power output with a higher cathode PVDF content was more severe during low humidity operation. MEAs with painted cathodes were also created with the same Nafion/PVDF compositions as the nanofiber MEAs. Each nanofiber cathode MEA produced higher power at BoL and EoL (after a carbon corrosion accelerated durability test that simulated start-stop cycling of fuel cell stack) than its GDE MEA analog and had higher ECA and mass activity.

MEAs with high PVDF cathode binder content (>50 wt%) showed an unusual result in that they produced more power after the carbon corrosion test than at BoL. This increase in power output was attributed to an increase in Pt activity as the cathode became more hydrophilic during the durability test and overcompensated for a reduction in ECA. Real time measurements of CO_2 in the cathode exhaust during the accelerated

voltage cycling tests confirmed the hypothesis that increasing the cathode catalyst binder hydrophobicity with the addition of PVDF slowed carbon corrosion. The cumulative carbon loss decreased with increasing cathode PVDF content, with 80/20 Nafion/PVDF cathodes losing 14 wt% and neat PVDF cathodes losing only 6 wt%. However, changes in MEA power output during the carbon corrosion experiment did not directly correlate with carbon loss. Changes in the hydrophilicity/hydrophobicity of the cathodes had a strong impact on mass activities and power output. While nanofiber cathodes with a higher Nafion content worked much better at BoL, the 100% RH polarization curves of MEAs with various Nafion/PVDF ratios showed a much smaller difference at EoL, with the 33/67 Nafion/PVDF nanofiber cathode MEA producing the most power.

5.5 References

(1) Litster, S. and G. McLean (**2004**) *Journal of Power Sources*, 130, 61-76.

(2) Gasteiger, H. A., S. S. Kocha, B. Sompalli, and F. T. Wagner (**2005**) *Applied Catalysis B: Environmental*, 56, 9-35.

(3) Zhang, W. and P. N. Pintauro (**2011**) *ChemSusChem*, 4, 1753-1757.

(4) Brodt, M., R. Wycisk, and P. N. Pintauro (**2013**) *Journal of the Electrochemical Society*, 160, F744-F749.

(5) Brodt, M., T. Han, N. Dale, E. Niangar, R. Wycisk, and P. Pintauro (**2015**) *Journal of the Electrochemical Society*, 162, F84-F91.

(6) Park, Y. C., K. Kakinuma, M. Uchida, D. A. Tryk, T. Kamino, H. Uchida, and M. Watanabe (**2013**) *Electrochim. Acta*, 91, 195-207.

(7) Young, A. P., J. Stumper, and E. Gyenge (**2009**) *Journal of the Electrochemical Society*, 156, B913-B922.

(8) Kocha, S. S., *Chapter 3 - Electrochemical Degradation: Electrocatalyst and Support Durability*, in *Polymer Electrolyte Fuel Cell Degradation*, M.M. Mench, E.C. Kumbur, and T.N. Veziroglu, Editors. 2012, Academic Press: Boston. p. 89-214.

(9) Mench, M. M., E. C. Kumbur, and T. N. Veziroglu, *Polymer Electrolyte Fuel Cell Degradation*. 2011: Elsevier Science.

(10) Parrondo, J., T. Han, E. Niangar, C. Wang, N. Dale, K. Adjemian, and V. Ramani (**2014**) *Proceedings of the National Academy of Sciences*, 111, 45-50.

(11) Stassi, A., I. Gatto, V. Baglio, E. Passalacqua, and A. S. Aricò (**2013**) *Applied Catalysis B: Environmental*, 142–143, 15-24.

(12) Kumar, A. and V. K. Ramani (**2013**) *Applied Catalysis B: Environmental*, 138–139, 43-50.

(13) Hara, M., M. Lee, C.-H. Liu, B.-H. Chen, Y. Yamashita, M. Uchida, H. Uchida, and M. Watanabe (**2012**) *Electrochim. Acta*, 70, 171-181.

(14) Debe, M. K., A. K. Schmoeckel, G. D. Vernstrorn, and R. Atanasoski (**2006**) *Journal of Power Sources*, 161, 1002-1011.

(15) Su, H. N., S. Pasupathi, B. Bladergroen, V. Linkov, and B. G. Pollet (**2013**) *Int. J. Hydrog. Energy*, 38, 11370-11378.

(16) Landis, F. A. and R. B. Moore (**2000**) *Macromolecules*, 33, 6031-6041.

(17) Wycisk, R., J. W. Park, D. Powers, and P. N. Pintauro (**2014**) *Meeting Abstracts*, MA2014-02, 1199.

(18) Oh, H.-S., K. H. Lim, B. Roh, I. Hwang, and H. Kim (**2009**) *Electrochimica Acta*, 54, 6515-6521.

(19) Ballengee, J. B. and P. N. Pintauro (**2011**) *Journal of the Electrochemical Society*, 158, B568-B572.

(20) Ohma, A., K. Shinohara, A. Iiyama, T. Yoshida, and A. Daimaru (**2011**) *ECS Transactions*, 41, 775-784.

(21) Mackey, M., L. Flandin, A. Hiltner, and E. Baer (**2011**) *Journal of Polymer Science Part B: Polymer Physics*, 49, 1750-1761.

(22) Broka, K. and P. Ekdunge (**1997**) *Journal of Applied Electrochemistry*, 27, 117-123.

(23) Xu, H., Y. Song, H. R. Kunz, and J. M. Fenton (**2005**) *Journal of the Electrochemical Society*, 152, A1828-A1836.

(24) Song, W., H. Yu, L. Hao, Z. Miao, B. Yi, and Z. Shao (**2010**) *Solid State Ionics*, 181, 453-458.

(25) Kang, J. and J. Kim (**2010**) *International Journal of Hydrogen Energy*, 35, 13125-13130.

(26) Sinha, P. K., W. Gu, A. Kongkanand, and E. Thompson (**2011**) *Journal of the Electrochemical Society*, 158, B831-B840.

(27) Peron, J., A. Mani, X. Zhao, D. Edwards, M. Adachi, T. Soboleva, Z. Shi, Z. Xie, T. Navessin, and S. Holdcroft (**2010**) *Journal of Membrane Science*, 356, 44-51.

(28) Seo, D., S. Park, Y. Jeon, S.-W. Choi, and Y.-G. Shul (**2010**) *Korean J. Chem. Eng.*, 27, 104-109.

(29) Selvaganesh, S. V., G. Selvarani, P. Sridhar, S. Pitchumani, and A. K. Shukla (**2011**) *Fuel Cells*, 11, 372-384.

(30) Janssen, G. J. M. and E. F. Sitters (**2007**) *Journal of Power Sources*, 171, 8-17.

(31) Ogasawara, H., L. A. Naslund, J. McNaughton, T. Anniyev, and A. Nilsson (**2008**) *ECS Transactions*, 16, 1385-1394.

(32) Kim, T., T. Xie, W. Jung, F. Gadala-Maria, P. Ganesan, and B. N. Popov (**2015**) *Journal of Power Sources*, 273, 761-774.

(33) Bi, W. and T. Fuller (**2007**) *ECS Transactions*, 11, 1235-1246.

(34) Neyerlin, K. C., H. A. Gasteiger, C. K. Mittelsteadt, J. Jorne, and W. Gu (**2005**) *Journal of the Electrochemical Society*, 152, A1073-A1080.

(35) Yli-Rantala, E., A. Pasanen, P. Kauranen, V. Ruiz, M. Borghei, E. Kauppinen, A. Oyarce, G. Lindbergh, C. Lagergren, M. Darab, S. Sunde, M. Thomassen, S. Ma-Andersen, and E. Skou (**2011**) *Fuel Cells*, 11, 715-725.

(36) Spernjak, D., J. D. Fairweather, T. Rockward, R. Mukundan, and R. Borup (**2011**) *ECS Transactions*, 41, 741-750.

(37) Maass, S., F. Finsterwalder, G. Frank, R. Hartmann, and C. Merten (**2008**) *Journal of Power Sources*, 176, 444-451.

(38) Kreitmeier, S., A. Wokaun, and F. N. Büchi (**2012**) *Journal of the Electrochemical Society*, 159, F787-F793.

(39) Lim, K. H., H.-S. Oh, S.-E. Jang, Y.-J. Ko, H.-J. Kim, and H. Kim (**2009**) *Journal of Power Sources*, 193, 575-579.

(40) Jo, Y. Y., E. Cho, J. H. Kim, T.-H. Lim, I.-H. Oh, S.-K. Kim, H.-J. Kim, and J. H. Jang (**2011**) *Journal of Power Sources*, 196, 9906-9915.

(41) Lee, T. K., J. H. Jung, J. B. Kim, and S. H. Hur (**2012**) *International Journal of Hydrogen Energy*, 37, 17992-18000.

(42) Tintula, K. K., A. Jalajakshi, A. K. Sahu, S. Pitchumani, P. Sridhar, and A. K. Shukla (**2013**) *Fuel Cells*, 13, 158-166.

(43) Hashimasa, Y., T. Shimizu, Y. Matsuda, D. Imamura, and M. Akai (**2013**) *ECS Transactions*, 50, 723-732.

(44) Guétaz, L., S. Escribano, and O. Sicardy (**2012**) *Journal of Power Sources*, 212, 169-178.

CHAPTER VI

CONCLUSIONS

(1) Nanofiber electrode mats were fabricated by electrospinning particle/polymer mixtures containing commercial Pt/C catalyst and one of the following binders: (i) Nafion/poly(acrylic acid) (PAA), (ii) Nafion/poly(vinylidene fluoride) (PVDF) with different Nafion/PVDF wt ratios, or (iii) PVDF. High magnification scanning electron microscopy images of electrospun nanofibers showed porous fibers with a highly roughened surface and a uniform distribution of catalyst and polymer over the fiber length. The average fiber diameter was typically in the range of 400-600 nm. These non-woven mats were incorporated as the anode and cathode in membrane-electrode-assemblies (MEAs) and evaluated in a hydrogen/air proton exchange membrane fuel cell. Experiments focused on the performance of nanofiber mats as the cathode in a fuel cell MEA. Additional tests were performed to determine the electrochemical surface area and mass activity of nanofiber cathodes for the electrochemical reduction of oxygen.

(2) MEAs with a nanofiber cathode were shown to have excellent performance in a hydrogen/air fuel and generate higher power at lower Pt loadings, as compared to conventional MEAs with a decal or gas diffusion electrode (GDE) cathode. For example, an MEA with an electrospun cathode composed of catalyst particles at 0.065 mg_{Pt}/cm^2 and Nafion/PAA binder generated 360 mW/cm^2 at 0.65 V as compared to the 280 mW/cm^2 for a 0.104 mg/cm^2 decal cathode MEA (29% more power with a nanofiber cathode) when operated at 80^oC with fully humidified feed gases and no back pressure.

The nanofiber cathode MEA generated higher power throughout the entire voltage range of the polarization curve (~0.20 to 0.95 V vs. SHE).

(3) An MEA with a 0.055 m_{gPt}/cm^2 nanofiber cathode and 0.059 m_{gPt}/cm^2 nanofiber anode produced 906 mW/cm^2 maximum power at 80°C and 100% RH with 2 atm backpressure and high feed gas flow rates. Based on this power density, the total mass of Pt in an 80 KW fuel cell stack would be 10 g (4.8 g for the cathode and 5.2 g for the anode). This Pt amount is at/near the U.S. Department of Energy's target for an automotive fuel cell power plant.

(4) A nanofiber cathode MEA with an ultra-low platinum cathode loading of 0.029 mg_{Pt}/cm^2 produced reasonable power in a hydrogen/air fuel cell (over 300 mW/cm^2 maximum power at 80°C with fully humidified feed gases and no back pressure).

(5) Nanofiber cathodes with Nafion/PAA binder had a higher electrochemical surface area than conventional GDE or decal cathodes with Nafion binder, for the same mg/cm^2 Pt loading (39-45 m^2/g for nanofibers as compared to 30-36 m^2/g for GDEs).

(6) Nanofiber cathodes with Nafion/PAA binder had a higher mass activity than conventional cathodes with Nafion binder for the same Pt loading. For example, 0.16-0.17 A/mg_{Pt} at 0.9 V for a nanofiber cathode vs. 0.11 A/mg_{Pt} for a conventional Nafion cathode MEA. These data were collected at 80°C in 150 kPa_{abs} H_2/oxygen.

(7) Nanofiber cathode MEAs had the same oxygen reduction reaction Tafel slope as conventional MEAs (64-84 mV/decade), indicating no change in the oxygen reduction reaction mechanism on Pt in a nanofiber cathode mat.

(8) The MEA fabrication procedure with nanofiber electrodes was optimized and streamlined. A separate thermal annealing step prior to hot-pressing a nanofiber mat to a membrane could be eliminated with no detrimental effect on MEA performance. The optimal conditions for hot-pressing a nanofiber mat cathode to a Nafion membrane for maximum fuel cell power output were found to be: 5 MPa, 140°C, and 1 minute. Power output was more sensitive to pressure than time and temperature.

(9) The MEA power output in a hydrogen/air fuel cell with Nafion/PAA binder nanofiber cathodes was insensitive to the Nafion/PAA binder composition, for binders of (i) 72 wt% Pt/C, 13 wt% Nafion, 15 wt% PAA, (ii) 63 wt% Pt/C, 22 wt% Nafion, 15 wt% PAA, and (ii) 55 wt% Pt/C, 30 wt% Nafion, 15 wt% PAA. Thus, at 0.65 V all of the Nafion/PAA binders produced a power output of 450-480 mW/cm^2 in a hydrogen/air fuel cell (0.10 mg/cm^2 cathode Pt loading, 80°C, 100% RH, no back pressure). The fiber diameter and physical appearance of the fibers mats prior to hot-pressing were insensitive to binder composition. This result showed that precise control of the nanofiber cathode binder composition is not required for optimal fuel cell performance.

(10) Nanofiber cathode MEAs (where the nanofiber binder is Nafion/PAA) could be soaked in hot 1 M sulfuric acid or 3 wt% hydrogen peroxide at room temperature without any visual changes to the nanofiber structure or changes in fuel cell power output. This

showed that the fiber mats were chemically robust in the presence of acid or strong oxidizing agent.

(11) A series of electrospinning mats with the same Pt/C binder (63 wt% Pt/C, 22 wt% Nafion, 15 wt% PAA) was fabricated where the average fiber diameter varied from 250 to 520 nm. When these mats were tested as the cathode in an MEA (0.10 mg/cm^2 cathode Pt loading, 80°C, 100% RH, no backpressure) there were only marginal differences in power densities (power densities at 0.65 V were 460 mW/cm^2 ± 7%). Therefore, precise control of nanofiber diameter in an electrospun cathode mat is not required for optimum fuel cell power output, which should ease scale-up and manufacturing.

(12) The nanofiber electrode architecture did not significantly change the way fuel cell cathodes degraded during load cycling tests (Pt dissolution tests). After 10,000 voltage cycles, both a nanofiber Nafion/PAA cathode MEA and a traditional GDE cathode MEA showed the same cathode ECA loss (40-50%), but the resulting power loss was minimal (a 5-10% loss at 0.65 V).

(13) A Nafion/PAA nanofiber cathode MEA had significantly better end-of-life performance with 100% RH feed gases than a traditional GDE cathode MEA, after an accelerated durability test that simulated start-stop cycling test (a carbon corrosion test). After the test, the nanofiber cathode MEA maintained 53% of its initial power at 0.65 V and 85% of its maximum power, as compared to only 28% power at 0.65 V and 59% maximum power for the GDE cathode MEA. Carbon losses during the voltage cycling

experiment, as determined by the CO_2 content in the cathode air exhaust, was the same for nanofiber cathode and conventional (sprayed) GDE cathode MEAs. The improvement in nanofiber cathode MEA power output after carbon corrosion was attributed to the absence of water flooding in the nanofiber cathode after the carbon support was partially oxidized and became more hydrophilic as well as the retention of the nanofiber structure after the corrosion test (there is substantial thinning and collapse of the cathode layer in a conventional GDE cathode due to carbon loss).

(14) A nanofiber cathode MEA (where the nanofiber binder was Nafion/PAA) had significantly better end-of-life performance after an accelerated carbon corrosion voltage cycling test with 40% RH feed gases, as compared to a conventional GDE cathode MEA. The nanofiber cathode MEA produced more power after carbon corrosion than before the test, e.g., 120 mW/cm^2 at BoL vs. 190 mW/cm^2 at EoL at 0.65 V, when operating at 80°C and 1 bar backpressure (where BoL and EoL denote beginning-of-life and end-of-life, respectively). This result is in sharp contrast to the GDE cathode MEA, where there was a 50% loss in power at EoL at 0.65 V (220 mW/cm^2 at BoL vs. 110 mW/cm^2 at EoL at 0.65 V). During carbon corrosion, surface oxide species are formed on the cathode carbon support material, making the catalyst and cathode more hydrophilic. Better water retention in the cathode nanofibers improved power output.

(15) A nanofiber cathode MEA with a neat PVDF cathode binder (no proton-conducting ionomer in the cathode) produced significant power densities (e.g., 291 mW/cm^2 at maximum power) in a hydrogen/air fuel cell operating at 80°C with fully humidified fed gases and no backpressure.

(16) A nanofiber cathode MEA with a cathode binder of 80/20 Nafion/PVDF (w/w) exhibited excellent BoL performance in a hydrogen/air fuel cell at 80°C with fully humidified feed gases. The 80/20 Nafion/PVDF cathode MEA had lower catalyst activity and produced slightly less power at low current densities (high voltages) as compared to a Nafion/PAA binder MEA, but this cathode produced high power at low voltages (high current densities) due to improved water removal. This MEA (with a cathode Pt loading of 0.10 mg/cm^2) produced a maximum power of 545 mW/cm^2 under ambient pressure air conditions, which was the highest power output of any MEA tested (a Nafion/PAA cathode MEA at the same Pt loading and fuel cell operating conditions generated at maximum power of 489 mW/cm^2). End-of-life performance of this MEA was excellent; for example at 0.65 V, it generated 230 mW/cm^2 at 0.65 V, which was similar to a nanofiber Nafion/PAA cathode MEA (238 mW/cm^2), and much better than a conventional MEA with GDE electrodes and Nafion binder (143 mW/cm^2).

(17) Decreasing the Nafion/PVDF ratio (increasing the PVDF content) of nanofiber cathode MEAs decreased BoL fuel cell performance at both 100% and 40% RH operating conditions. For example at 0.65 V, an 80/20 Nafion/PVDF cathode MEA produced 385 mW/cm^2 with 100% RH feed gases and 138 mW/cm^2 with 40% RH feed gases, as compared to 180 mW/cm^2 and 10 mW/cm^2, respectively, for a 20/80 Nafion/PVDF cathode MEA with the same Pt loadings and operating conditions. Increasing the PVDF content relative to Nafion (while keeping the total binder content constant) had no effect on the measured electrochemical surface area of cathode Pt, but the catalyst mass activity decreased with decreasing Nafion/PVDF binder ratio. The

decrease in mass activity was attributed to less water near the Pt surface (due to the presence of more hydrophobic PVDF) which hinders the oxygen reduction reaction.

(18) Increasing the hydrophobicity of the cathode binder by decreasing the Nafion/PVDF ratio slowed catalyst carbon support corrosion in the cathode, presumably by reducing the amount of water near the catalyst surface. Thus, after an accelerated carbon corrosion durability test, cathodes with a binder of 80/20 Nafion/PVDF lost 14 wt% carbon (similar to a Nafion/PAA binder nanofiber or a conventional cathode GDE MEA with Nafion binder), while cathodes with a neat PVDF binder lost only 6 wt% carbon. Nanofiber and GDE cathodes with the same Nafion/PVDF binder composition lost the same about of carbon after an accelerated carbon corrosion test. This result indicates that cathode composition and not morphology was controlling carbon corrosion.

(19) There was no correlation between the measured carbon loss of a cathode after an accelerated carbon corrosion voltage cycling test and EoL fuel cell power output for MEAs with nanofiber cathodes containing Nafion/PVDF and neat PVDF binders. With fully humidified feed gases, cathodes with a Nafion/PVDF binders of 80/20 and 67/33 (i.e., where the major binder component was Nafion) generated less power at EoL vs. BoL, while cathodes with a Nafion/PVDF binder of 20/80 and 33/67 (i.e., where the major binder component was PVDF) generated more power at EoL vs. BoL. With 40% RH feed gases, all Nafion/PVDF nanofiber cathode MEAs showed an increase in EoL power (at 0.65 V) as compared to their BoL power densities. All nanofiber cathodes with a Nafion/PVDF binder showed a carbon loss and decrease in electrochemical Pt surface area after an accelerated carbon corrosion voltage cycling durability test. Nafion/PVDF

nanofiber cathodes that generated more power at EoL (at 100% RH) also exhibited an increase in Pt mass activity at EoL (vs. BoL). This unusual finding was attributed to a more hydrophilic cathode at EoL; where surface oxide species were formed on the Pt catalyst support. At EoL, the MEA that produced the highest power at 100% RH had a binder composition of 33/67 Nafion/PVDF, and the MEA that produced the highest power at 40% RH had a cathode binder composition of 80/20 Nafion/PVDF.

(20) A nanofiber cathode MEA with a binder of 50/50 Nafion/PVDF produced stable/constant power densities at 0.65 V before/during and after a carbon corrosion voltage cycling test. This power was significantly less than the BoL power output obtained with a nanofiber cathode with 80/20 Nafion/PVDF binder nanofibers (265 mW/cm^2 for 50/50 Nafion/PVDF vs. 385 mW/cm^2 got 80/20 Nafion/PVDF at 0.65 V).

CHAPTER VII

SUGGESTIONS FOR FUTURE WORK

(1) Membrane-electrode-assemblies (MEAs) should be further optimized to create high power densities with low Pt loadings. This dissertation primarily used Nafion® 211 as the membrane which has a 25 μm thickness and a conductivity of about 0.09 S/cm. Thinner membranes have lower sheet resistances and therefore result in higher fuel cell performance as long as the hydrogen gas crossover from the anode to the cathode is not severe. Membranes with < 25 μm and high proton conductivity should be used for nanofiber MEAs, such as a GORE-SELECT® membrane. Additionally, all MEAs in this dissertation used Sigracet 25 BCH as the gas diffusion media (this material is polytetrafluoroethylene (PTFE)-coated microporous carbon paper with a 235 μm thickness). Other gas diffusion layers, with various thicknesses, porosities, and hydrophilic/hydrophoblic characteristics should be examined.

(2) A dual-fiber electrospinning approach[1] should be explored to optimize the performance of electrospun catalyst mat cathodes. Dual fiber spinning offers many potentially advantages for improved cathode design, including (i) electrospinning fibers with the best beginning-of-life performance simultaneously with fibers of a binder composition that will give the best long-term durability, or (ii) preparing layered electrode mats, such as electrospinning more hydrophilic fibers near the membrane and more hydrophobic fibers farther from the membrane.

(3) This dissertation showed no fundamental change in load cycling Pt dissolution durability tests (0.6-0.95 V vs. SHE voltage cycles) for nanofiber cathodes with a Nafion/PAA binder as compared to conventional cathode. Similar tests should be performed on nanofiber cathodes with various Nafion/PVDF wt ratio binders.

(4) Experiments should be preformed that provide three-dimensional mapping/imaging of the catalyst/binder distribution in a nanofiber. Ideally, such studies could provide information on the thickness/uniformity of the polymer coating on catalyst particles, the degree of particle agglomeration, and the spatial distribution of catalyst particles as a function of fiber diameter, catalyst type and binder type and composition. The high ECA and excellent performance of nanofiber cathodes is thought to be due to a better distribution of catalyst and polymer in a nanofiber mat. This hypothesis should be substantiated with imaging studies. While such catalyst/Nafion imaging is notoriously difficult[2], recently M. Lopez-Haro *et al.*[3] successfully rendered 3-D images of portions of a fuel cell cathode layer by exchanging the Nafion sulfonic acid sites with Cs+ and then using electron tomography in a high angle annular dark-field scanning transmission electron microscope (HAADF-STEM).

(5) One of the present challenges of using non-platinum group catalysts in hydrogen/air fuel cells is the low density of active catalyst sites which necessitates the need for very thick electrode layers. Oxygen and water mass transfer in such electrodes is slow/problematic.[4,5,6] The inherent porosity of nanofiber catalyst mats may help

mitigate the problem with thick electrode layers. Future work should explore the merits of thick electrospun cathodes with non-platinum group catalysts.

(6) Novel Pt-alloy catalysts have been synthesized with much higher activity than the Pt/C powder used in this dissertation.[7-9] These new powders should be incorporated into electrospun cathodes and evaluated for MEA performance and durability in a hydrogen/air fuel cell.

(7) Conventional decal or GDE cathode layers have shown extreme thinning after accelerated carbon corrosion voltage cycling tests.[10] SEM cross-sectional analyses should be performed on nanofiber cathodes before and after such durability tests to determine the existence/extent of thinning of electrospun nanofiber cathodes. This result should be compared with traditional cathodes to better understand why nanofiber cathodes exhibit excellent durability. Additionally, TEM analysis should be performed on nanofiber cathodes before and after accelerated durability tests to investigate platinum agglomeration.

(8) Neat PVDF has been shown to be an effective catalyst binder in a high temperature PEMFC with a polybenzimidazole **(**PBI) membrane.[11] Cathodes with PVDF were shown to have less mass transfer limitations (to phosphoric acid) than cathodes with a Nafion binder due to the higher hydrophobicity of PVDF. Nanofiber PVDF-bound electrodes should be incorporated and tested in high temperature hydrogen/air fuel cells (160°C). As shown in this dissertation in a moderate temperature (80°C) fuel cell, the

increased catalyst surface area and high porosity of nanofiber electrode structures should produce higher power densities than standard/conventional thin film electrodes.

(9) In this dissertation, catalyst was electrospun with a Nafion/PAA, Nafion/PVDF, and neat PVDF binders. Binders with Nafion and both PAA and PVDF (a high PAA content for electrospinning and varying amounts of PVDF for hydrophobic property adjustment) should be investigated to determine: (i) the compositional range of blended binders that can be electrospun with Pt/C or non-PGM catalyst, and (ii) the effect of such binders on fuel cell power and durability. Additionally, other catalyst binders should be explored. Poly(vinyl alcohol) has also been used to electrospin Nafion and, in principle, could be used as the Nafion carrier polymer for electrospun electrodes.[12] Nafion could also be replaced by PFSAs with a lower equivalent weight and higher proton conductivity, such as Aquivion®.

(10) Anion exchange membrane (AEM) fuel cells can use non-noble metals (e.g. nickel or silver) as electrode catalysts. Such metals cannot be used in a proton exchange membrane (PEM) fuel cell because they would dissolve in the acidic PEM media.[13] The elimination of platinum catalyst electrodes would significantly lower the price of fuel cells. However, like PEM fuel cells, AEM fuel cells also suffer from sluggish reaction kinetics and could benefit from a nanofiber electrode morphology. It is recommended that electrospun nanofiber electrodes with non-noble metal catalysts be fabricated and tested in an AEM fuel cell.

(11) PEM electrolyzers can be used to produce high purity hydrogen gas streams.[14] They operate as a PEM fuel cell in reverse (add electrical energy and water; produce hydrogen and oxygen gases), with operating voltages as high as 2.0 V vs. SHE. Carbon catalyst supports cannot be used for the oxygen generation electrodes due to carbon corrosion concerns.[15] Electrospun electrodes with PVDF-bound Pt/C may help rectify this problem, since it was shown in this dissertation that a PVDF binder greatly reduced the carbon corrosion rate of Pt/C catalyst powders in a fuel cell cathode.

(12) This dissertation showed that electrospun nanofiber electrodes increase the active surface area of catalysts and provide a porous structure suitable for heterogeneous reactions. These features should make nanofiber electrodes excellent candidates for batteries and sensors and for organic electrochemical syntheses in a fuel cell reactor.[16] In a battery, a nanofiber-based electrode will increase the interfacial area between ionic reactants in the electrolyte and electrode surface sites, thus allowing for faster kinetics and better reactant utilization. An increase in the porosity of the electrode (due to the inherent void volume in nanofiber mats), will allow for complete electrolyte impregnation throughout the entire electrode structure, with faster mass for decreased battery charging times. In a sensor, high surface area electrospun electrodes will have a higher sensitivity and, thus, may be able to detect lower concentrations with faster response times than conventional devices

7.1 References

(1) Ballengee, J. B. and P. N. Pintauro (**2013**) *Journal of Membrane Science*, 442, 187-195.

(2) Scheiba, F., N. Benker, U. Kunz, C. Roth, and H. Fuess (**2008**) *Journal of Power Sources*, 177, 273-280.

(3) Lopez-Haro, M., L. Guetaz, T. Printemps, A. Morin, S. Escribano, P. H. Jouneau, P. Bayle-Guillemaud, F. Chandezon, and G. Gebel (**2014**) *Nature Communications*, 5.

(4) Serov, A., M. H. Robson, M. Smolnik, and P. Atanassov (**2013**) *Electrochimica Acta*, 109, 433-439.

(5) Othman, R., A. L. Dicks, and Z. Zhu (**2012**) *International Journal of Hydrogen Energy*, 37, 357-372.

(6) Maldonado, S. and K. J. Stevenson (**2004**) *J. Phys. Chem. B*, 108, 11375-11383.

(7) Long, N. V., Y. Yang, C. Minh Thi, N. V. Minh, Y. Cao, and M. Nogami (**2013**) *Nano Energy*, 2, 636-676.

(8) Ma, Y., H. Zhang, H. Zhong, T. Xu, H. Jin, and X. Geng (**2010**) *Catalysis Communications*, 11, 434-437.

(9) Mukerjee, S., S. Srinivasan, M. P. Soriaga, and J. McBreen (**1995**) *Journal of the Electrochemical Society*, 142, 1409-1422.

(10) Hashimasa, Y., T. Shimizu, Y. Matsuda, D. Imamura, and M. Akai (**2013**) *ECS Transactions*, 50, 723-732.

(11) Su, H. N., S. Pasupathi, B. Bladergroen, V. Linkov, and B. G. Pollet (**2013**) *Int. J. Hydrog. Energy*, 38, 11370-11378.

(12) Chang, X. F., Y. Hu, and Z. L. Xu (**2011**) *Mater. Lett.*, 65, 1719-1722.

(13) Matsumoto, K., T. Fujigaya, H. Yanagi, and N. Nakashima (**2011**) *Advanced Functional Materials*, 21, 1089-1094.

(14) Grigoriev, S. A., V. I. Porembsky, and V. N. Fateev (**2006**) *International Journal of Hydrogen Energy*, 31, 171-175.

(15) Barbir, F. (**2005**) *Sol. Energy*, 78, 661-669.

(16) An, W. D., J. K. Hong, P. N. Pintauro, K. Warner, and W. Neff (**1999**) *Journal of the American Oil Chemists Society*, 76, 215-222.

APPENDIX A

ADDITIONAL DATA FOR NAFION/PVDF CATHODE MEAS: LOW HUMIDITY OPERATION

In Figure 5.4, polarization curves that were collected with 100% RH feed gases were shown comparing nanofiber and GDE Nafion/PVDF cathode MEAs. The polarization curves collected with 40% RH feed gases for these same MEAs were not explicitly shown in Chapter 5, though the power densities at 0.65 V were summarized in Figure 5.6. Below, the 40% RH polarization curves are shown.

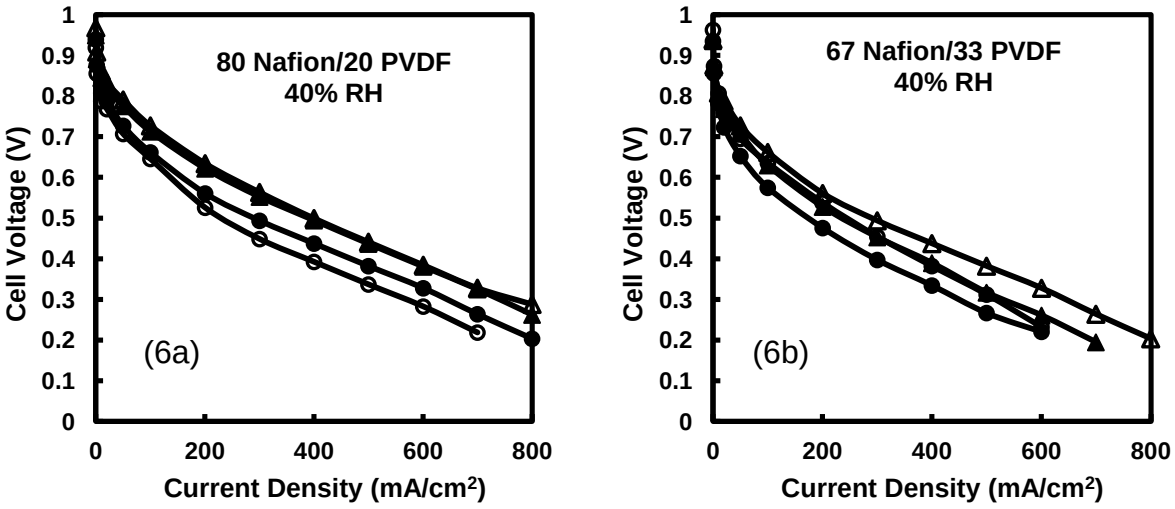

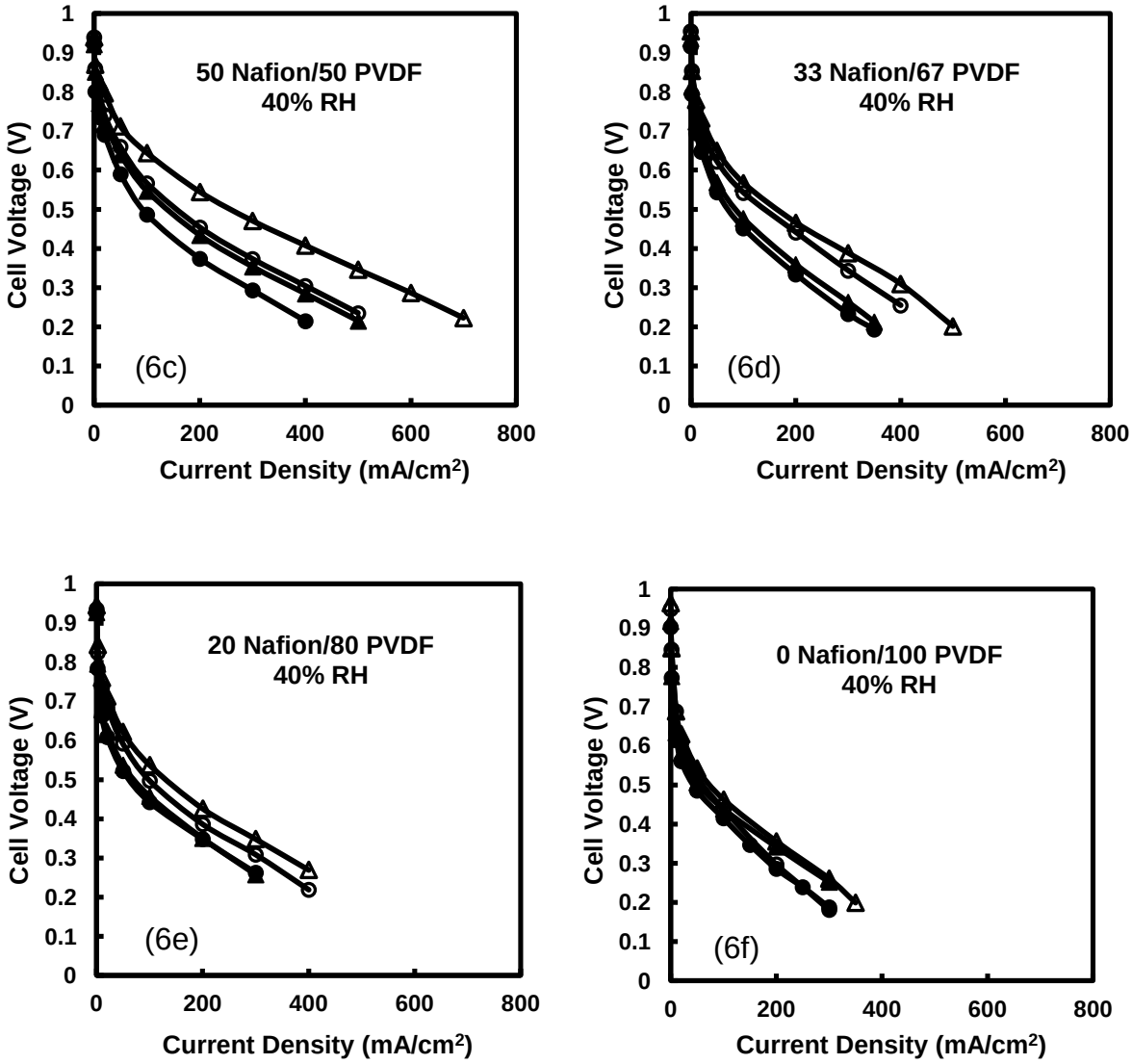

Figure A.1. BoL (solid symbols) and EoL (open symbols) polarization curves for 5 cm^2 MEAs with a Nafion 211 membrane and 0.10 mg_{Pt}/cm^2 cathode and anode after 1,000 voltage cycles. Fuel cell operating conditions: 80°C, 40% RH, 125 sccm H_2 and 500 sccm air at ambient pressure. Each plot shows data for an MEA with a nanofiber cathode (triangles) and an MEA with a painted GDE cathode (circles) with the same Nafion/PVDF cathode composition: (a) 80/20, (b) 67/33, (c) 50/50, (d) 33/67, (e) 20/80, or (f) 0/100.

At BoL with 40% RH feed gases, the Nafion/PVDF nanofiber MEAs also produced higher current densities (and thus higher power densities) than their GDE MEA analogous at all voltages as shown in Figure A.1. The advantage of the nanofiber MEAs was more pronounced at higher Nafion/PVDF ratios; the nanofiber MEA produced 8% more power at 0.65 V than a GDE MEA with a neat PVDF binder, 25% more power with an 20/80 Nafion/PVDF binder, and ~35% more power when the Nafion content was 33-80% of the total binder. The advantage of the nanofiber MEAs is primarily higher ECA and mass activity (as shown previously in this dissertation in Table 5.2) as the shapes of the polarization curves in the middle and high current regions are essentially identical. A higher ECA provides more accessible catalyst sites to protons and oxygen and thus reduced voltage loss in the kinetically-controlled high voltage region of the polarization curve. At 40% RH, all MEAs with more than 20% PVDF in the cathode binder produced higher power at EoL due to a favorable increase in hydrophilicity after voltage cycling.